Development of a Harmonic Motion Imaging guided Focused Ultrasound system for breast tumor characterization and treatment monitoring

Yang Han

Submitted in partial fulfillment of the

requirements for the degree

of Doctor of Philosophy

in the Graduate School of Arts and Sciences

COLUMBIA UNIVERSITY

2018

Abstract

Development of a Harmonic Motion Imaging guided Focused Ultrasound system for breast tumor characterization and treatment monitoring

Yang Han

Breast cancer is the most common cancer and the second leading cause of cancer death among women. About 1 in 8 U.S. women (about 12%) will develop invasive breast cancer over the course of their lifetime.

Existing methods of early detection of breast cancer include mammography and palpation, either by patient self-examination or clinical breast exam. Palpation is the manual detection of differences in tissue stiffness between breast tumors and normal breast tissue. The success of palpation relies on the fact that the stiffness of breast tumors is often an order of magnitude greater than that of normal breast tissue, i.e., breast lesions feel ‘‘hard’’ or ‘‘lumpy’’ as compared to normal breast tissue. A mammogram is an x-ray that allows a qualified specialist to examine the breast tissue for any suspicious areas. Mammography is less likely to reveal breast tumors in women younger than 50 years with denser breast than in older women. When a suspicious site is detected in the breast through a breast self-exam or on a screening mammogram, the doctor may request an ultrasound of the breast tissue. A breast ultrasound can provide evidence about whether the lump is a solid mass, a cyst filled with fluid, or a combination of the two. An invasive needle

biopsy is the only diagnostic procedure that can definitely determine if the suspicious area is cancerous. In the clinic, 80% of women who have a breast biopsy do not have breast cancer.

Most women with breast cancer diagnosed will have some type of surgery to remove the tumor. Depending on the type of breast cancer and how advanced it is, the patient might need other types of treatment as well, such as chemotherapy and radiation therapy. Image-guided minimally-invasive treatment of localized breast tumor as an alternative to traditional breast surgery, such as high intensity focused ultrasound (HIFU) treatment, has become a subject of intensive research. HIFU applies extreme high temperatures to induce irreversible cell injury, tumor apoptosis and coagulative necrosis. Compared with conventional surgical procedures the main advantages of HIFU ablation lie in the fact that it is non-invasive, less scarring and less painful, allowing for shorter recovery time. HIFU can be guided by MRI (MRgFUS) or by conventional diagnostic ultrasound (USgFUS). Worldwide, thousands of patients with uterine fibroids, liver cancer, breast cancer, pancreatic cancer, bone tumors, and renal cancer have been treated by USgFUS.

In this dissertation, the objective is to develop an integrated Harmonic Motion Imaging guided Focused Ultrasound (HMIgFUS) system as a clinical monitoring technique for breast HIFU with the added capability of detecting tumors for treatment planning, evaluation of tissue stiffness changes during HIFU ablation for treatment monitoring in real time, and assessment of thermal lesion sizes after treatment evaluation. A new HIFU treatment planning method was described that used oscillatory radiation force induced displacement amplitude variations to detect the HIFU focal spot before lesioning. Using this method, we were able to visualize the HMIgFUS focal region at variable depths. By comparing the estimated displacement profiles with lesion locations in pathology, we demonstrated the feasibility of using this HMI-based technique to localize the HIFU focal spot and predict lesion location during the planning phase. For HIFU monitoring, a

HIFU lesion detection and ablation monitoring method was first developed using oscillatory radiation force induced displacement amplitude variations in real time. Using this method, the HMIgFUS focal region and lesion formation were visualized in real time at a feedback rate of 2.4 Hz. By comparing the estimated lesion size against gross pathology, the feasibility of using HMIgFUS to monitor treatment and lesion formation without interruption is demonstrated. In order to reduce the imaging time, it is shown in this dissertation that using the steered FUS beam, HMI can be used to image a 2.3 times larger ROI without requiring physical movement of the transducer. Using steering for HMI can be used to shorten the total imaging duration without requiring physical movement of the transducer. For the application of breast tumor, HMI and HMIgFUS were optimized and applied to *ex vivo* breast tissue. The results showed that HMI is experimentally capable of mapping and differentiating stiffness in normal and abnormal breast tissues. HMIgFUS can also successfully generate thermal lesions on normal and pathological breast tissues. HMI has also been applied to post-surgical breast mastectomy specimens to mimic the *in vivo* environment. In the end, the first HMI clinical system has been built with added capability of GUP-based parallel beamforming. A clinical trial has been approved at Columbia University to image breast tumor on patient. The HMI clinical system has shown to be able to map fibroadenoma mass on two patients with valid HMI displacement. The study in this dissertation may yield an early-detection technique for breast cancer without any age discrimination and thus, increase the survival rate.

Table of Contents

List of Figures

List of Tables

Acknowledgements

"The Lord is my strength and my shield; My heart trusted in Him, and I am helped; Therefore my heart greatly rejoices, And with my song I will praise Him."

-Psalm 28:7

After an intensive 64 months of study and research, today is the day to write this note of thanks as a final touch on my dissertation. It has been a period of intense learning for me, not only in the scientific arena, but also on a personal level. Writing this dissertation has been one of the most important things happened in my life. I would like to reflect on the people who have supported and helped me so much throughout this period.

Foremost, I would like to express my sincere gratitude to my advisor Prof. Elisa Konofagou for the continuous support of my Ph.D. study and research, for her patience, motivation, enthusiasm, and immense knowledge. Her guidance helped me in all the time of research and writing of this thesis. I could not have imagined having a better advisor and mentor for my Ph.D. study.

I would like to thank the rest of my thesis committee: Prof. Andrew Laine, Prof. Andreas Hielscher, Dr. Bret Taback and Dr. Richard Ha for their support, encouragement and insightful comments. A very special gratitude goes out to Dr. Bret Taback for his support and collaboration in the past five years.

I also feel so grateful to be part of the Ultrasound Elasticity Imaging Laboratory and the Harmonic Motion Imaging team. Thank you, Shutao Wang, Gary Hou and Thomas Payen, for

your wonderful mentorship and collaboration. You supported me greatly and were always willing to help me.

I would also like to thank my husband for his unconditional love and support. To my parents for their encouragement and sympathetic ear. You are always there for me.

CHAPTER 1. Introduction

1.1 Breast Cancer

Breast cancer is the most common cancer and the second leading cause of cancer death among women. In 2017, approximately 252,710 women will be diagnosed with breast cancer and approximately 40,160 will die from the disease in the US. About 1 in 8 U.S. women (about 12.4%) will be diagnosed with breast cancer over the course of their lifetime. A woman's risk of breast cancer nearly doubles if she has a first-degree who has been diagnosed with breast cancer. In the meanwhile, most breast cancer cases (85%) had no family history of breast cancer [1], which is why screening examination is important for women.

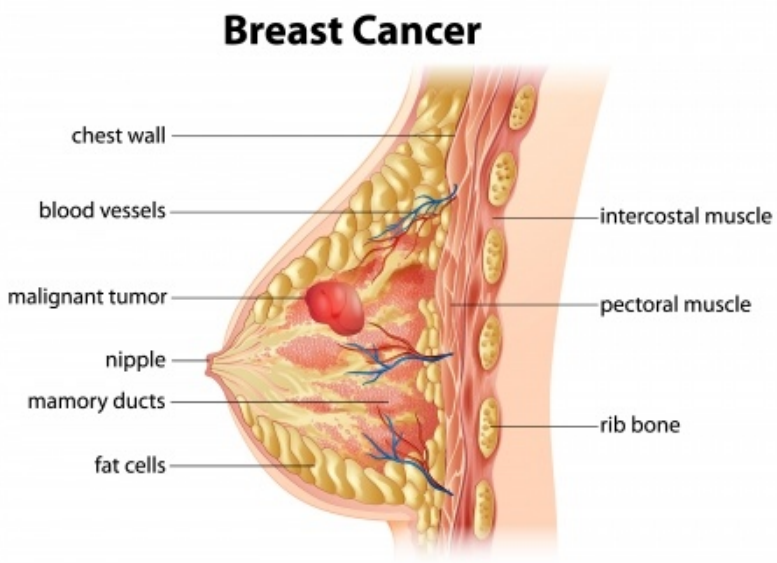

Figure 1.1 Illustration - Needle biopsy of the breast. Source: http://slu.adam.com

1.2 Breast Cancer diagnosis

Breast cancer typically produces no symptoms at early stages, which is why screening is important for early detection as when the tumor is small it is most easily treated. Breast cancer can begin anywhere in the breast, most commonly in the lobules, which are the milk-producing glands, or the ducts, the passages that drain milk from the lobules to the nipple.

The standard diagnostic process for breast cancer often has 3 stages: clinical examination, imaging, and needle biopsy. The first stage involves a medical history and clinical examination, followed in the second stage by imaging of the breast, and finally in the last stage laboratory testing of the sample breast tissue obtained using a needle biopsy procedure [2]. Existing common methods of the first and second stage include mammography and palpation, either by patient self-examination or clinical breast exam. Palpation is the manual detection of differences in tissue stiffness between breast tumors and normal breast tissue. The success of palpation relies on the fact that the stiffness (or Young's modulus) of breast tumors is often an order of magnitude greater than that of normal breast tissue [3], i.e., breast lesions feel ''hard'' or ''lumpy'' as compared to normal breast tissue [4]. Most masses seen on a mammogram and most breast lumps turn out to be benign (not cancerous). However, to determine the extent of stage and characterize the type of the disease when cancer is suspected, a needle biopsy (Figure 1.2) is necessary to obtain the tissue for microscopic analysis.

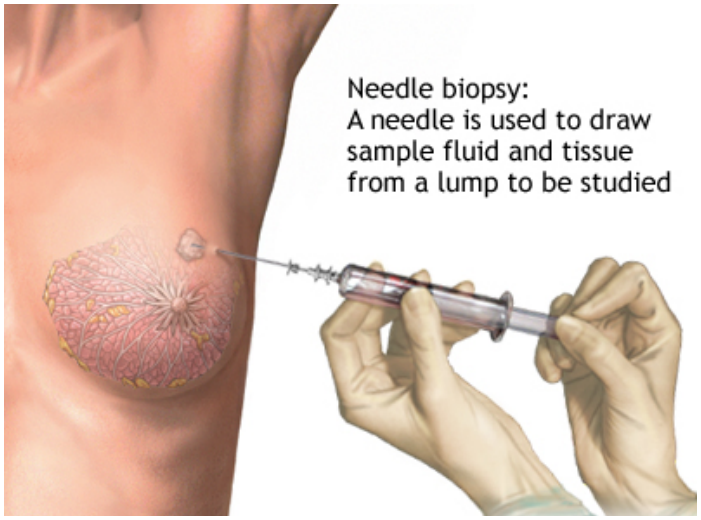

Figure 1.2 Illustration - Needle biopsy of the breast. Source: http://slu.adam.com

1.2.1 Conventional breast cancer imaging

Mammography is the most common and recommended method for breast cancer screening of women in the general population. It is also the only method of screening for breast cancer shown to decrease mortality [5], [6]. The ability of a mammogram to detect breast cancer may depend on the size of the tumor, the density of the breast tissue, and the skill of the radiologist administering and reading the mammogram. Mammography is less likely to reveal breast tumors in women younger than 50 years than in older women. This may be because younger women have denser breast tissue that appears white on a mammogram. Likewise, a tumor appears white on a mammogram, making it hard to detect.

Therefore, mammography alone does not perform as well as mammography plus supplemental screening in high-risk women, particularly those with dense breasts [7]. Therefore, supplemental screening with MRI or ultrasound is recommended in selected high-risk populations.

Ultrasound is useful for looking at some breast changes, such as lumps (especially those that can be felt but not seen on a mammogram) or changes in women with dense breast tissue. It also can be used to look at a change that was seen on a mammogram. It is especially useful to tell the difference between fluid-filled cysts (which are very unlikely to be cancer) and solid masses (which might need further testing to be sure they're not cancer). However, ultrasound B-mode alone had the highest false-negative rate compared with mammography and MR [8].

Breast MRI in high-risk women has been shown to have higher sensitivity than mammography, and the combination of mammography and MRI has the highest sensitivity. Screening MR imaging had a higher biopsy rate but helped detect more cancers than either mammography or ultrasound B-mode [9].

In addition, the conflict of sensitivity versus specificity also matters. Most of the current methods are highly sensitive yet lack specificity, resulting in an alarming number of false-positive cases. Consequently, the increased false-positive results also increase the rate of unnecessary biopsies [2]. Therefore, improved methods of differential diagnosis based on quantitative measures of elasticity have been gaining support and interest for clinical utilization.

1.2.2 Breast elasticity imaging

Ultrasound elasticity imaging is used in addition to traditional B-mode ultrasound as a tool for differential diagnosis between normal and tumor in human breast based on tissue stiffness as it provides information not only on morphology but also on tissue elasticity. Qualitative and quantitative tissue strain analyses using acoustic radiation force impulse imaging (ARFI) technology has been developed for the diagnosis of breast masses [4], [10], [11]. The response of tissue to the acoustic radiation force is tracked as tissue displacement, which has been found to be

correlated with local stiffness of the tissue. Vibro-acoustic tissue mammography is also a radiation force-based method, uses focused ultrasound to vibrate tissue at frequency (kHz) and utilizes the resulting response to produce images that are related to the hardness of the tissue [12], [13]. Supersonic shear imaging (SSI) utilizes a very fast (5000 frames/s) acquisition sequence to capture the propagation of shear waves [14] that provide information of the local viscoelastic properties [15], [16].

1.3 Breast Cancer treatment

1.3.1 Conventional breast cancer treatment

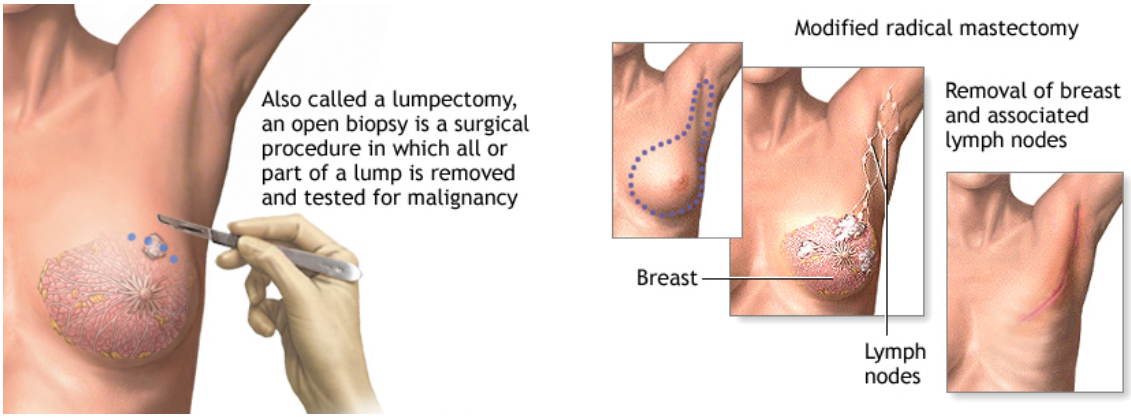

Figure 1.3 Illustration – Lumpectomy (left) and mastectomy (right). Prior to surgery, a radiologist often first marks the lump with a wire, making it easier for the surgeon to find. Source: http://slu.adam.com

Once diagnosed, there are several ways to treat breast cancer, depending on its type and stage. Some treatments are local, meaning they treat the tumor without affecting the rest of the body. Types of local therapy used for breast cancer include surgery and radiation therapy. Drugs used to treat breast cancer are considered systemic therapies because they can reach cancer cells

almost anywhere in the body. They can be given by mouth or put directly into the bloodstream. Depending on the type of breast cancer, different types of drug treatment might be used, including chemotherapy, hormone therapy and targeted therapy.

Most women with breast cancer will have some type of surgery to remove the tumor. Breast conserving surgery, also called lumpectomy (Figure 1.3(left)), only remove the part of the breast containing the cancer. The goal is to remove the cancer as well as some surrounding normal tissue. The other type of surgery, mastectomy (Figure 1.3(right)), removes the entire breast, including all of the breast tissue and sometimes other nearby tissues. Modified radical mastectomy includes removal of the entire breast, plus a full axillary lymph node dissection. Some women may also get a double mastectomy, in which both breasts are removed [1].

1.3.2 Noninvasive and minimally invasive cancer therapy

However, open surgery has been linked to significant risk of morbidity and mortality. Despite the surgical risk involved and the fact that the vast majority of breast cancers at diagnosis are non-metastatic, 94% of the patients still undergo surgery (58% lumpectomy and 36% mastectomy) [17], including in the case of a benign mass, with several risks and prolonged recovery periods. In the meanwhile, breast conservation or lumpectomy is dependent on clear margins, defined as no tumor cells visible on ink on the resected specimen according to American Society for Radiation Oncology (ASTRO) guidelines [18]. However, during surgery the surgeon is unable to visualize the tumor to aid in determining clear margins. This lack of intraoperative target definition results in high rates of reoperation to excise residual tumor. There is a clinical need to develop minimally invasive ablative techniques to define better the target and tumor margins during treatment [19].

Image-guided minimally-invasive treatment of localized breast tumor has become a subject of intensive research and several studies have assessed the feasibility of minimally-invasive breast tumor ablation techniques, such as radiofrequency ablation (RFA), cryo-ablation and high intensity focused ultrasound (HIFU) ablation [20]. Minimally-invasive treatment applies extreme temperatures, either high or low, to induce irreversible cell injury, tumor apoptosis and coagulative necrosis [21]. Compared with conventional surgical procedures the main advantages of minimally-invasive ablation lie in the fact that they are less invasive, less scarring and less painful, allowing for shorter recovery time [22]. With the widespread use of screening examination and improved patient education, smaller invasive breast tumors and in situ cancers are being identified more often for minimally-invasive treatment. RFA has been used as a local therapy to treat early stage breast carcinomas [23]–[25] and elderly patients with inoperable breast cancer [26]. However, as soon as the RFA treatment starts, the region of the targeted lesion becomes invisible or masked by a shadow in ultrasound guided images. Therefore, it is difficult to monitor during the RFA procedure and even more difficult to control it [27]. A completely non-invasive technique on the rise is HIFU. During HIFU, the ultrasound beam is transmitted and focused into a small target volume to reach high focal power levels, resulting in temperature elevations causing cell damage in short duration. HIFU can be guided by MRI (MRgFUS) or by conventional diagnostic ultrasound (USgFUS). Worldwide, thousands of patients with uterine fibroids, liver cancer, breast cancer, pancreatic cancer, bone tumors, and renal cancer have been treated by USgFUS [20].

1.3.3 High Intensity Focused Ultrasound for breast

The breast is ideally suited for HIFU therapy due to its superficial position, with no intervening vital structures [28]. HIFU was first investigated as a non-invasive therapeutic

technique in the 1940s to thermally coagulate tissue at the focus to produce thermal lesions in living animals [29]. The HIFU beam is finely focused on a small region of the tissue and produces rapid and intense heating. Over the past several decades, HIFU has been increasingly explored as an extracorporeal modality to ablate tumors in cancer treatment, but is only recently beginning to emerge as a vital alternative to conventional therapies [30], [31]. Numerous studies and clinical trials have used HIFU to treat local diseases in organs such as the thyroid, prostate, breast, pancreas and liver [32]–[36]. The clinical translation and accessibility of HIFU relies heavily on improving its treatment monitoring.

HIFU is an entirely non-invasive technique which focuses the ultrasound beam onto a small target volume to reach high focal power, resulting in temperature elevations causing coagulative necrosis in the target while surrounding structures are spared. Since the ultrasound wave penetrates through soft tissue without any surgical incision nor needle insertion, there are no damages to the skin or underlying tissues. Acoustic energy can induce temperature elevations at the focal spot in a few seconds and simultaneously induce cellular damage and vascular destruction in normal and tumor tissues [37]. Because of the steep thermal gradients involved, the boundaries of the ultrasound-treated volumes can be closely spaced until the entire target is covered.

HIFU has also been used to ablate early stage malignant breast tumors in elderly patients who are not surgical candidates. Huber et al [38] used MRI-guided HIFU to treat a 56-year-old patient with breast cancer. Post-procedural tissue pathological examination indicated that HIFU induced lethal and sub-lethal tumor ablation without damage to the surrounding healthy tissue or systemic effects. In 2003, Wu et al. [39] reported the first clinical trial exploring the efficacy and safety of HIFU in the treatment of patients with breast cancer in China. The results showed that no severe side effects were observed in the HIFU-treated patients. Pathological findings revealed that

HIFU-treated tumor cells underwent complete coagulative necrosis, and tumor vasculature was severely damaged. In 2007, Furusawa et al. [40] reported a follow-up study of 21 patients who underwent MRI-guided HIFU treatment. After an average of 14 months, one case had local recurrence, but no evidence of recurrence was detected in the remaining 20 (95%) patients. HIFU has then been applied to treat solid breast tumors in the past decade or so.

Recently, the use of ultrasound has been shown to have potential in cancer immuno-therapy. In addition to direct destruction of the primary tumor, HIFU thermos ablation may elicit long-term systemic host anti-tumor immunity [41]–[43]. Based on many pre-clinical and clinical studies, different possible mechanisms are suggested to explain the positive effect of anti-cancer immune response following focused ultrasound treatment, although clinical significance of this HIFU-induced immuno-modulation is still unknown [44], [45].

CHAPTER 2. Background and significance

2.1 Harmonic Motion Imaging

2.1.1 Tissue elasticity imaging

Mechanical properties of tumor tissues are known to differ from the surrounding tissues, as indicated by the use of palpation in the clinic as a first step diagnostic tool. Elasticity imaging is a medical imaging technology that maps the elastic properties of soft tissue providing diagnostic information about the presence or status of disease. Differences in Young's moduli are the basis for the investigation of elasticity imaging modalities that provide information about the stiffness of tissue.

In the field of ultrasound, Jonathan Ophir et al. introduced elastography as a new method for quantitative imaging of strain and elastic modulus distributions in soft tissues based on external tissue compression [46]. Cross-correlation techniques were used on radiofrequency (RF) ultrasonic signals to estimate the displacement and strain in the tissue resulting from the compression. By measuring the stresses applied by the compressing device, the strain profile can then be converted to an elastic modulus profile. In 1998, Krouskop et al. [47] estimated vibration motion amplitudes and related them to estimates of elastic modulus by measuring the Doppler shifts of ultrasonic tone bursts.

Remote application of the mechanical stimuli, such as radiation force, was introduced in the late 1990s to overcome the shortcomings of an external excitation. A radiation force based ultrasound method, Vibro-Acoustic Spectrography, was presented for imaging the acoustic response of a material to mechanical excitation by Fatemi et al. [48]. Radiation force was generated by a two-element confocal ultrasound annular array driven by two continuous wave sources at

frequencies equal to ω_1 and $\omega_2 = \omega_1 + \Delta\omega$, where these frequencies are very close to the central frequency of the elements, and $\Delta\omega$ is much smaller than the center point. The low-frequency force on a target at the focal point can be expressed by

$$F_1(t) = d_r \iint_s < E_{focal}(t,x,y) >_T dxdy = C d_r \cos(\Delta\omega t) \quad (2.1)$$

where C is a constant, S is the area over which E_{focal} the total energy density in the focal plane, and $<>_T$ indicates a short-term time average. The sound field resulting from object vibrations at each position is received by a hydrophone and recorded. Nightingale et al. [4] developed a method of acoustic remote palpation using focused ultrasound is used to apply localized radiation force within tissue, and the resulting tissue displacements are mapped using ultrasonic correlation-based methods. In this study, the radiation force is given by

$$\mathrm{F} = (\prod a + \prod s - \int \gamma cos\theta r \, dr \, d\theta)\langle E \rangle \quad (2.2)$$

where $\prod a$ is the total power absorbed by the target is, $\prod s$ is the total power scattered by the target, γ is the magnitude of the scattered intensity, θ is the scattering angle, $r \, dr \, d\theta$ is an area element of the projection of the target onto the axial/lateral plane, and $\langle E \rangle$ is the temporal average energy density of the propagating acoustic wave. The tissue displacements are inversely proportional to the stiffness of the tissue, and thus a stiffer region of tissue exhibits smaller displacements than a more compliant region. Localized Harmonic Motion Imaging was developed taking advantages of localized oscillatory harmonic motion resulting from the harmonic radiation force produced by two focused ultrasound transducer elements with overlapping beams oscillating at distinct frequencies [49]. Different from Vibro-Acoustic Spectrography using an external hydrophone for detection, Localized Harmonic Motion Imaging use a separate ultrasound beam to probe the induced tissue motion avoid the artefacts. In addition, the use of ultrasound to detect the motion

using cross-correlation techniques successfully decoupled ultrasound attenuation effects from the mechanical effects in different tissues.

Ultrasound elasticity imaging has been further developed and refined to enable quantitative assessments of tissue stiffness. Supersonic Shear Imaging (SSI) was first introduced by Bercoff et al. [50] as a new ultrasound-based technique for real-time visualization of soft tissue viscoelastic properties. Relaying on mechanical vibration generated by ultrasonic focused beams, SSI proposed to create such a source moving at a supersonic speed. These waves propagate through the medium and are progressively distorted by tissue heterogeneities. Using ultrafast scanner prototype (5000 frames/s), SSI was able to image (5000 frames/s) the propagation of the resulting shear waves. As measurement of the shear wave speed results in qualitative and quantitative estimates of tissue elasticity, an elasticity maps were obtained in heterogeneous medium containing hard inclusions and on healthy breasts. To date, the following commercially available systems use shear wave elastography technology: FibroScan™ (Echosens, Paris, France), Virtual TouchTM Imaging Quantification (VTIQ/ARFI) by Siemens, Shear Wave™ Elastography by SuperSonic Imagine (SSI), Shear Wave Elastography by Philips, Acoustic Structure Quantification™ (ASQ) by Toshiba, and 2D-SWE by GE Healthcare [51]–[53].

In elasticity imaging, local tissue characters are determined by measuring local displacements that occur during global tissue compression or acoustic radiation forced induced vibration (Figure 2.1). The magnitude of the tissue displacement is inversely proportional to the local stiffness of the tissue. Therefore, a relative stiffness map can be generated using ultrasound-based elasticity imaging.

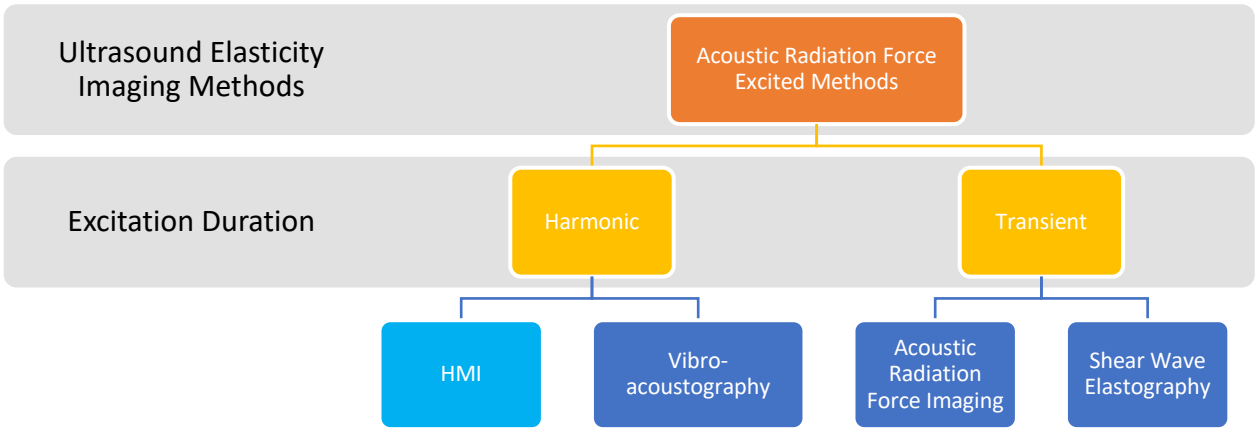

Figure 2.1 Ultrasound-based elasticity imaging methods can be categorized by the excitation source used to deform soft tissue. As presented herein, acoustic radiation force-based elasticity imaging methods can be further classified according to the duration of the applied acoustic radiation force excitation.

2.1.2 Harmonic Motion Imaging

The harmonic motion imaging (HMI) technique using single focused ultrasound transducer was first described our group [54]. Using a single focused ultrasound transducer as opposed to two separate elements [49] has shown the advantage of sustaining the application of the radiation force at a constant, stable focus within the tissue region. The displacement amplitudes are measured at the location of the applied force using a pulse-echo transducer. A finite-element mode (FEM) study was presented with an experimental validation [55] to show that HMI can be used as a reliable tumor-mapping technique based on the tumor's distinct stiffness comparing with its surrounding tissue. On the other hand, HMI has shown the feasibly for attenuation measurements which may provide an alternative to conventional techniques [56]. HMI was also used as method

for measuring elastic properties non-invasively by using internal indentation [57]. The HMI elastic modulus E_{HMI} was defined as the ratio of the applied force to the axial strain measured. Initial feasibility was also shown very good correlation and agreement was found between the measured Young's modulus and the HMI modulus in the numerical study and on polyacrylamide gels.

2.2 Harmonic Motion Imaging guided Focused Ultrasound

2.2.1 HIFU monitoring

Over the past 70 years, researchers have investigated the potential of utilizing high intensity focused ultrasound (HIFU) as a minimally, or non- invasive, cancer treatment modality. Currently, MRI and sonography are being used for guidance and monitoring of HIFU therapy. Both MR-guided HIFU (MRgFUS) and ultrasound-guided HIFU (USgFUS) methods have their advantages and disadvantages.

It has been well known that most endogenous MRI- sensitive parameters are temperature sensitive. Based on the temperature dependence of T1 relaxation time in tissue, T1 is proportional to 1/T over a small range of temperatures, MRI was shown to be compatible with focused ultrasound treatment [58], [59]. MRI-based techniques can provide reliable functional and anatomical information during HIFU treatment can currently be provided only by using MRI-based techniques. In one of its first breast cancer clinical trials, nine patients (eleven fibroadenomas) were treated over two hours for 2-cm and 45 min for 1-cm lesion sizes with an average temperature rise of up to 45.9 °C. Common side-effects, such as skin burn or swelling following the treatment, were not observed six months after treatment and no sign of tumor re-growth in the same treated region was detected 3-4 years following treatment [60]. Despite its exquisite imaging quality and thermometry feedback, MRIgFUS incurs low temporal resolution resulting in lengthy procedures

(up to 3 hours for uterine fibroid HIFU ablation [61]) together with co-registration challenges, restrictions in the patient pool and large physical space requirements. MRI has also been shown particularly challenging in the breast. Proton-resonance frequency shift (PRFS)-based MRT is the most widely used method during MR-guided thermal therapies. Unfortunately, this technique does not work for protons in fat molecules. Fat-suppression techniques therefore have been employed during PRFS-based MR thermometry in fat-containing tissues. However, during breast tumor ablation, preferably both the temperature of the tumor and surrounding adipose tissue should be measured. Monitoring of temperatures in fat tissue is important to reduce the risk of skin burns and also when treating a margin around the tumor. Furthermore, a second problem related to the use of PRFS-based MRT for breast thermometry has been recently raised. This problem is the occurrence of temperature-induced susceptibility changes of fat, which can introduce significant errors in PRFS-based MR thermometry and may cause inaccurate temperature measurements in the fibroglandular breast tissue during MR-HIFU ablation [62]. An additional problem is caused by respiration. The fact that the air volume inside the lungs changes over the respiratory cycle gives rise to time-varying changes in the magnetic field inside the breasts that can cause considerable temperature errors in PRFS-based MR thermometry [63], [64]. As a result, despite the promise shown in studies over the past 15 years, breast HIFU remains unavailable to patients unlike other breast ablative procedures in the clinic.

In addition, thermometry only provides temperature elevation (or, thermal dose) but not the coagulation onset, which is most important for informing lesioning and reported to occur at distinct temperatures across organs or even within the same organ. The thermal dose for changing temperature exposure was calculated using the technique suggested by Sapareto and Dewey.

Numerical integration was used to calculate the time that would yield an equivalent thermal dose at a reference temperature for different temperature profiles, as given by

$$t_{43} = \sum_{t=0}^{t=final} R^{(43-T_t)}\Delta t \quad (2.3)$$

where t_{43} is the equivalent time at 43 °C, and Tt is the average temperature during Δt. The value of R was 0.25 for temperatures lower than 43 °C and 0.5 for temperatures higher than 43 °C. These values were chosen because they are the most common values measured [65]. However, studies have shown that different tissues respond differently to heat exposure requiring different thermal doses for ablation [66].

Therefore, elasticity-based HIFU monitoring aims at detecting and tracking the relative changes in tissue elasticity upon formation of thermal lesion have been developed and implemented. Magnetic resonance elastography (MRE) has shown to be capable of quantitatively estimating the differences in shear modulus between the HIFU lesion and the untreated tissue, indicating that the ablated regions were stiffer than the untreated ones [67]. In addition to MRE, many ultrasound-based elasticity imaging studies also investigated the Young's modulus of HIFU lesions for comparative analyses with mechanical testing. Past studies include, but are not limited to, elastography for HIFU treatment [68]–[75].

2.2.2 HMIgFUS

In prior work by our group, a theoretical framework of HMIgFUS was built, comprising a customized nonlinear wave propagation model, a finite-element (FE) analysis module and an image-formation model to assess the fundamental performance of HMIgFUS in detecting HIFU lesions based on the change in tissue apparent elasticity [76]. For a lesion-to-background Young's modulus ratio of 3, 6 and 9, the FE and estimated HMI displacement ratios were equal to 1.83,

3.69 and 5.39 and 1.65, 3.19 and 4.59, respectively. In addition, moderate agreement in lesion size growth was found in both simulations (16.2, 73.1 and 334.7 mm^2) and experiments (26.2, 94.2 and 206.2 mm^2). Therefore, the feasibility of HMIgFUS for HIFU lesion detection based on the underlying tissue elasticity changes was verified through the developed theoretical framework, i.e., validation of the fundamental performance of the HMIgFUS system for lesion detection, localization and quantification, was demonstrated both theoretically and *ex vivo*. HMIgFUS was performed to investigate both elastic and acoustics-independent viscoelastic tissue changes using the Harmonic Motion Imaging (HMI) displacement, axial compressive strain and change in relative phase shift during high energy HIFU treatment with tissue boiling [77], [78]. HMIgFUS had been applied in a transgenic breast cancer mouse model to monitor changes in mechanical properties of tissues during thermal therapy *in vivo* [79]. Results from two mice with eight lesions formed in each mouse (16 lesions total) showed that the average peak-to-peak displacement amplitude before and after lesion formation was respectively equal to 17.34 ± 1.34 μm and 10.98 ± 1.82 μm ($p < 0.001$). Cell death was also confirmed by hematoxylin and eosin (H&E) histology. HMIgFUS was also applied for abdominal tumor detection in a transgenic mouse model of pancreatic cancer [80], [81]. HMI monitoring of HIFU ablation found significant decrease in the peak-to-peak HMI displacements before and after HIFU ablation with a reduction rate ranging from 15.8% to 57.0%. The formation of thermal lesions after HIFU exposure was confirmed by histological analysis.

2.3 Overview and significance

The objective is to develop an integrated HMIgFUS system as a clinical monitoring technique for breast HIFU with the added capability of detecting tumors for treatment planning,

evaluation of tissue stiffness changes during HIFU ablation for treatment monitoring in real-time, and assessment of thermal lesion sizes after treatment evaluation. In achieving the goal, the HMIgFUS system for both imaging and real-time treatment monitoring will be developed and evaluated in *ex vivo* post-surgical breast tissue specimens. Finally, a clinical HMI system will be developed for initial feasibility testing in patients.

In order to develop, test and optimize and a HMIgFUS system for breast tumor characterization and ablation monitoring, there is a need to localize the HIFU focal spot within the tissue in the treatment planning stage. A real-time lesion formation monitoring method is also essential for treatment monitoring. *Ex vivo* study on human breast tumor is needed for feasibility test and system optimization before the clinical trial of HMI in patents. The dissertation is thus separated into five specific chapters: HIFU focal spot localization, real-time lesion quantification, HMI with electronic beam steering, HMIgFUS for *ex vivo* breast tumor characterization and treatment monitoring, clinical HMI initial results.

Chapter 3: HMI is capable of HIFU focal spot localization in 1D and 2D

The objective of this chapter is to develop and test the feasibility of using the HMIgFUS method to localize the focus of the HIFU beam. To our knowledge, this is the first radiation-force-based all-ultrasound elasticity imaging method designed for focal spot localization, which is also robust to temperature limit and motion artifact. In this chapter, both 1D and 2D HMI systems were used to assess the feasibility of focal spot localization on tissue-mimicking phantom, *in vitro* liver, and *ex vivo* human breast specimens. The focal spots detected by HMI were validated with gross histology.

Chapter 4: Real-time lesion quantification in HMIgFUS

The objective of this chapter is first to develop a HMIgFUS-based lesion quantification method to detect and quantify HIFU-induced thermal lesions. We have also demonstrated the accuracy as well as reproducibility of the lesion quantification method through gross pathology validation *in vitro* and *in vivo*. We have shown the implementation of a lesion quantification method for on-line processing by incorporating a GPU-based, sparse-matrix algorithm to achieve lesion development monitoring during HMIgFUS treatment in real time.

Chapter 5: Focused ultrasound steering for Harmonic Motion Imaging (HMI)

The objective of this chapter is to develop and demonstrate initial feasibility of electronic steering of focused ultrasound for HMI using a HIFU phased array to facilitate the scanning process. The main interest of the electronic steering compared to the mechanical movement arises from the dramatically shorter time required to move the focal spot. In this chapter, we have demonstrated that HMI can be used to image a 2.3 times larger region of interest without requiring physical movement of the transducer using the steered focused ultrasound beam. Using electronic steering for HMI can be used to shorten the total imaging duration without requiring physical movement of the transducer.

Chapter 6: HMIgFUS is capable of human breast tumor characterization and treatment monitoring *ex vivo*

The overall objective of this chapter is to investigate the potential complementary role of HMI, which can provide measurements of the locally generated mechanical responses and inherent

mechanical properties of breast tissues *ex vivo*. This chapter has demonstrated the initial feasibility of HMI and HMIgFUS on both small piece and large piece *ex vivo* human mastectomy specimens.

Chapter 7: Clinical HMI in patients

In this chapter, the goal is to develop and build a clinical HMI system with parallel beamforming and automatic rater scan using a robotic arm. The HMI clinical system consisted of 3 parts: 1) an ultrasound imaging research system with a designated host PC for system control, real-time display and data acquisition; 2) a FUS transducer and a phased array imaging probe for imaging and motion tracking; 3) a robotic arm for automatic raster scan. Finally, the optimized clinical HMI system has been developed for initial testing in human subjects.

CHAPTER 3. Harmonic Motion Imaging (HMI) for focused ultrasound focal spot localization

3.1 Introduction

Treatment planning constitutes one of the most critical aspects of HIFU treatment. Correct placement of HIFU beam and securing clear acoustic path to the target tissue is critical in order to avoid unnecessary thermal damage on normal tissues. The targeting step is essential because the apparent focal spot can be shifted from the geometric focus due to phase aberrations caused by tissue inhomogeneity [82]. To this end, many researchers have been developing techniques and methods for HIFU treatment planning. As of now, HIFU treatment planning and real-time monitoring are performed by two major imaging modalities, magnetic resonance imaging (MRI) and ultrasound imaging. During the planning stage of MR-guided focused ultrasound (MRgFUS) treatment, a small temperature increment is generated at the focal spot. MR thermometry is used to generate a quantitative temperature map of tissues and detects the focal spot with a small temperature elevation as low as 1˚C [83].MR acoustic radiation force imaging (MR-ARFI) has previously been proposed to locate the beam using tissue displacement map at low intensities to avoid heat deposition in the target during planning [84]–[86]. Despite its advantages, MRgFUS still relies on a high-cost hybrid system and has relatively low temporal resolution. Compared to MRI, ultrasound itself is a low-cost imaging modality offering several advantages, including high temporal resolution and lower compatibility requirements. Conventional B-mode has been found to be capable of detecting hyperechoic regions due to cavitation and/or boiling at the focus but these phenomena are by definition random and unreliable especially after HIFU cessation [87]. Ultrasound-based temperature mapping relies on the temperature dependence of the speed of

sound in tissues, which increases with temperature between 37˚C and 50˚C in non-fatty tissues [88]–[90]. However, the limitation of ultrasound-based temperature measurements lies in the fact that the linear relationship between the speed of sound and temperature is no longer valid at temperatures above 50˚C or higher. Based on RF data, Vaezy et al. aimed at targeting by monitoring the focal RF signal increase immediately and showed that the focal RF amplitude increased immediately after HIFU started at subablative intensities [91]. However, it may lose accuracy for *in vivo* application where motion disturbance is much more significant on a pixel-to-pixel basis.

Instead of estimating temperatures or quantification of the backscatter RF signals, Harmonic Motion Imaging guided Focused Ultrasound (HMIgFUS) monitors the localized displacement at the focus as an indicator of the HIFU focal zone placement. HMIgFUS is a dynamic, all-ultrasound based system for both ablation and imaging, which utilizes a HIFU transducer by emitting an amplitude-modulated (AM) beam to simultaneously thermally ablate and induce a stable oscillatory tissue displacement at its focal zone. The oscillatory response is then estimated by a cross-correlation-based motion tracking technique on the RF signal collected by a confocally-aligned diagnostic transducer. It is based on the radiation force to induce vibration at the focal zone for the detection of localized stiffness changes [92].

The main objective in this chapter is to study the feasibility of using the HMIgFUS method to localize the focus of the HIFU beam. To our knowledge, this is the first radiation force based all-ultrasound elastography method designed for focal spot localization, which is also robust to temperature limit and motion artifact. In this chapter, we will use a 1D and 2D based system to assess the feasibility of focal spot localization on phantom, *in vitro* liver, and *ex vivo* human breast

specimens. We expect HMIgFUS to detect the focal spots with verifications based on gross histology.

3.2 Methods

3.2.1 HIFU focal spot localization experimental materials

3.2.1.1 Tissue-mimicking phantom preparation

Phantom experiments were conducted to verify the efficacy of the proposed method. Gelatin powder (Gelatin 50 bloom, MP Biomedicals, Irvine, CA, USA) was used to construct the tissue mimicking phantoms. Three homogeneous phantoms with elastic modulus of 10 kPa were constructed. The concentration of gelatin powder was 50.7g/L yielding a stiffness of 10 kPa. Phantom preparation was completed using the following steps [93]: 1) gelatin powder was hydrated in a solution of deionized water and isopropanol and heated above its gelling point to disperse the colloid, clarify the solution, and release trapped gasses; 2) the mixture was then placed into an ice water bath for the purpose of cooling. While the gel solution is liquid, agar powder was added to increase the absorption and the scattering. Note that the agar melted only at temperatures higher than 80˚C; thus, it did not significantly contribute to the increase of the phantom stiffness. The mixture was constantly stirred until the temperature decreased to 25˚C; 3) and the solution was poured into a mold carefully and placed in a refrigerator overnight.

3.2.1.2 *In vitro* and *ex vivo* specimen preparation

Experiments were performed in 9 *in vitro* canine liver specimens on three to six different ablation locations (dependent on the size of the liver) within each specimen. Liver was chosen for the experiment because of its relatively homogenous structure and allowing lesions to be optical

contrast in gross pathology. Tissue samples were degassed in phosphate buffered saline (PBS) for 1 hour at room temperature prior to each experiment. In experiments, each specimen was immersed in degassed PBS and fixed on an acoustic absorber using metallic needles.

3.2.2 HIFU focal spot localization in 1D

The 1D HMI system was comprised of a 4.755-MHz HIFU transducer (Riverside Research Institute, New York, NY, USA) and a 7.5 MHz single-element transducer (Olympus NDT Inc., Waltham, MA, USA). The HIFU transducer (outer diameter = 80 mm, inner diameter = 16.5 mm, focal depth = 90 mm) was used to generate the acoustic force using a low frequency amplitude-modulated RF signal. The -6 dB pressure focal region has an ellipsoidal shape with 7.7 mm in the axial direction and 0.67 mm in the lateral direction. A function generator (33120A, Hewlett-Packard, Palo Alto, CA, USA) was used to generate a low frequency amplitude modulation waveform at 25 Hz. A second function generator (33220A, Agilent Technologies Inc., Santa Clara, CA, USA) was used to construct the continuous carrier signal at 4.755 MHz with 200% amplitude modulation using the input from the first function generator. The single-element transducer was driven by a pulser/receiver (5072PR, Olympus, Waltham, MA, USA) with a frame rate at 1000 Hz. RF signals within 10 cm from the transducer surface were recorded using a data acquisition unit (Gage applied, Lockport, IL) at a sampling frequency of 100 MHz. The received RF signals

from the pulser/receiver were filtered using an analog band-pass filter (Reactel Inc., Gaithersburg, Maryland, USA) with cutoff frequencies of fc1 = 5.84 MHz and fc2 = 8.66 MHz (Figure 3.1).

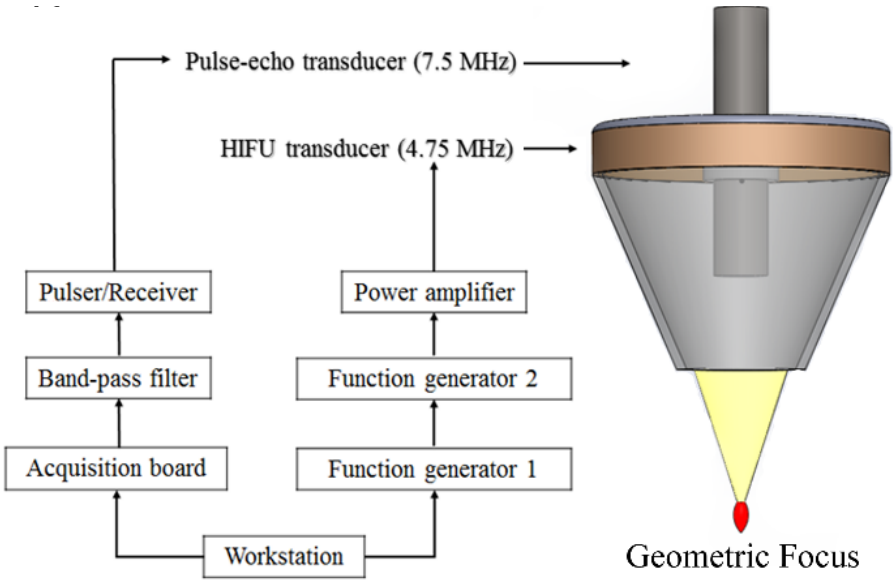

Figure 3.1 Schematic of the 1D HMI setup.

In this study, a short, continuous AM HIFU wave was used for localizing the focused ultrasound beam. A 1-s duration was sufficient to obtain stabilized HMI displacement while short enough to avoid significant temperature rise [76].

One-dimensional cross-correlation [94] of the consecutively acquired RF signals was applied on the acquired frames acquired at a frame rate of 1000 frames/s with a kernel size equal to 5 wavelengths of the imaging probe and 90% overlap to estimate incremental axial displacement as a result of oscillatory radiation force. Cross-correlation coefficient maps were also generated to determine the level of decorrelation noise, which is an indicator of the estimation accuracy. After low-pass filtering with a cutoff frequency at 100 Hz, the 50-Hz displacement was obtained, and a peak-to-peak displacement map could be generated across the axial direction. A maximum peak-to-peak displacement value was found across the axial direction. Based on the maximum peak-to-

peak displacement value, we calculated -3 dB and -6 dB displacement focal zone over the axial direction. The results allowed for monitoring of tissue displacement profile across targeting depth during both focal spot localization and HIFU ablation. The peak-to-peak displacement profiles were estimated across all imaging depths for all specimens and were plotted against imaging depth.

In HMI, the acoustic radiation force can be described by [95], [96]

$$\mathrm{F(t)} = \frac{2\alpha I(t)}{c} \tag{3.1}$$

where c is the speed of sound (1540 m/s in soft tissue), $I(t)$ (W/cm2) is the intensity and α (dB/cm/MHz) is the absorption coefficient of the tissue. Assuming the homogeneity within the specimen, the change in the radiation force F was thus only dependent on the intensity $I(t)$. Subsequentially, higher HMI displacement D is indicative of higher radiation force which induced vibration. Therefore, the amplitude of peak-to-peak HMI displacement is directly correlated with acoustic intensity in a homogenous phantom or tissue. Based on this relationship, the -3 dB and -6 dB focal zones were computed based on the maximum peak-to-peak displacement amplitude in the same trial. In *in vitro* liver experiments, 2-min tissue ablation was performed to generate lesion in the targeted area. Lesion locations were compared with corresponding focal spot localization results.

During ablation, the in situ acoustic intensity was equal to 4200 W/cm2 and the duration was equal to 120 s. Once a thermal lesion was generated, a post-ablative HMI was performed ($Isptp$ = 4200 W/cm2, duration = 1s) to obtain the stiffness contrast map. The midpoint of the lesion in histology was measured to represent the location of the lesions. The midpoint of the -3dB focal region was thus estimated to represent the focal spot localization method for comparison purposes.

3.2.3 HIFU focal spot localization in 2D

A 93-element, PZT-4 ceramic focused transducer (individual element diameter = 10 mm, overall out diameter = 110 mm, inner diameter = 41 mm, and focal depth=70 mm. H-178, Sonic Concepts Inc., Bothell, WA, USA) was used for HIFU. The HIFU center opening is designed to always locate the imaging array confocally. All HIFU channels were synchronously excited by a 25-Hz amplitude-modulated 4.5 MHz signal generated by a dual-channel waveform generator (33522A, Agilent Technologies Inc., Santa Clara, CA, USA). The -6dB focal region has an ellipsoid shape with 1.35 mm in the axial direction and 0.25 mm in the lateral direction. A 64-element phased array transducer (P4-2, ATL., Bothell, WA USA) with a center frequency at 2.5 MHz was confocally aligned with the HIFU transducer to transmit and receive through a 4-board VDAS system (V-1, Verasonics, Bothell, WA, USA) at a sampling frequency of 10 MHz (Figure 3.2).

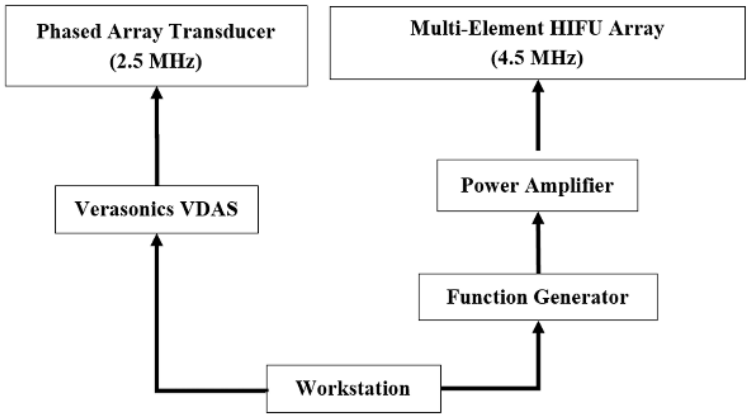

Figure 3.2 Flowchart of the 2D HMI setup.

In the 1D system, RF signals were directly acquired from the single-element transducer. While in the 2D system, graphical processing unit (GPU) was used to perform efficient beamforming [97]–[99]. The channel signals were acquired individually through the 64-channel

phased array probe through VDAS system using a custom flash plane wave transmits imaging sequence. A GPU-based algorithm was used to beamforming and upsampling the RF signal to 80MHz. The lateral resolution is 0.5 mm in obtained 2D HMI images. The acquired element data to the RF signals. The frame rate of both systems was 1000 frames/s.

To assess the capability of the method in the presence of aberration, an aberration layer [100], [101] was introduced between the HIFU transducer and the gel phantom. The aberration layer made of agar was placed above the gel phantom in order to create phase distortion within the incident HIFU beam. The incidence angle between the primary beam direction and the wedge-shaped aberration layer is 11°.

In order to assess the accuracy of the aforementioned focal spot localization method, it is idealistic to detect the apparent focal region by searching for the highest rate of temperature change as a comparison. Nevertheless, the thermocouple could not be used in this study in order to avoid imaging artifacts. Here, we propose an alternative approach to measure the apparent focal spot based on the relative change of monitoring displacement profiles during HIFU ablation across the imaging depth. That is, the location with earliest decreasing of displacement decrease is identified as the focal spot where the temperature rose fastest. From our previous work [92], the peak-to-peak amplitude of the HMI focal displacement first increases then decreases as tissue undergoes initial softening followed by stiffening during slow thermal ablation, which is the pattern of stiffness change under slow denaturation (Figure 3.2(B)). Assuming that the targeted *in vitro* liver tissue is homogeneous and the target region coagulates at the same temperature, then the time point at which the tissue starts to stiffen can indirectly indicate that the tissue has reached the temperature causing irreversible protein denaturation [67], [102]. In order to successfully find the peak in this variation, an envelope detection algorithm was applied across the 2-min long monitoring

displacement to detect the time-point at which the tissue started to undergo stiffening. The time to undergo stiffening was computed across all acquired depths. The depth with the shortest time to stiffening (TTS) was considered as the actual focal spot (AFS) since thermal dosage was delivered most at this depth.

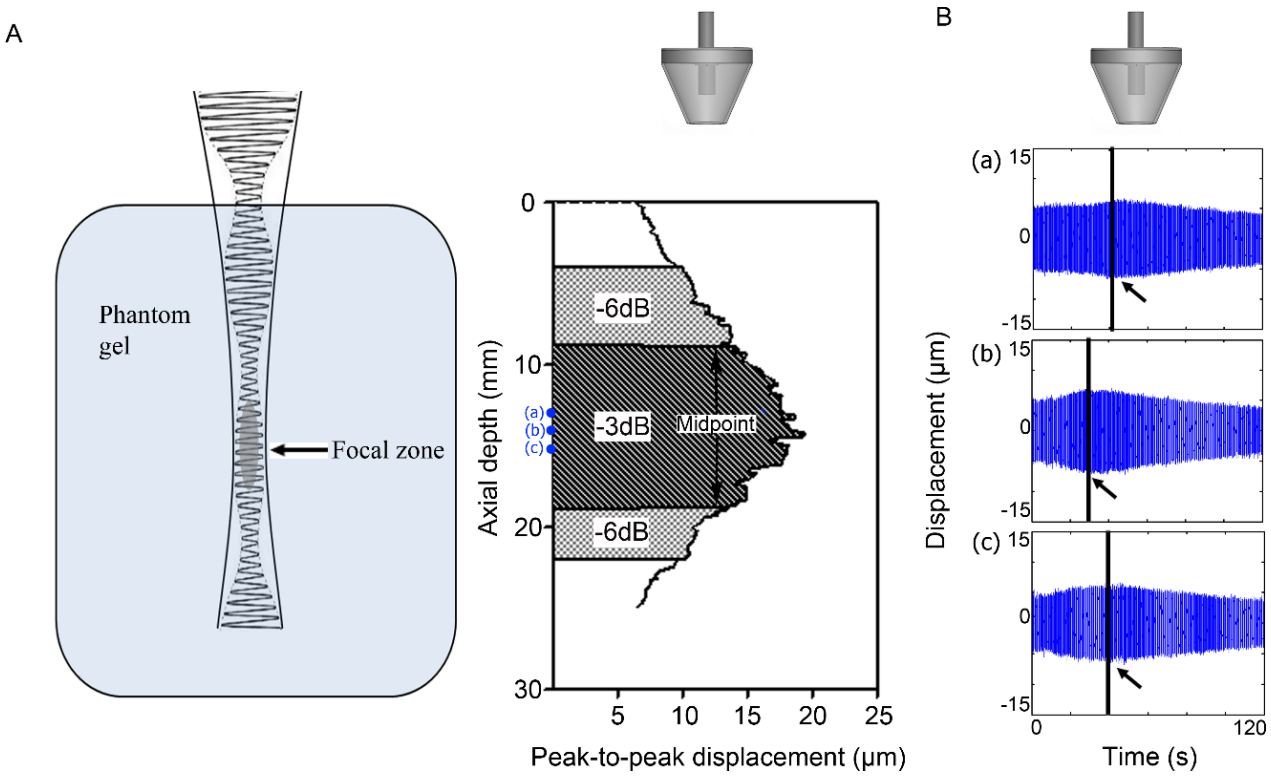

Figure 3.3 (A) Overview of the generation of oscillatory radiation force and an example of HMI peak-to-peak displacement recorded *in vitro* canine liver specimen. The -3dB and -6dB focal zone was computed based on the maximum peak-to-peak displacement amplitude. (B) HMI monitoring during 2-minute ablation at 3 depths (a), (b) and (c). The 3 depths are marked in (A).

3.3 Results

3.3.1 Experimental validation in 1D

3.3.1.1 1D HMI on phantoms

The intensity of the focused ultrasound beam was detectable by estimating the harmonic displacement in homogeneous gelatin phantoms. Figure 3.3(A) depicts an example of 1D peak-to-peak displacement profile along the axial direction in a gelatin phantom. The targeted region could be represented as the -3dB focal zone. Figure 3.3(B) shows the representative 2-min HMI displacement of 3 depths (a), (b) and (c) within the focal region. The displacement at all three depths initially increased then decreased as tissue underwent initial softening followed by stiffening during slow thermal ablation. The time point at which the tissue started to stiffen is marked with a black line and arrow. The time taken to reach this time point was computed as the time to stiffening (TTS).

3.3.1.2 1D HMI on *in vit*ro liver specimens

An example of HMI displacement image of an *in vitro* canine liver specimen using the 1D system before and after ablation is shown in Figure 3. The -3dB and -6dB focal zone was estimated based on the 1-s HMI before ablation. A post-ablative HMI was recorded after 2-min ablation monitoring. The peak-to-peak displacement contrast was capable of delineating the lesion generated when compared against gross pathology. The midpoint of the lesion in pathology on the right panel was measured to represent the location of the lesion.

Linear regression was performed in nine thermal lesions in order to establish the relationship between the focal spot location identified with HMI and the shortest TTS location. The R^2 value from the statistical regression analysis equals to 0.879 and $p<0.0002$. The slope of

the best-fit line is 0.930 ± 0.155 with a 95% confidence interval of 0.562 to 1.298. Another linear regression was performed on those lesions between the location of focal regions from focal spot localization and the location of true physical lesions from histology. The R^2 value from the statistical regression analysis is 0.638 and $p<0.001$ as shown in Figure 4. The slope of the best-fit line is 0.743 ± 0.212 with a 95% confidence interval of 0.242 to 1.243.

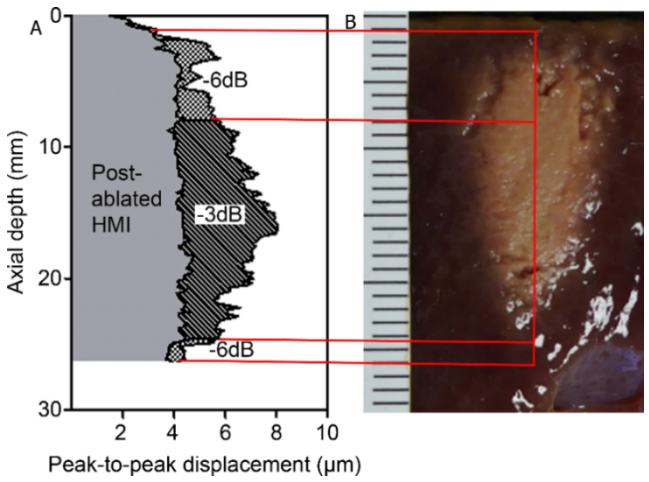

Figure 3.4 1D HMI displacement image of an *in vitro* canine liver specimen before and after ablation. The -3dB and -6dB focal zone was estimated based on the maximum peak-to-peak displacement amplitude. A post-ablative HMI was recorded after 2-min ablation. The peak-to-peak displacement contrast could indicate the lesion generated when comparing with the transverse section in gross pathology on (B). The red lines are indicating the corresponding -3dB and -6dB regions in gross pathology.

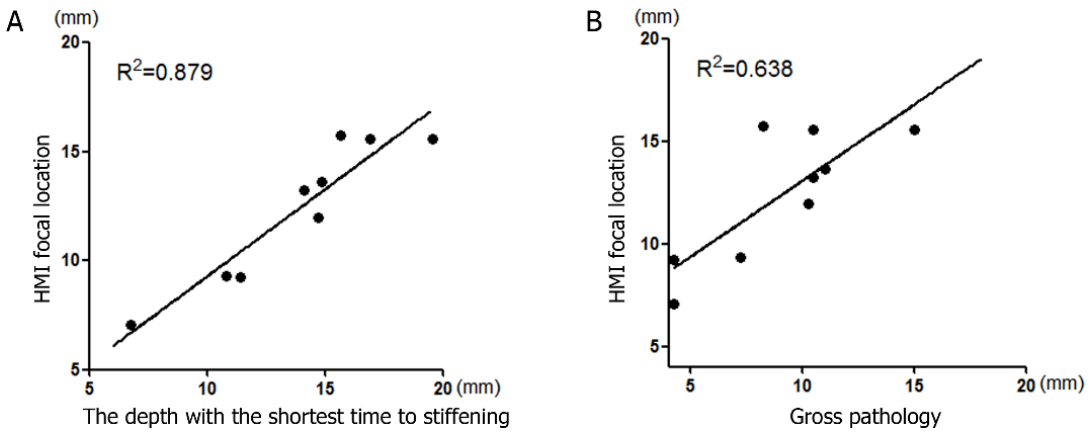

Figure 3.5 Verification of focal spot localization results. (A) Comparison between the midpoint of -3dB focal zone computed from focal spot localization with the location of the corresponding shortest TTS points. The R^2 value from the statistical regression analysis is 0.879 for the 9 data points used in this study. The corresponding p value is <0.0002. (B) Comparison between the midpoint of -3 dB focal zone computed from focal spot localization with midpoint of lesion from gross pathology. The R^2 value from the statistical regression analysis is 0.638 for the 9 data points used in this study. The corresponding p value is < 0.001.

3.3.2 Experimental validation in 2D

3.3.2.1 2D HMI on phantoms and *in vitro* liver specimens

Figure 3.6(A)-(C) shows the estimated focal region using the HMI-based focal spot localization method overlaid onto the B-mode image of gelatin phantoms. The yellow region represents the -6dB focal region, and the red region represents the -3dB focal region. The transducer was moved across various lateral and axial locations within the phantom. In Figure 3.7, the aberration layer is delineated by the blue dash line. The red region represents the -3dB focal region without the aberration layer, and the blue region represents the -3dB focal region with the aberration layer. A shift of the focal spot due to aberration was detected. The axial movement of

the focal spot was within the range of 66.3 to 69.8 and 65.9 mm to 69.7 mm in phantom and liver respectively. Figure 3.8 shows the estimated focal region using the HMI focal spot in *in vitro* liver specimens. In Figure 3.9, linear regression was performed in eight lesions in order to establish the relationship between the location of focal regions from focal spot localization and the location of the corresponding shortest TTS points. The R^2 value from the statistical regression analysis is 0.869 and $p < 0.001$. The slope of the best-fit line is 1.079 ± 0.171 with a 95% confidence interval of 0.661 to 1.498. Another linear regression was performed in those lesions between the location of the focal regions predicted by HMI and the true location of the lesions from histology. The R^2 value is 0.821 at $p < 0.002$. The slope of the best-fit line is 1.415 ± 0.269 with a 95% confidence interval of 0.756 to 2.074.

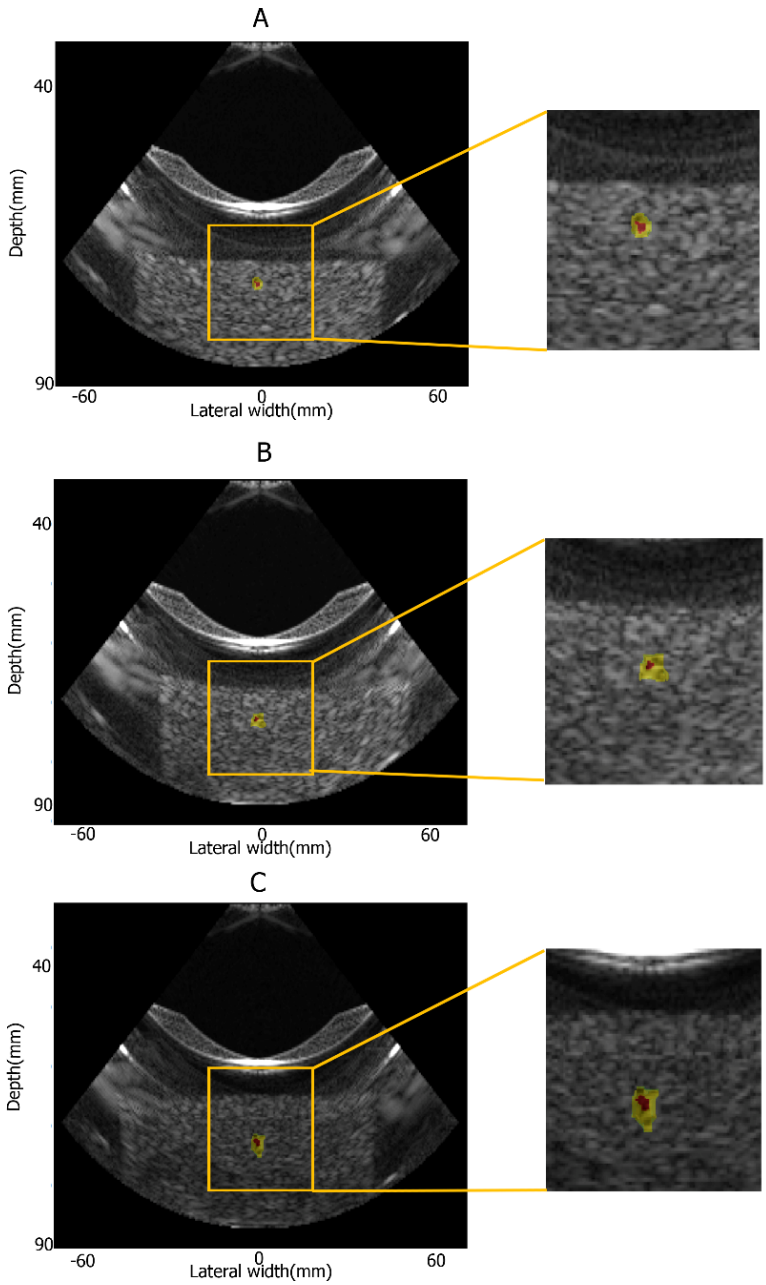

Figure 3.6 Focal spot localization application on phantom in 2D HMI system. The focal region from focal spot localization method was overlaid to the B mode image in (A) (B) and (C): the yellow region represents the -6dB focal region, and the red region represents the -3dB focal region.

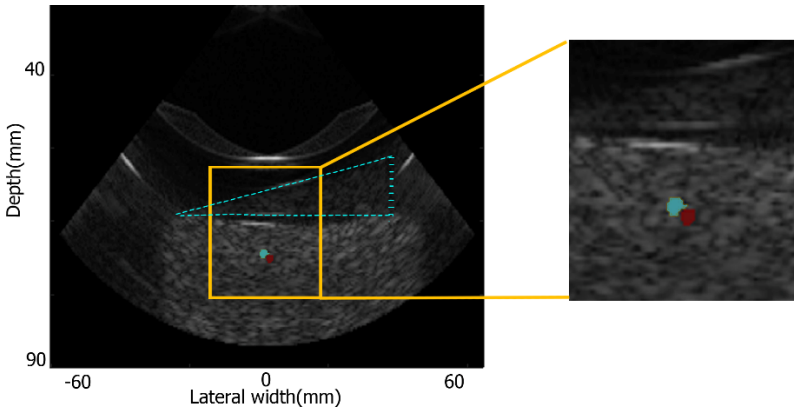

Figure 3.8 Focal spot localization application on phantom in 2D HMI system. The aberration layer is delineated with blue dash line. The red region represents the -3dB focal region without the aberration layer, and the blue region represents the -3dB focal region with the aberration layer.

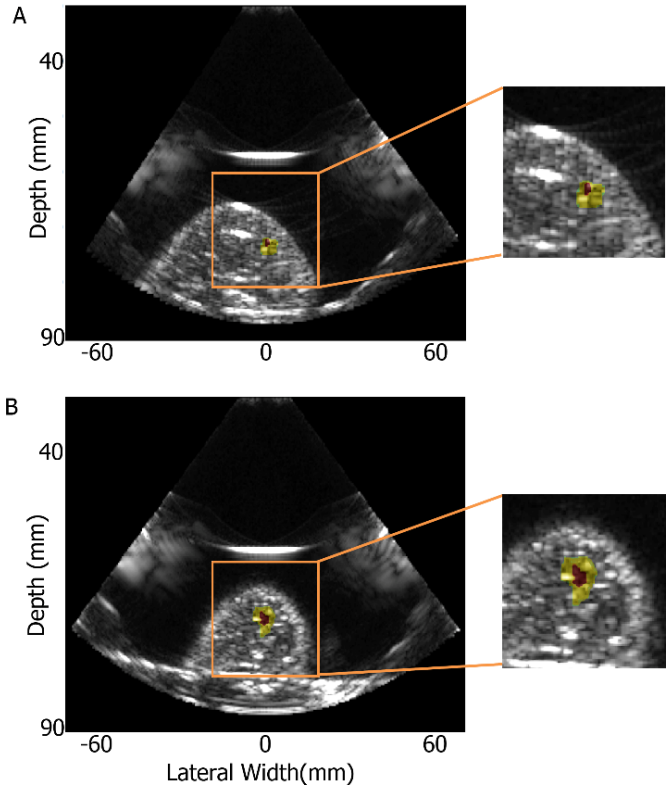

Figure 3.7 Focal spot localization application on *in vitro* liver in 2D HMI system. The focal region of the focal spot localization method was overlaid on the B mode image: the yellow region represents the -6dB focal region, and the red region represents the -3dB focal region.

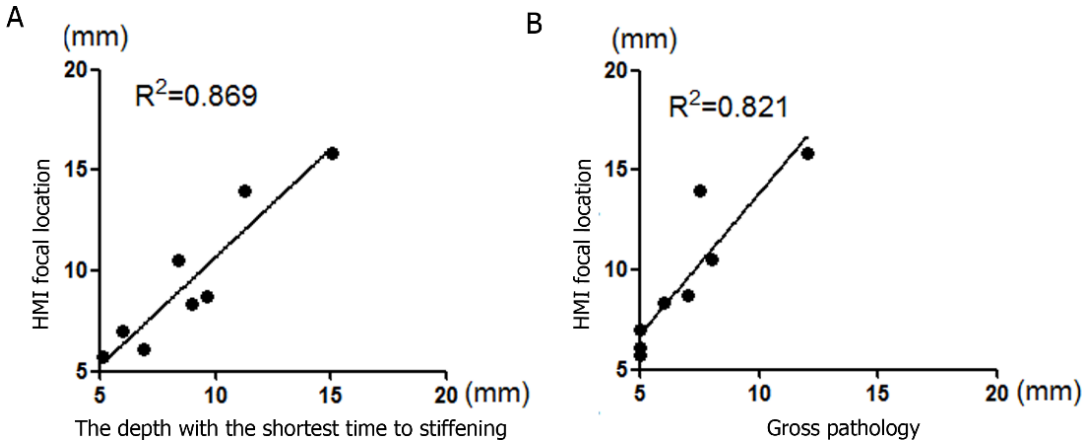

Figure 3.9 Verification of focal spot localization results in 2D HMI system. (A) Comparison between the midpoint of -3dB focal zone computed from focal spot localization with the location of the corresponding shortest TTS points. The R^2 value from the statistical regression analysis is 0.869 for the 8 data points used in this study. The corresponding p value is < 0.001. (B) Comparison between the midpoint of -3dB focal zone computed from focal spot localization with midpoint of lesion from gross pathology. The R^2 value from the statistical regression analysis is 0.821for the 8 data points used in this study. The corresponding p value is < 0.002.

3.3.2.2 2D HMI on *ex vivo* human breast tumor specimens

A representative application of the estimated focal region using the HMI focal spot in *ex vivo* human breast specimens is shown in Figure 3.10: (A) normal breast tissue and (B) IDC. The focal region of the focal spot localization method was overlaid on the B mode image: the yellow region represents the -6dB focal region, and the red region represents the -3dB focal region.

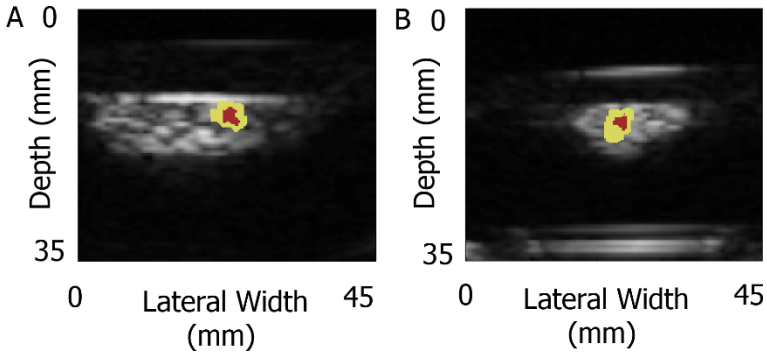

Figure 3.10 Focal spot localization application on *ex vivo* human breast tissue in 2D HMI system: (A) normal breast tissue and (B) IDC. The focal region from focal spot localization method was overlaid on the B mode image: the yellow region represents the -6dB focal region, and the red region represents the -3dB focal region.

3.4 Discussion

Several ultrasound-based imaging modalities have been proposed for image guidance and monitoring of HIFU surgery. However, accurate localization and characterization of the effective region of treatment in real-time remain as the obstacles in the clinical implementation of HIFU ablation. In this study, we investigated on an important challenge for focused ultrasound treatment planning, i.e. the visualization of the focal region prior to treatment. In this study, a focal spot localization method was developed with a radiation-force-based technique of HMI based on both 1D and 2D systems. The capability of HMI to simultaneously generate oscillatory radiation force and monitor the induced local displacement at the focus are considered unique advantages. Minimal interference between high power FUS and diagnostic beams is achieved by performing analog and digital filtering, thus phantom/tissue displacements can be accurately estimated using the filtered RF signals.

The method presented herein was also shown to be efficient requiring under 1s for data acquisition. Based on previous thermometry studies, a one second excitation under 25 Hz modulation frequency consisted of 50 oscillation cycles was used to reliably obtain steady-state HMI displacement while avoiding any significant temperature rise [78]. It is noteworthy that despite the speed of sound can vary with temperature, the offset caused by the speed of sound change could be filtered out as DC component from the oscillation in the focal spot localization process.

The midpoint of the -3dB focal region was thus estimated to represent the focal spot. The midpoint of the -6dB focal region was also estimated but tend to be less accurate because the -6dB focal region is bigger than the -3dB on which could have introduced noise in the focal spot estimation. We have shown that the region with the highest heating rate is also the region with the shortest time to stiffening. This was in agreement with its predicted focal spot by HMI in Figure 3.7(A). However, Figure 3.7(B) shows a slight discrepancy between our method and gross pathology in the evaluation of the location of the lesion in this study. The lesions measured by gross pathology tend to be closer to the transducer by an average difference of 2.59 mm than the locations estimated by HMI. The discrepancy can be due mainly to the heat diffusion of HIFU-induced lesions. It is known that the geometry of the lesion axial cross section may not be ideal ellipsoidal shape but a tadpole lesion with centroids displaced from the focus toward the transducer [103]–[105]. It is likely that the discrepancy between the gross pathology location and the HMI location is due to the tadpole-shaped lesions that have grown towards the transducer. This is consistent with the linear regression results in Figure 3.5(B) where the axial midpoint of lesions tends to be closer to the tissue surface than the estimated focuses. A single expert was used for manual segmentation of the lesion. The manually segmented lesion on the pathology may have

also introduced discrepancies. In 2D HMI, the axial and lateral resolutions were 0.087 mm and 0.3 mm respectively. In lesion measurement, although the boundaries of the lesions have sharp contrast from the surrounding normal tissue, the physical measurement was on 0.1 mm scale.

Despite our successful implementation on both 1D and 2D HMI platforms, there are several limitations. One limitation of this study is the absence of temperature measurement during HIFU treatment. The placement of a thermocouple within the tumor typically generates additional heat accumulation due to the beam interference with the thermocouple. This would influence the associated displacement estimation. Hence, simultaneous temperature measurement was excluded in this study. However, a location with shortest TTS, which may suggest quickest coagulation, was considered as the focal spot in the axial direction. Furthermore, although off-line processing was used in this study, the 2D HMI system has the fundamental capability of on-line monitoring.

3.5 Conclusions and Summary

A new HIFU treatment planning method was described that used oscillatory radiation force induced displacement amplitude variations to detect the HIFU focal spot before lesioning. This method was applied on tissue-mimicking phantoms and *in vitro* tissues with both the 1D and 2D HMI systems. Using this method, we were able to visualize the HMIgFUS focal region at variable depths. By comparing the estimated displacement profiles with AFS point and with lesion locations in pathology, we demonstrated the feasibility of using this HMI-based technique to localize the HIFU focal spot and predict lesion location during the planning phase. The same application feasibilities were also demonstrated in a 2D preclinical system. We concluded that HMI has the potential of providing the capability for HIFU planning.

CHAPTER 4. Real-time lesion quantification in Harmonic Motion Imaging guided Focused Ultrasound (HMIgFUS)

4.1 Introduction

There are several techniques currently being investigated to detect real-time treatment performance of HIFU. Magnetic resonance imaging (MRI) thermometry [106], [107] is used to detect temperature rise across the treatment area. However, MRI guidance can be expensive and time consuming compared to ultrasound-based HIFU guidance; the temporal resolution for this clinical applications is usually between 2 and 6 s [36]. Among the ultrasound guidance techniques, conventional B-mode-based 'hyperecho' tracking is not robust for HIFU monitoring as it is sensitive to air bubbles, which occur at high temperatures and usually lead to over-treatment of the targeted region [108], [109]. Passive acoustic mapping (PAM) has also been investigated regarding it capability of monitoring HIFU ablation by reconstructing the emissions generated by inertially cavitating bubbles during HIFU. However, the estimates of cavitation location and intensity are also prone to errors due to the limited axial resolution [110], [111].

Over the past two decades, ultrasound elasticity imaging has expanded from diagnostic technique to include therapy guidance and monitoring based on tissue stiffness change [71], [73], [112]. Compared to bubble- or cavitation-based methods, elasticity imaging does not rely on, or is affected by, boiling air bubbles formed at the focus but monitors the change in the tissue characteristics. However, most elasticity imaging techniques require HIFU to be interrupted for reliable monitoring, and therefore cannot detect the onset of lesion formation in real time, significantly increasing the treatment duration and cumulatively reduces the efficiency of a HIFU treatment.

Harmonic Motion Imaging (HMI) is a radiation-force-based ultrasound elasticity imaging technique which is designed for both tissue relative stiffness imaging and reliable HIFU treatment monitoring. An amplitude-modulated (AM) HIFU beam is transmitted through a focused ultrasound (FUS) transducer to induce tissue vibration at the focal region. The oscillatory response from the tissue can be tracked using radio-frequency (RF) signals acquired with a confocally-aligned imaging transducer [49], [92]. The oscillatory displacement amplitude, namely HMI displacement, is monitored continuously to provide real-time tissue stiffness change during the treatment. Without interrupting the ablative procedure, Harmonic Motion Imaging guided Focused Ultrasound (HMIgFUS) can be applied with optimal efficiency to the targeted area. Several studies have been published showing feasibility of HMI in post-surgical human breast tissue [113], *ex vivo* canine liver [78], [114] and *in vivo* mice [80], [81]. A fast imaging and processing algorithm is essential to ensure real-time lesion mapping. Recently, HMI was shown capable of streaming HMI displacement in real time at 15 frames per second [115]. Although the oscillatory HMI displacement contains important information on tissue stiffness change, it does not provide information on the lesion location or lesion size itself in real time. A fast lesion mapping method that can inform physicians intuitively on the progression of thermal lesioning in real time without sacrificing the frame rate is thus wanted.

Our objective in this chapter is first to develop a HMIgFUS-based lesion quantification method to map and quantify HIFU-induced thermal lesions. We also aimed at demonstrating the accuracy as well as reproducibility of the lesion quantification method through gross pathology validation *in vitro* and *in vivo*. Finally, we aimed at implementing a fast lesion mapping method for online processing to achieve lesion formation monitoring during HMIgFUS treatment in real time.

4.2 Methods

4.2.1 Development of lesion quantification method

In HMI, the oscillatory displacement is monitored continuously through a phased array imaging transducer. The changes in estimated displacement amplitude can be used to indicate the relative stiffness change when the lesion is starting to form at the focal region.

Figure 4.1 shows an illustration of the experiment setup. The HMIgFUS system consisted of a FUS transducer and a phased array imaging probe confocally-aligned through the central opening (diameter = 41 mm) of the FUS transducer. The FUS transducer was a 93-element phased array (f_c= 4.5 MHz, and D = 70 mm, Sonic Concepts Inc., Bothell WA, USA). The imaging probe was a 64-element phased array (f_c = 2.5 MHz, P4-2, ATL/Philips, Bothell, WA, USA). A dual-channel arbitrary waveform generator (AT33522A, Agilent Technologies Inc. Santa Clara, CA, USA) was used to generate an AM sinusoidal signal to drive the FUS transducer through a 50-dB power amplifier (325LA, E&I, Rochester, NY, USA). The imaging probe was inserted through the central opening and confocally aligned with the FUS transducer. The imaging probe was transmitting and receive through an ultrasound imaging research system (Vantage, Verasonics, Bothell, WA, USA) with a pulse repetition frequency (PRF) at 1000 Hz. The FUS total output acoustic power was within the range of 6.4 - 8.6 W from radiation force balance measurements [116]. A T-type bare wire thermocouple with a diameter of 80 μm (Physitemp Instruments Inc., Clifton, NJ, USA) was inserted into the tissue and aligned with the focal spot for temperature monitoring at the focal region.

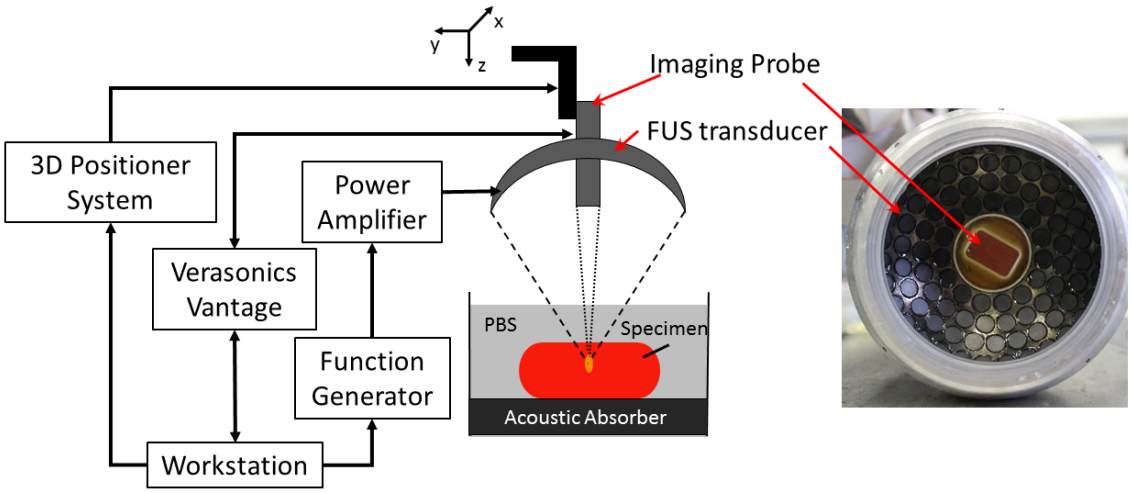

Figure 4.1 HMIgFUS experimental setup and transducers.

During real-time HMIgFUS, the RF channel data was acquired at a PRF of 1000 frames/s. In order to calculate the peak-to-peak HMI displacement without sacrificing the display frame rate, only 10 consecutive frames within a single HMI vibration were obtained at each acquisition and transferred to a host computer. The RF channel data matrix was placed into a GPU matrix within Matlab and multiplied by a beamforming sparse matrix to get the beamformed RF data [99], [115]. A 1D cross-correlation method [94] was used to estimate the incremental axial displacement between 2 consecutive RF frames. HMI peak-to-peak displacement maps were calculated over each of the 10 frames of HMI displacement maps by subtracting the minimum displacement from the maximum displacement on each pixel. When the processing is finished, another 10 frames will be acquired for processing. The peak-to-peak HMI displacement map averaged over the first 1s of treatment served as a reference map. The HMI lesion map was generated by subtracting the

reference HMI image from the current HMI peak-to-peak displacement map (Figure 4.2) to be displayed on computer screen (Figure 4.3).

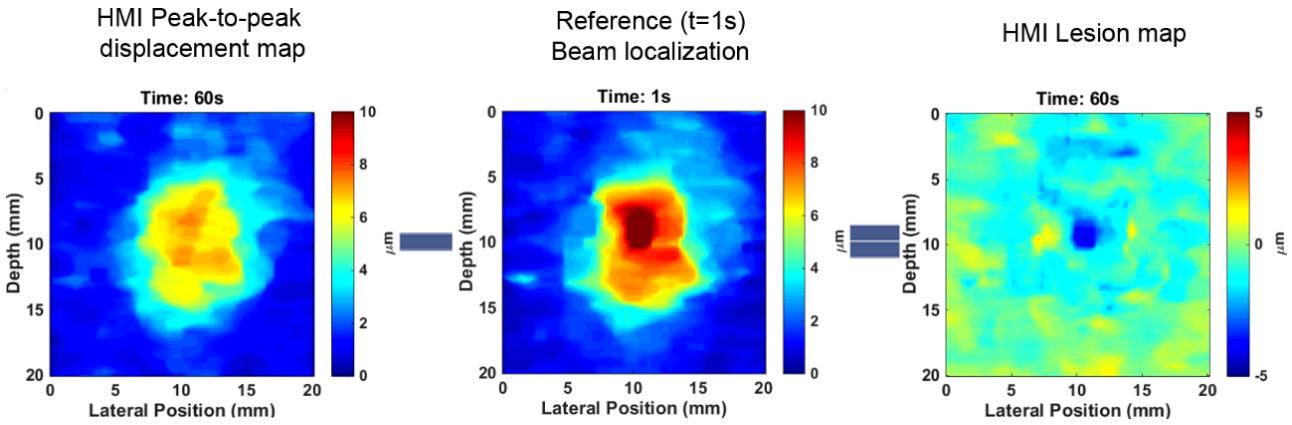

Figure 4.2 Schematic of HMI lesion map generation.

Six *in vitro* canine liver specimens were used for this study as they are relatively homogeneous, allowing easy optical delineation of the lesions in gross pathology. Liver specimens were prepared and degassed for 2 hours before each experiment. After ablation, each liver specimen was carefully sectioned at the imaging plane under the guidance of B-mode for gross pathology. The lesion area was delineated based on the color change in tissue. The depth, width and area of the lesions measured on gross pathology were compared with HMI lesion mapping. We tested 0 dB, -1.5 dB, -3 dB and -6 dB thresholding. We then chose to set a -3 dB or 30% displacement decrease as the threshold to discriminate the ablated from unablated tissue as it yields the best correlation with gross pathology. The largest region closest to the geometric focus was identified as the lesion.

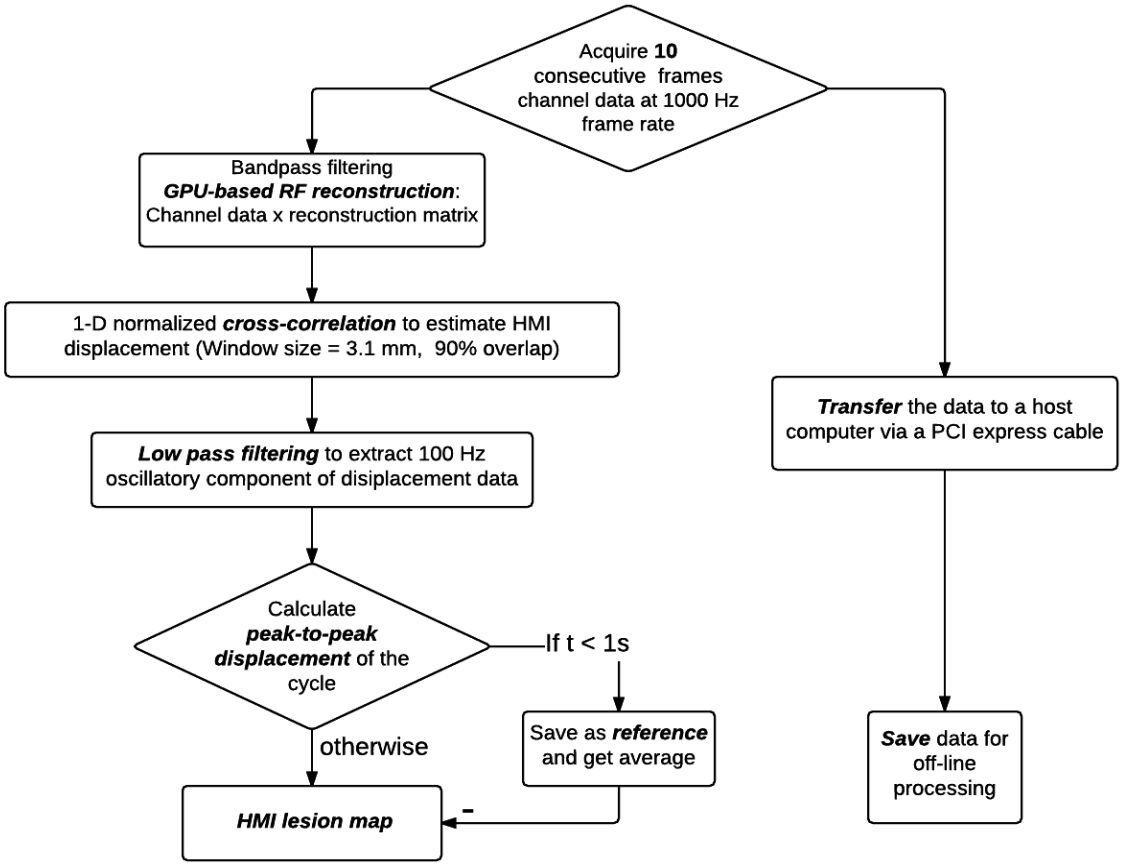

Figure 4.3 Flowchart of real-time HMI reconstruction algorithm.

4.2.2 *In vivo* implementation of lesion quantification

The animal experiment protocol was approved by the Institutional Animal Care and Use Committee (IACUC) of the Columbia University. The transgenic mouse model (K-rasLSL.G12D/+; p53R172H/+; PdxCre (KPC)) [117], [118] was used to develop pancreatic tumor which is pathophysiologically resembling human pancreatic ductal adenocarcinoma (PDA). One KPC mouse was used for this study. The mouse was laying supine under isoflurane anesthesia with it abdomen shaved and covered with ultrasound gel, with a degassed water tank on top to be coupled for ultrasound imaging. To precisely locate the pancreas, an 18.5-MHz diagnostic probe

(L22-14v, Verasonics, Bothell, WA, USA) was used in the planning stage providing high resolution B-mode images to locate and differentiate organs. By aligning the HMI imaging plane with the high-resolution B-mode images, the HMI images are spatially registered with the B-mode images. In the treatment monitoring stage, the center imaging probe of HMIgFUS was replaced with a 104-element phased array (f_c = 7.8 MHz, P12-5, ATL/Philips, Bothell, WA, USA) for higher resolution more adapted to small animals. The treatment power on the tumor was 6.4 W with 60 s duration.

The mouse was immediately sacrificed after the previously described procedure. Because gross pathology was incapable of distinguishing the ablated lesion from the pancreatic tumor, the whole pancreas along with the tumor was harvested for histological evaluation. The excised tissue was first fixed in 4% paraformaldehyde. After post-fixation processing, tissue was embedded in paraffin, sectioned, and stained with hematoxylin and eosin (H&E). Bright field microscopy images were acquired and evaluated by a trained expert.

4.3 Results

4.3.1 Real-time HMIgFUS ablation monitoring

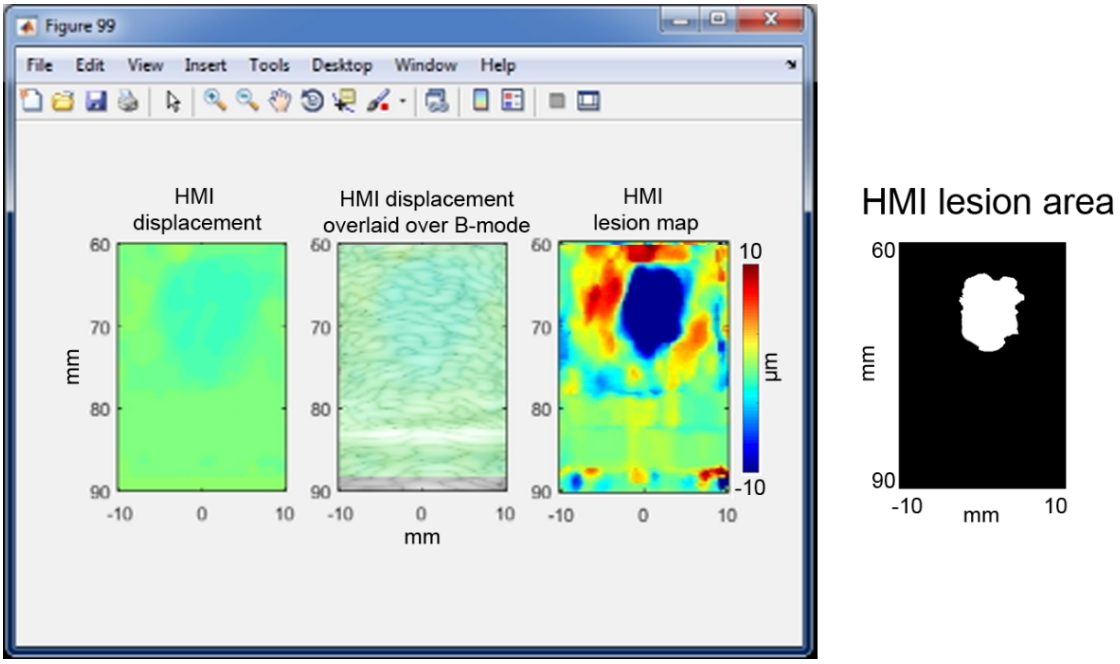

Figure 4.4 Real-time HMI displacements. A computer screenshot is shown with the left panel showing real-time HMI displacements. The middle panel shows the filtered HMI displacements overlaid on the B-mode image. A HMI lesion map (right) is shown in the right panel with blue denoting lesion. Corresponding HMI lesion area after -3 dB thresholding is shown on the right side.

The fast lesion mapping of HMIgFUS can stream the HMI displacement, HMI displacement overlaid on B-mode and HMI lesion map to the computer screen (Figure 4.4) at an average frame rate of 2.4 Hz. In the HMI displacement map, positive displacement is towards the transducer and negative displacement is away from the transducer

4.3.2 *In vitro* experimental validation

In order to prove the reproducibility of the technique, we have generated 13 lesions with HMIgFUS using different acoustic powers (6.4 W and 8.6 W) with different treatment durations varying from 90s to 120s. The lesions were detected and visualized at 2.4 Hz.

Figure 4.5 shows a representative case of HMIgFUS lesion monitoring over 90s ablation. Yellow indicates HMI peak-to-peak displacement amplitude increase (softening) and blue indicates HMI peak-to-peak displacement amplitude decrease (stiffening). No lesioning was found by HMI until 50s into the treatment when a dark blue spot was detected at the focal spot region (Figure 4.5(a)) indicating tissue stiffening. The lesion was found to grow during ablation, which is also quantified in Figure 4.5(d) showing that the lesion size increased after 50s. When temperature rises above a certain threshold, liver tissue undergoes irreversible stiffening change, which is caused by protein denaturation. According to established studies [58], [119], [120], 58–60°C is the conventional "threshold" for the formation of HIFU lesions in the liver. The temporal temperature profile (Figure 4.5(e)) was obtained showing the temperature at the focal spot reaching the threshold of 60°C at 30s (denoted with red line). Normalized HMI displacement within the focal region (Chapter 3) was plotted against the temperature clearly showing the displacement change with temperature increase. A gross pathological cross section of the lesion was shown in Figure 4.5(b) for comparison with the final HMI lesion map Figure 4.5(c).

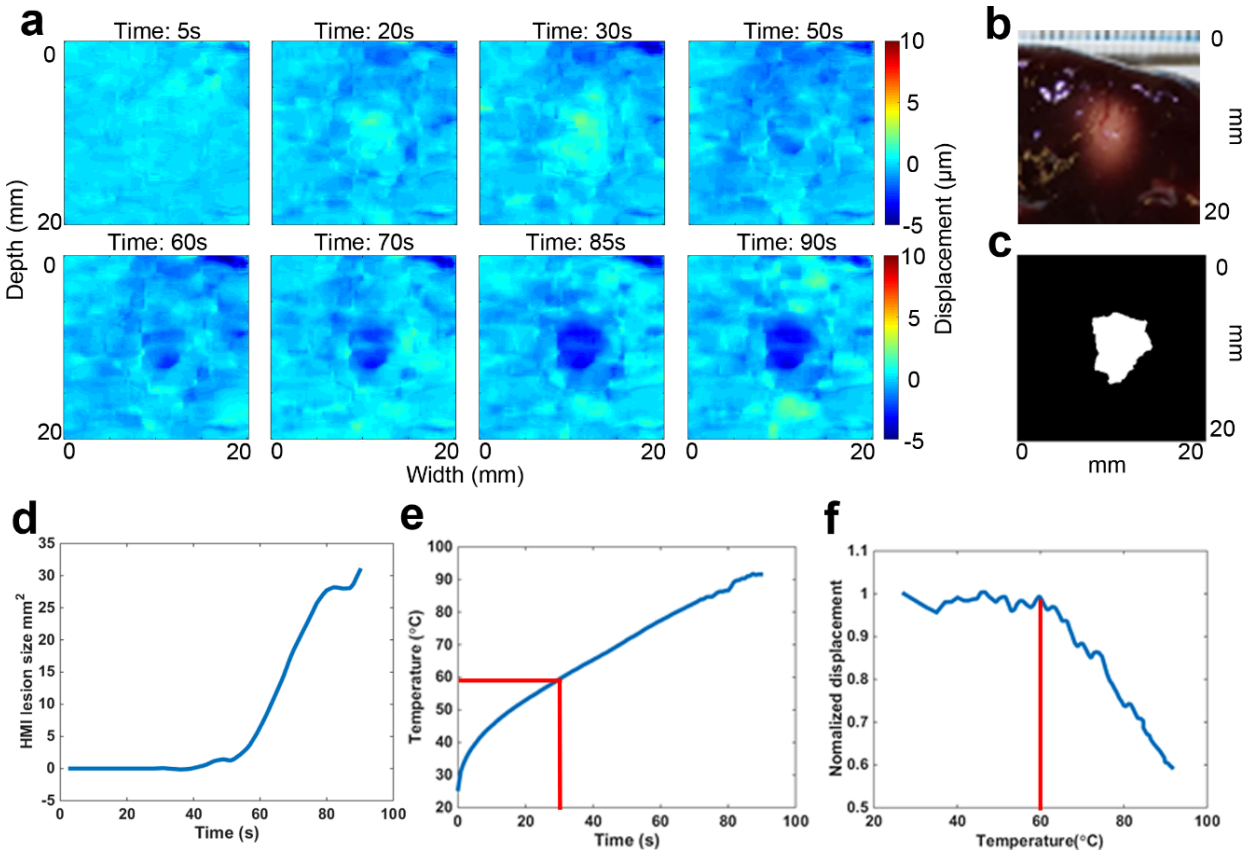

Figure 4.5 Example case of HMIgFUS lesion monitoring on 90s ablation. Lesion developing overtime is shown in (a) with blue indicating the formation of the lesion. Gross pathology of the lesion (b) is shown along with the HMI lesion map at the end of ablation (c). (d) HMI lesion size development overtime. (e) Temperature measurement from thermocouple. (f) HMI displacement change during the ablation.

Figure 4.6 is another representative case of 120s HMIgFUS lesion monitoring. Lesioning was detected by HMI after 40s of sonication with a decrease in displacement at the focal spot indicating tissue stiffening (Figure 4.6(a)). Lesion growth during ablation is also quantified in Figure 4.6(d) showing that the lesion size increased after 50s. The temperature profile over time

(Figure 4.6(e)) showed that the temperature at the focal spot reached the 60°C threshold at 30s (denoted with red line). Normalized HMI displacement within the focal region was also plotted against temperature clearly showing the displacement change with temperature. A gross pathological cross-section of the lesion was shown in Figure 4.6(b) in comparison with the HMI final lesion map Figure 4.6(c).

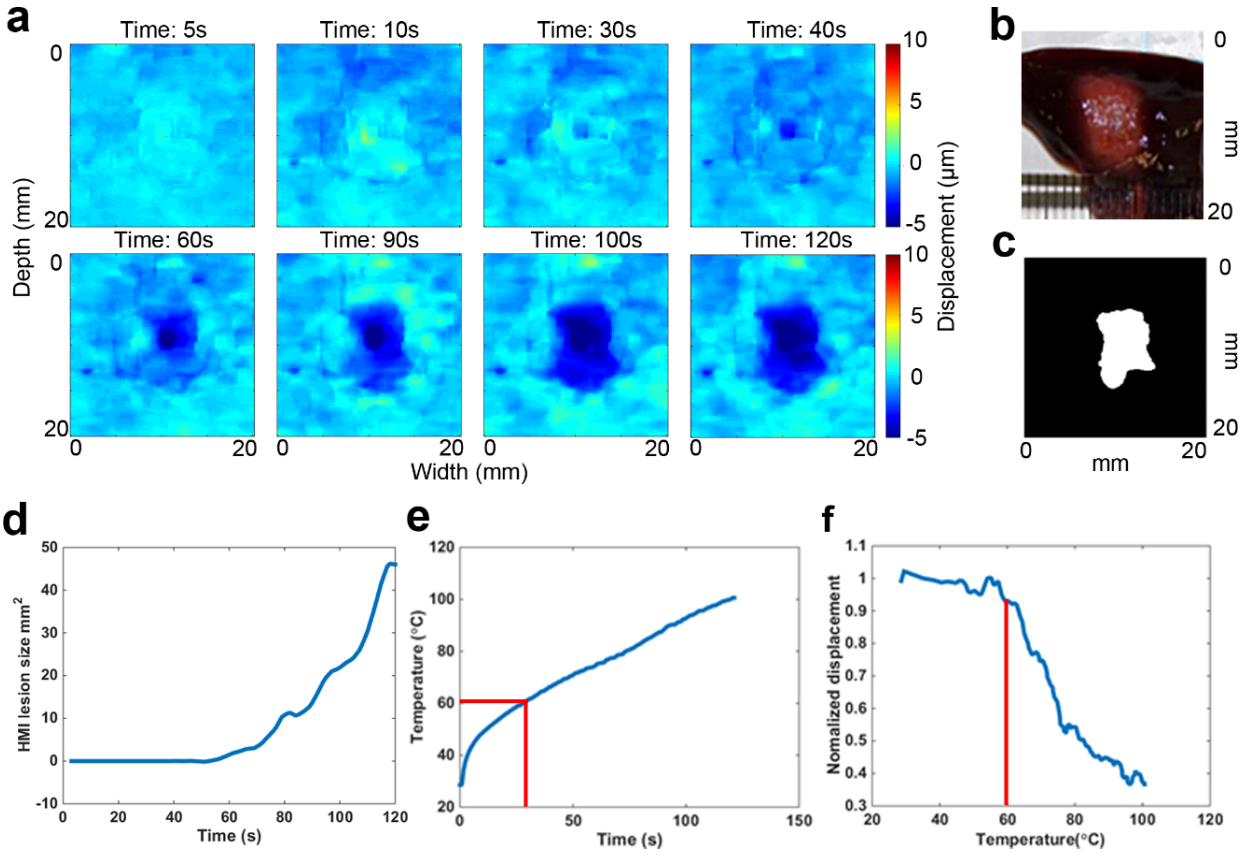

Figure 4.6 Example case of HMIgFUS lesion monitoring on 120s ablation. Lesion developing overtime is shown in (a) with blue indicating the formation of the lesion. Gross pathology of the lesion (b) is shown along with the HMI lesion map at the end of ablation (c). (d) HMI lesion size development overtime. (e) Temperature measurement from thermocouple. (f) HMI displacement change during the ablation.

Statistical analysis was performed with linear regression in 13 HMIgFUS-induced lesions to compare the lesion dimension identified with HMI and gross pathology. The R^2 value from the linear regression analysis equal to 0.81 and 0.85 in depth and width. The linear regression performed in the lesion area gives a R^2 equals to 0.75 (Figure 4.7).

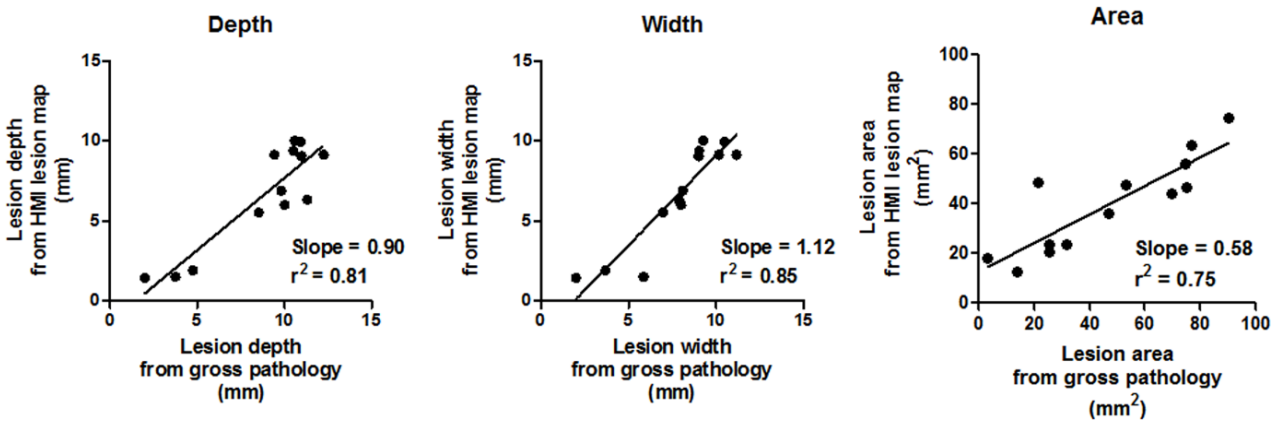

Figure 4.7 Lesion dimension comparison between gross pathology and HMI lesion map in depth (left), width (middle) and area (right).

In HIFU clinical applications, multiple-lesion ablations are often needed to treat the entire target region. When a few lesions come close together, the lesions generated later start to merge into those created before. An example of a three-lesion HMIgFUS case was shown in Figure 4.8. The three lesions are 3 mm apart at the same ablation power and duration starting from location 1 and then moving towards the right to locations 2 and 3 (Figure 4.8(a)). Same lesion quantification protocol was used in each location. After combining lesion maps from 3 locations, a final combined HMI lesion map was obtained in Figure 4.8(d).

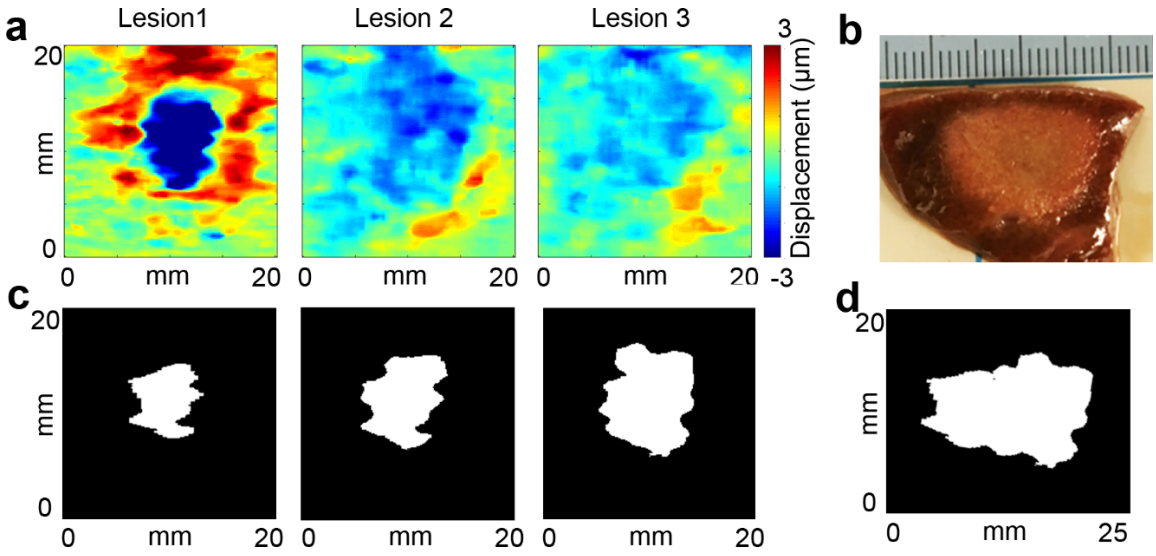

Figure 4.8 Multiple-lesion map using HMI in comparison with gross pathology. (a) HMI lesion map at lesion 1, 2 and 3. (b) Lesion gross pathology. (c) HMI lesion map at the end of ablation at lesion 1, 2 and 3. (d) Combined HMI lesion map.

4.3.3 *In vivo* experimental validation

HMIgFUS lesion maps within the tumor area at the beginning (t = 3s) and the end (t = 59s) of the ablation are shown in Figure 4. (a-b). The pancreatic tumor was delineated based on the high-resolution B-mode images. In Figure 4.9(a), the lesion map within the tumor was homogeneous and no lesion was indicated at the onset of ablation. Figure 4.9(b) exhibits stiffening within the tumor after a 59s-ablation with a displacement reduction rate of 43.3%, suggesting lesion formation. The H&E staining results in Figure 4.9(c) confirmed that the thermal lesion was generated in the tumor with apparent hemorrhage and tissue disruption.

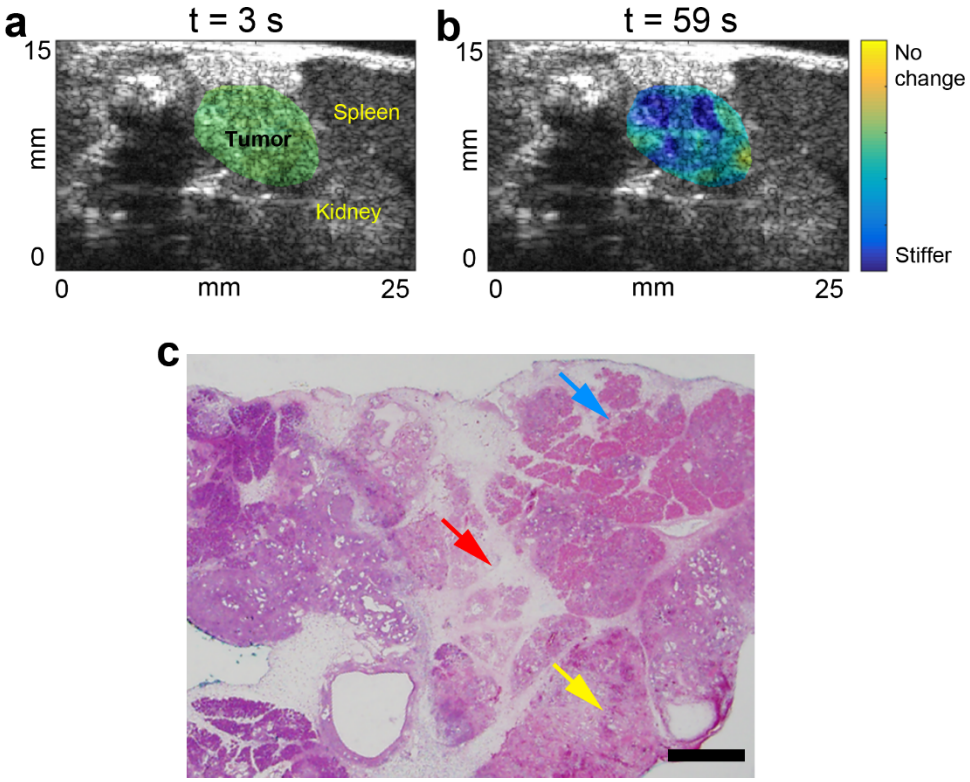

Figure 4.9 HMIgFUS lesion formation monitoring in mouse pancreatic tumor. HMIgFUS lesion map at (a) the beginning (t = 3 s) and (b) the end (t = 59 s) of ablation with tumor and adjacent organs marked. (c) H&E stained image of the pancreatic tumor after HIFU ablation show tissue disruption (red arrow), hemorrhaging (yellow arrow) and cell death (blue arrow). The scale bar represents 1 mm.

4.4 Discussion

In the field of MRI and ultrasound imaging, numerous guidance techniques have been developed for the 3 stages of HIFU treatment: planning, monitoring and assessment. Although numerous methods have been developed to assist the 3 stages of HIFU treatment, real-time HIFU monitoring still remain as a challenge. Real-time HIFU monitoring, especially lesion mapping, is

essential during HIFU procedure as it can help avoid any over- or under-treatment. HMIgFUS is capable of performing HIFU monitoring based on the stiffness change of the tissue without interrupting treatment. Throughout this study, we developed a lesion quantification method using HMIgFUS, and investigated the feasibility of real-time lesion formation monitoring, which incorporated a GPU-based, fast beamforming method. The lesion quantification method was validated through *in vitro* experiments in liver and showed promising results *in vivo*.

In addition to lesion stiffening, softening was also detected at the focal spot when temperature is within the range of 40-60°C before the lesion started to form (Figure 4.5(a) at 30s). This agreed with previous literature on liver showing a slow, reversible shear modulus decrease under HIFU treatment before reaching the threshold of irreversible protein denaturation [67]. At the end of treatment, softening is also detected around the lesion boundary area in most cases indicating heat diffusion to adjacent region. We found that heat diffusion after HIFU is turned off will not affect the lesion size significantly by comparing it with another lesion map acquired 5 min after ablation. According to the temperature profile obtained by the thermocouple, temperature measured from the focal spot drops back to room temperature rapidly within 1 min after HIFU is turned off. A post-treatment HMI was performed 5 min after HIFU exposure showing the lesion dimensions remain the same. Therefore, the lesion map at the end of HMIgFUS can represent the final lesion. Since the speed of sound change is filtered out from the displacement map [92], the effect of speed of sound change due to temperature increase can also be excluded. Furthermore, the increase in attenuation can occur during thermal lesioning [87], resulting in increased absorption therefore increased radiation force within the stiffer lesioning area. However, it has been shown that the decrease in displacement amplitude occurs approximately after reaching 60°C due to the combined effect of viscoelasticity changes and lesion growth overpowering the effect

of attenuation [77], [121]. The increased radiation force during ablation may generate an opposite lesion-to-background contrast by generating higher HMI displacement inside the lesion, which was not observed in this study. It is therefore concluded that the stiffening process is dominant over the change of absorption coefficient in HIFU ablation in liver.

Despite our successful implementation on real-time HMIgFUS platforms, one limitation was that there was no absolute threshold of relative stiffness change to distinguish ablated liver tissue. However, the displacement change during and after treatment has shown enough contrast to delineate the HIFU lesion. -3 dB or 30% decrease out of 0 dB, -1.5 dB and -6 dB showed the best agreement with the gross pathology. This can be improved by optimization study, which can adapt the lesion threshold for each specific specimen. The lesion size was not quantifiable on H&E staining for 2 reasons: 1) it was difficult to register the imaging plane with the cutting plane in histology due to the harvest process; 2) soft tissue shrinks in the paraformaldehyde fixing process, which makes the lesion size smaller when compare with the actual lesion size *in vivo*. A registration method will be used in the future to register the orientation of the lesion with the help of surrounding organs. Another limitation of this study lies in the fact that only slow denaturation induced ablation was included in the study. However, previous work [77] from our group has shown that HMIgFUS is robust under faster treatments such as boiling in monitoring the lesion formation in the presence of strong cavitation events with good displacement contrast across the entire treatment window. The present study may have the potential to be applied on cavitation induced HIFU treatment in the future.

As a final point, HMIgFUS combines HIFU and real-time elasticity imaging on the same device with the advantage of lesion formation monitoring without interfering HIFU treatment.

Future studies will consider the correlation between tissue structures and HMI characteristics to better understand tissue mechanical responses during HMIgFUS ablation.

4.5 Conclusions and Summary

A real-time (2.4 Hz) lesion detection and ablation monitoring method was developed using oscillatory radiation force induced displacement amplitude variations in real time. Lesion size monitoring was achieved in canine liver *in vitro* and initial *in vivo* feasibility was shown in a mouse pancreatic tumor model. Using this method, the HMIgFUS focal region and lesion formation were visualized in real time at a feedback rate of 2.4 Hz. By comparing the estimated lesion size against gross pathology, we have shown the feasibility of using HMIgFUS to monitor treatment and lesion formation without interruption. The study presented herein validated that HMIgFUS could map lesion formation during HIFU treatment and capable of real-time HIFU monitoring.

CHAPTER 5. Focused ultrasound steering for Harmonic Motion Imaging (HMI)

5.1 Introduction

Over the past two decades, several radiation-force-based elasticity imaging techniques have been developed to estimate tissue stiffness and thus detect tumors using various forms of tissue perturbation for the detection of stiffer masses, including acoustic radiation force impulse(ARFI) imaging[122], vibro-acoustography[123] and shear wave elasticity imaging[124]. Harmonic Motion Imaging (HMI) is capable of monitoring the displacement in seamless synchronization with the application of radiation force, with applications to monitoring thermal ablation and tissue viscoelasticity evaluation [113], [121], [125].

Electronic steering is achieved by varying the delay of the sinusoidal signal applied to each element of the transducer to move the focal spot position from the geometric focal spot. The main interest of the electronic steering compared to the mechanical movement arises from the dramatically shorter time required to move the focal spot. The response time for electronic steering is approximately equal to the time-of-flight of the ultrasonic beam from the transducer to the focus (less or equal to 100 μs). Studies have indicated that using electronic steering can greatly increase the rate of tissue coagulation and reduce the total treatment time [126]. Using electronic steering can also help avoid poor coupling between transducer/skin interfaces introduced by mechanical movement. The main limitation of the electronic steering approach lies in the spatial steering range, typically on the order of 1 cm along a given direction [127], [128].

In this chapter, electronic steering is proposed for facilitating HMI by electronically steering the focal spot to several different predetermined locations. This method offers the

advantages of significantly increasing the imaging area and shortening the imaging duration without physical movement of the transducer.

5.2 Methods

HMI measures the oscillatory response of the targeted region to an oscillatory radiation force. The radiation force is caused by applying amplitude modulation (AM) on the acoustic wave as it propagates through a medium. When an AM waveform is used to drive the focused ultrasound (FUS) transducer, the radiation force is oscillating at the modulation frequency ω_m, which is 25 Hz in this study.

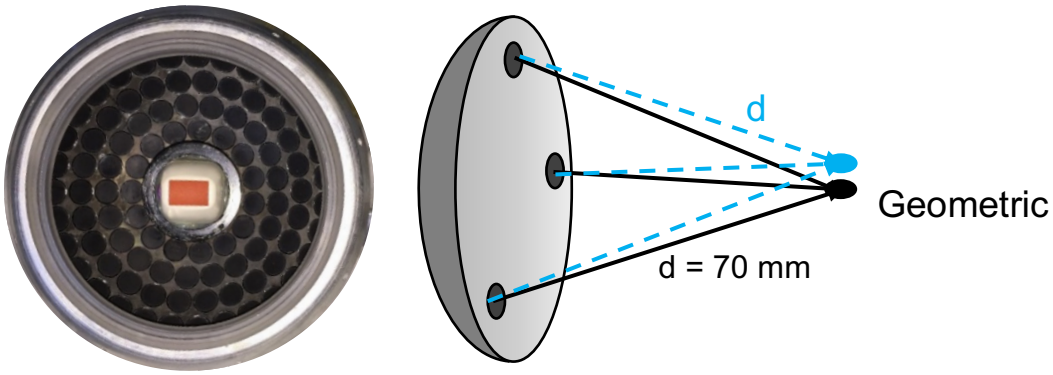

Figure 5.1 HMI phased array transducers and schematic of steering.

In HMI, an oscillatory response is induced at the FUS focal zone due to the AM-FUS excitation, i.e., the HMI displacement [49], [55], [114]. Imaging was performed in a plane wave flash mode with a frame rate of 1000 Hz. The incremental axial tissue displacements were estimated by performing a fast 1D normalized cross-correlation [94] between sequentially acquired tracking lines.

The HMI system consisted of a FUS phased array and an imaging phased array confocally-alignedthrough the central opening (diameter = 41 mm) of the HIFU transducer. The FUS transducer had 93 elements (f_c= 4.5 MHz, and D = 70 mm, Sonic Concepts Inc., Bothell WA, USA). The -3 dB focal size was equal to 0.3 mm (transverse) by 1.1 mm (axial) in water. The imaging probe had 64 elements (f_c = 2.5 MHz, P4-2, ATL/Philips, Bothell, WA, USA). The FUS phased array operated through a four-board ultrasound system (V-1, Verasonics, Bothell, WA, USA) and the diagnostic probe is operated through another ultrasound imaging research system (Vantage 256, Verasonics, Bothell, WA, USA). A Fiber Optic Hydrophone (HFO-690, Onda, Sunnyvale, CA, USA) was used to measure the pressure field and assess steering range in water. HMI using a steered FUS beam was acquired in tissue-mimicking phantoms. Gelatin powder (Gelatin 50 bloom, MP Biomedicals, Irvine, CA, USA) was used to construct 3 homogeneous tissue-mimicking phantoms with elastic modulus of 10 kPa. The concentration of gelatin powder was 50.7 g L−1 yielding a stiffness of 10 kPa [93].

Using the Verasonics V-1 four-board ultrasound system with external power supply, the longest single transmit burst is 31 x 64 half-cycles, or 992 cycles. To get longer burst for continuous wave transmission for HMI, several transmit-only events were put together in sequence in the script, with no other sequence control commands in between them. Therefore, the system could start the next event as fast as it can after completing the prior transmit-only event, resulting in an idle time of roughly 10 microseconds between the transmit bursts.

Assembling several transmit events in rapid sequence was also necessary to accomplish the amplitude modulation. Because the transmit power supply to the system's square wave transmitters was fixed at a DC level, there is no mechanism for changing that supply voltage rapidly to provide amplitude modulation. Therefore, the amplitude control of each transmit output

at the fundamental frequency was implemented by varying the pulse width of the transmit waveform using the "B" value in the parametric waveform definition on V-1. So to produce an overall amplitude-modulated transmit output, a number of transmit-only events were put together each using a different "B" parameter value.

The "B" parameter varied from a maximum of 100% down to a minimum of two (the shortest pulse the V1 transmit hardware can produce). The amplitude of the fundamental term in the Fourier series for a square wave with relative pulse width PW is given by

$$\text{Amplitude} = \sin\left(PW \times \frac{\pi}{2}\right) \times \frac{\pi}{4} \tag{5.1}$$

where PW was represented by parameter "B" when setting up each transmission.

Another constraint of the V-1 system hardware design is that it cannot drive the transmit devices continuously at transmit frequencies above 2 MHz. With the 4.5 MHz FUS transducer, it constraint the transmit sequence to be 'chopped' into a series of active 4.5 MHz transmit pulses interleaved with idle intervals long enough that the average cycle rate over the entire interval remains below 2 MHz as shown in Figure 5.2.

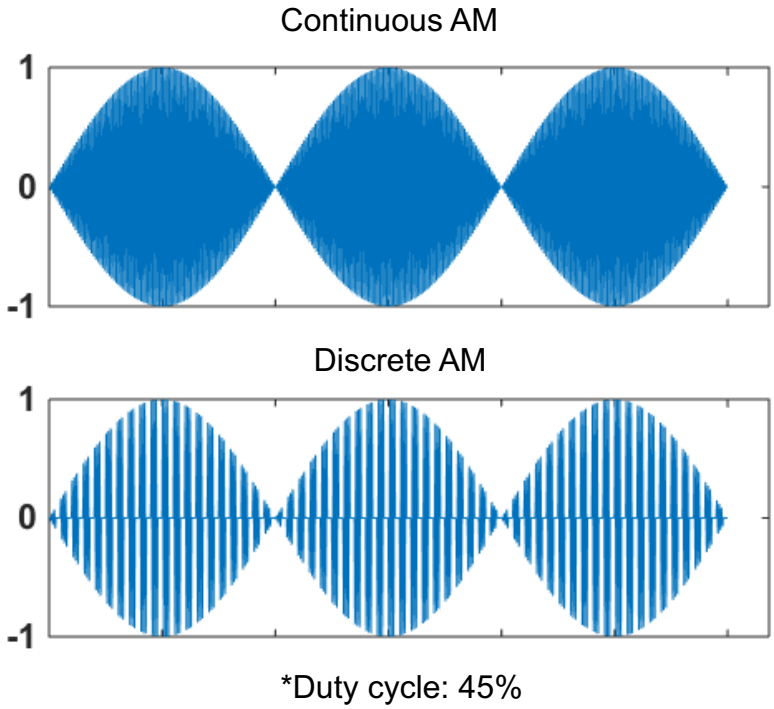

Figure 5.2 Comparison of continuous AM transmission waveform using function generator and discrete AM transmission wave form using Verasonics V-1 system with a duty cycle of 45 %.

5.3 Results

A pressure profile with steering was acquired in free field to calculate the focal pressure loss due to beam steering. A safe steering range was assumed when the highest grating lobe amplitude was under -6 dB. Figure 5.3 shows the FUS pressure field in water with lateral steering at 0 mm, 0.85 mm, 1.7 mm and 2.55 mm. The grating lobe amplitude keeps increasing with the steering distance and exceeds -6 dB of the maximum pressure when the steering distance is over 1.7 mm in lateral direction.

The HMI displacement was imaged within the steering range of +/-1.7 mm and +/-2 mm in the lateral and axial direction in tissue-mimicking phantoms, respectively. A peak-to-peak displacement map was generated, and a maximum peak-to-peak displacement amplitude value was found. The maximum peak-to-peak displacement location was also found and plotted in Figure 5.4(B) and Figure 5.4(C). Figure 5.4(B) shows that the maximum peak-to-peak displacement spot moves laterally from the geometric focus when lateral steering is applied (n = 5). Figure 5.4(C) shows that the maximum peak-to-peak displacement spot moves away in axial direction from the geometric focus when axial steering is applied (n = 5).

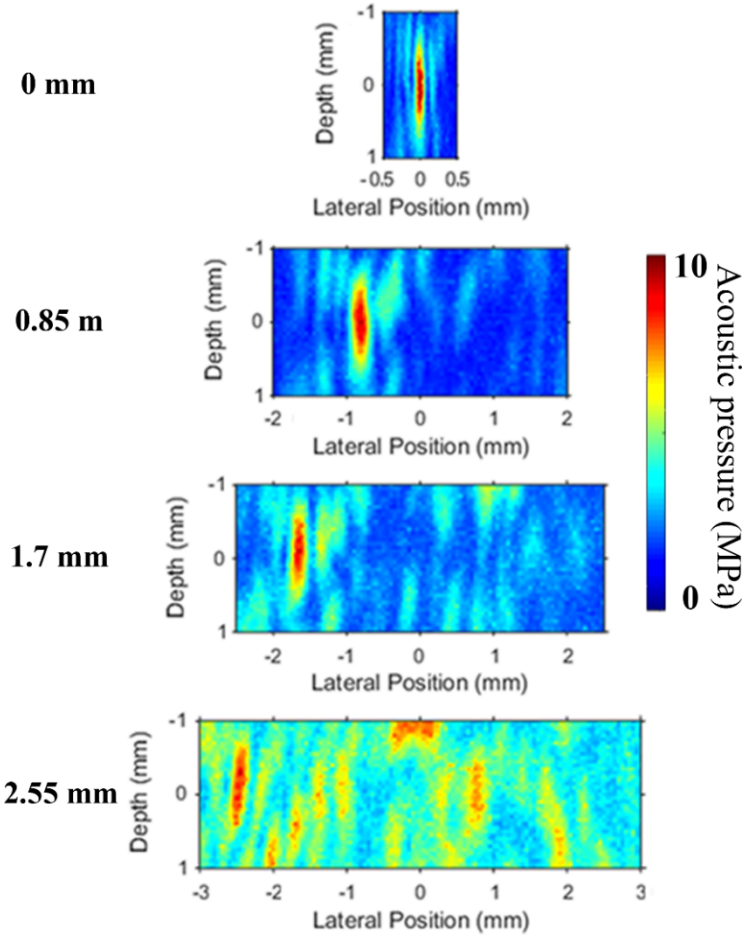

Figure 5.3 Hydrophone measured peak positive pressure profile with corresponding intended steering distance in free field.

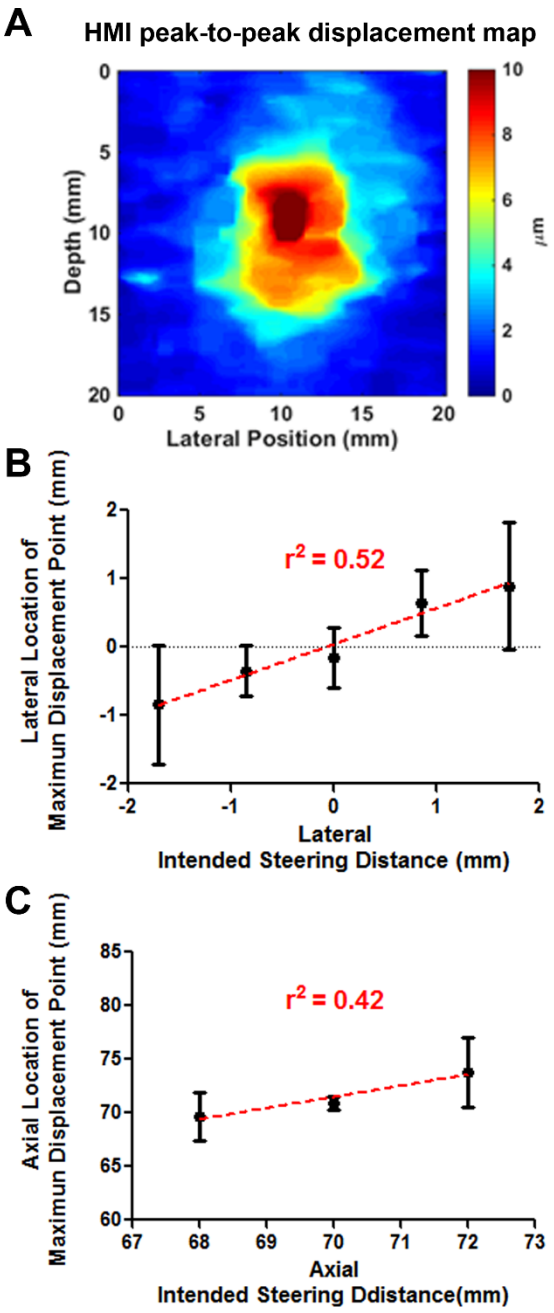

Figure 5.4 (A) Example of HMI peak-to-peak displacement map from a tissue-mimicking gelatin phantom. (B) In tissue-mimicking gelatin phantom, lateral location of maximum displacement point with corresponding lateral intended steering distance (n = 5). (C) In tissue-mimicking gelatin phantom, axial location of maximum displacement point with corresponding axial intended steering distance (n = 5).

Using the maximum peak-to-peak displacement amplitude value, we calculated -6 dB displacement focal zone to represent the radiation force engaged area. The peak-to-peak HMI displacement amplitude is directly correlated with acoustic intensity in a homogenous phantom or tissue [114]. Based on this relationship, the areas of the -6 dB displacement focal zone were computed based on the maximum displacement amplitude. In Figure 5.5, the ellipses indicating the theoretical targeted area were overlaid onto the focal area defined by -6 dB displacement focal zone. In Figure 5.5(a), the white area indicated the -6 dB displacement focal zone, which is also the radiation- force engaged region in the phantom. The focal zone has been found to be larger than the FUS spot in water due to the connectivity in the material. Regarding the shape of the focal zone, perfect ellipse is rarely seen in experiments as a result of the inhomogeneity in the phantom. With +/-1.7 mm lateral and +/-2 mm axial steering, the 5 raster steering sequences generated a total -6 dB excited region equaling 46.0 mm^2, which is 2.3 times larger than the original -6 dB excited region of 19.9 mm^2. Using the maximum speed of the positioner at 10mm/s, it takes 200ms to move the focal spot to the next axial location in Figure 5.5 (b). In order to raster scan the entire excited region in Figure 5.5(b), the transducer requires to be moved at least 15 times which total 3s of mechanical movement plus the communication time between the PC and the positioner. In the meanwhile, the time duration of electronic steering was negligible comparing to the physical movement.

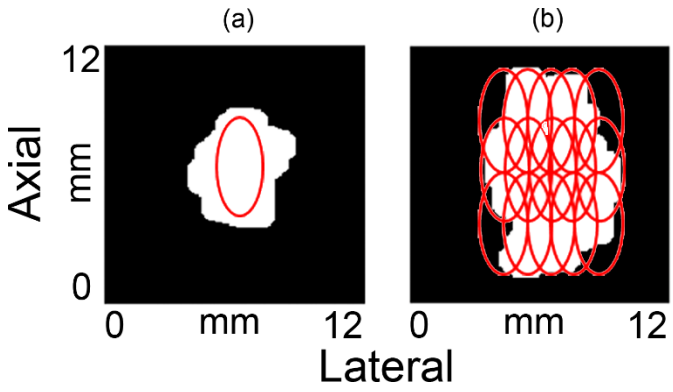

Figure 5.5 Representative image of -6 dB excited region without steering (a) and with 2D steering (b). The ellipses indicating the theoretical targeted area were overlaid onto the focal area defined by -6 dB displacement excited region.

5.4 Discussion

Using the steered FUS beam, HMI can be used to image a 2.3 times larger ROI without requiring physical movement of the transducer. Using steering for HMI can be used to shorten the total imaging duration without requiring physical movement of the transducer. The main limitation of this study lies in the design of the FUS transducer, which constrained the effective steering range of the FUS beam to +/-1.7 mm and +/-2 mm in the lateral and axial direction.

CHAPTER 6. Harmonic Motion Imaging guided Focused Ultrasound (HMIgFUS) based human breast tumor characterization and treatment monitoring *ex vivo*

6.1 Introduction

Breast cancer is the most common cancer and the second leading cause of cancer death among women. In 2013, approximately 300,000 women were diagnosed with breast cancer and almost 40,000 died from the disease in the US [129]. Image-guided minimally-invasive treatment of localized breast tumor has become a subject of intensive research and several studies have assessed the feasibility of minimally-invasive breast tumor ablation techniques, such as radiofrequency ablation (RFA), cryoablation and high intensity focused ultrasound (HIFU) ablation [20]. Minimally-invasive treatment applies extreme temperatures, either high or low, to induce irreversible cell injury, tumor apoptosis and coagulative necrosis [21]. Compared with conventional surgical procedures the main advantages of minimally-invasive ablation lie in the fact that they are less invasive, less scarring and less painful, allowing for shorter recovery time [22].

HIFU is an entirely non-invasive technique which focuses the ultrasound beam onto a small target volume to reach high focal power, resulting in temperature elevations causing coagulative necrosis in the target while surrounding structures are spared. Since the ultrasound wave penetrates through soft tissue without any surgical incision nor needle insertion, there are no damages to the skin or underlying tissues. Acoustic energy can induce temperature elevations at the focal spot in a few seconds and simultaneously induce cellular death and vascular destruction in normal and

tumor tissues [37]. Because of the steep thermal gradients involved, the boundaries of the ultrasound-treated volumes can be closely spaced until the entire target is covered.

Clinically, fibroadenoma (FA) is the most common benign breast mass and may be accompanied by pain [130]. FA does not require treatment; however, palpable FA may cause distress in some patients, who then request removal. Compared with conventional surgical excision or other minimally invasive techniques, HIFU is completely non-invasive which provides better cosmetic results and shorter recovery time. Recently, a multicenter study using HIFU as an outpatient procedure treated 42 women with 51 FA [131]. They demonstrated that HIFU is effective in reducing the volume and other clinical symptoms of FA. HIFU has also been studied to ablate early stage malignant breast tumors in elderly patients who are not surgical candidates [38]–[40].

Currently, MRI and sonography are being used for guidance and monitoring of HIFU therapy. Both MR-guided HIFU (MRgFUS)[59], [132] and ultrasound-guided HIFU (USgFUS) methods have their advantages and disadvantages. MRI has the advantage of providing temperature data within seconds after HIFU exposure. However, MRI guidance is expensive and lengthy. Ultrasonic guidance provides the benefit of imaging using the same form of energy that is being used for therapy. Therefore, if the target can be well visualized with sonography, then the HIFU therapy may avoid potentially causing thermal injury to normal tissue. Worldwide, thousands of patients with uterine fibroids, liver cancer, breast cancer, pancreatic cancer, bone tumors, and renal cancer have been treated by USgFUS [30], [133], [134].

Ultrasound elasticity imaging is used in addition to traditional B-mode ultrasound as a tool for differential diagnosis between normal and tumor in human breast based on tissue stiffness. Qualitative and quantitative tissue strain analyses using acoustic radiation force impulse imaging

(ARFI) technology has been developed for the diagnosis of breast masses [4], [10], [11]. The response of tissue to the acoustic radiation force is tracked as tissue displacement, which has been found to be correlated with local stiffness of the tissue. Vibro-acoustic tissue mammography is also a radiation force-based method, uses focused ultrasound to vibrate tissue at frequency (kHz) and utilizes the resulting response to produce images that are related to the hardness of the tissue [12], [13]. Supersonic shear imaging (SSI) utilizes a very fast (5000 frames/s) acquisition sequence to capture the propagation of shear waves [14] that provide information of the local viscoelastic properties [15], [16].

Over the past decade, ultrasound elasticity imaging was not limited to the area of disease diagnosis but also emerged in the application of therapy guidance and monitoring [135], [136]. Harmonic Motion Imaging (HMI) is an all-ultrasound-based elasticity imaging technique designed for both reliable diagnosis and HIFU treatment monitoring. It utilizes a HIFU transducer to emit an amplitude-modulated (AM) beam for both thermal therapy while inducing a stable oscillatory tissue displacement at its focal zone. The oscillatory response, namely HMI displacement, is estimated using the radio-frequency (RF) signals recorded during the HIFU treatment through a confocally-aligned imaging transducer [49], [92]. The localized tissue response is monitored continuously from the onset of HIFU treatment and aims at providing clinicians the change in local tissue stiffness in order to prevent any under- or over-treatment. Since the HMI does not interrupt HIFU ablation, HIFU sonication was operated with a duty cycle of 100%. Several studies have been published as feasibilities *ex vivo* [78], [114], and *in vivo* [79], [80] using 1D [54] and 2D [99] systems. The overall goal of this study is to develop and test HMI system for real-time imaging and ablation monitoring in post-surgical breast specimens.

6.2 Methods

6.2.1 Post-surgical breast specimen collection

Collection and handling of post-surgical breast specimens were approved by the Institutional Review Board (IRB) board of Columbia University and informed consent was obtained from all enrolled patients. Thirty-six small tissue specimens from mastectomy were obtained from 24 patients who underwent lumpectomy or mastectomy including 19 normal, 15 invasive ductal carcinoma (IDC) and 2 fibroadenoma (FA). The age range of patients was 21-89 years (age: 60 ± 18). Eleven entire mastectomy tissue specimens from 12patients who underwent mastectomy procedure, and all 12 contain malignant tumor. Experiment timeline is shown is Figure 6.1. All specimens were immediately immersed in phosphate-buffered saline (PBS) after surgery and transported in ice. The small piece specimens used for the experiments were approximately 2 cm × 2 cm × 1 cm in size and were received from the department of Pathology at CUMC. Small piece specimens were embedded in agar gel matrix soaked in degassed PBS in a water tank as shown in Figure 6.2, while the entire mastectomy specimens were directly soaked in degassed PBS without embedding. The tank wall was lined with a layer of sound-absorbing material to reduce undesired echoes from below.

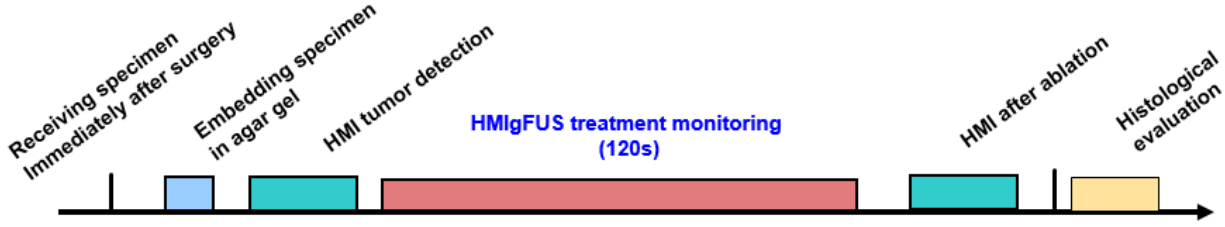

Figure 6.1 Experiment timeline.

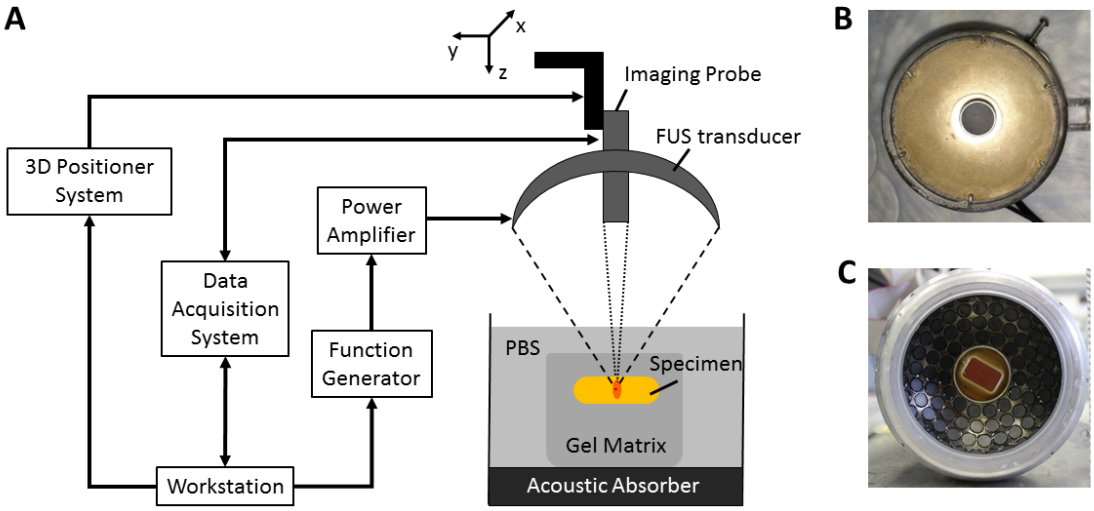

Figure 6.2 Schematic of Harmonic Motion Imaging (HMI) system with experiment setup. (A) Block diagram of HMI system. The red region indicates the focus of the FUS transducer. (B) The 1D HMI system comprised of a single-element FUS transducer (outer diameter = 80 mm, inner diameter = 16.5 mm) confocally-aligned with a single-element pulse-echo transducer (diameter = 15 mm). (C) The 2D HMI system consisted of a 93-element FUS phase array transducer (outer diameter = 110 mm, inner diameter = 41 mm) and a 64-element phase array imaging probe.

6.2.2 Experiment setup

HMI measures the vibrational response of the target region to an oscillatory radiation force. The radiation force is caused by the change in momentum of the acoustic wave as it propagates through a medium. When an AM waveform is used to drive the FUS transducer, the radiation force is oscillating at the modulation frequency ω_m, which is 25 Hz in this study. In HMI, an oscillatory response is induced at the HIFU focal zone due to the AM-HIFU excitation, namely the HMI displacement. This HMI displacement can be monitored throughout the entire HIFU treatment

duration. The change of the peak-to-peak HMI displacement amplitude can be correlated with the relative change in local tissue stiffness as the thermal lesion develops.

A schematic illustration of the main components of the HMI system is shown in Figure 6.2. HMI was performed using both 1D and 2D HMI systems in this study. The 1D HMI system comprised of a single-element focused ultrasound (FUS) transducer (outer diameter = 80 mm, inner diameter = 16.5 mm, center frequency = 4.75 MHz, focal depth = 90 mm. Riverside Research Institute, New York, NY) confocally-aligned with a single-element pulse-echo transducer (diameter = 15 mm, center frequency = 7.5 MHz, focal depth = 60 mm, Olympus-NDT, Waltham, MA, USA) (Figure 6.2). The FUS transducer was driven by an amplitude-modulated (AM frequency ω_m = 25 Hz) sinusoidal signal generated by a dual-channel arbitrary waveform generator (AT33522A, Agilent Technologies Inc. Santa Clara, CA, USA) and amplified by a nominal 50 dB gain power amplifier (325LA, E&I, Rochester, NY, USA). The pulse-echo transducer was mounted through the center hole of the FUS transducer and confocally aligned with it. It was connected to a pulser/receiver (Olympus-NDT, Waltham, MA, USA) operating at 1 kHz. The received RF signals from the pulser/receiver were band-pass filtered (Reactel Inc., Gaithersburg, Maryland, USA) with cutoff frequencies of f_{c1} = 5.84 MHz and f_{c2} = 8.66 MHz and then recorded by a digitizer (Gage applied, Lockport, IL, USA) at a sampling frequency of 100 MHz. To generate a 3D HMI displacement map, point-by-point raster scan acquisition was used with a step size of 0.5 mm in transverse plane. At each spot, the FUS exposure varied from 0.1 to 0.6-s long (5 to 30-cycle oscillations at 50 Hz), during which 100 to 600 RF lines at 1 kHz pulse repetition frequency (PRF) were acquired.

The 2D HMI system consisted of a 93-element FUS phase array transducer (individual element diameter = 10 mm, overall outer diameter = 110 mm, inner = diameter 41 mm, center

frequency = 4.5 MHz, and focal depth = 70 mm. H-178, Sonic Concepts Inc. Bothell WA, USA) and a 64-element phase array imaging probe (center frequency = 2.5 MHz, P4-2, ATL, Bothell, WA, USA) (Figure 5.1). In this feasibility study, the 93-element FUS transducer was driven in phase using the same function generator and power amplifier as the 1D system. The imaging probe was inserted through an opening in the center of the FUS transducer and confocally aligned with it. The imaging probe was operated by an ultrasound imaging research system (V-1, Verasonics, Bothell, WA, USA). The FUS total output acoustic power was 11 W in 1D system and 8.7 W in 2D system from radiation force balance measurement [116].

HMIgFUS ablation monitoring was only performed in 34 small piece specimens, including 19 normal, 15 IDC and 2 FA specimens using either 1D or 2D HMI system and each specimen was ablated at 1-2 different targeted locations depending on the size of the specimen. Prior to HIFU ablation, a standard B-mode image of the targeted region was acquired using the imaging probe. Then, HIFU was applied for a total duration of 120 s in a single location. Since HMIgFUS does not require interruption of HIFU ablation, HIFU sonication was operated with a duty cycle of 100%. A customized plane wave imaging sequence was developed using the VDAS (Verasonics Data Acquisition System) platform. A GPU-based sparse-matrix algorithm was used for fast beamforming [99]. During HMIgFUS exposure, 200 beamformed frames at a frame rate of 1 kHz were acquired and transferred to the host workstation every 3 s. An interpolation was performed to up-sample the RF signals by a factor of 8 to achieve a sampling frequency of 80 MHz before storing the RF signals on the host workstation. After 120 s of continuous HIFU ablation, a total of 40 date sets were acquired. The main parameters of two systems are summarized in Table 6.1.

	1D HMI/ HMIgFUS	2D HMI/ HMIgFUS
FUS transducer	4.75 MHz single-element transducer	4.5 MHz 93-element FUS phased array
Imaging transducer	7.5 MHz single-element pulse-echo transducer	2.5 MHz 64-element phased array
Parameters		
AM frequency	25 Hz	25 Hz
Sampling frequency	100 MHz	80 MHz
Frame rate	1000 Hz	1000 Hz
Acoustic Power	11 W	8.7 W
Imaging duration	0.6 s	0.1 - 0.6 s
Ablation duration	120 s	120 s

Table 6.1 Main parameters of 1D and 2D HMI/ HMIgFUS systems.

The signal processing techniques were the same for the 1D and 2D HMI systems. Each set of continuously acquired RF lines using the 1D HMI system, or each set of the 200 continuously acquired RF frames using the 2D HMI system, was processed together. The interference of the FUS beam with the RF signals was removed by digital low-pass filtering (f_{cutoff} = 4 MHz) during processing using the 2D system. In the 1D system, the interference of the FUS beam was removed by e analog band-pass filter as described previously. The incremental axial tissue displacements were estimated by performing a fast 1D normalized cross-correlation between sequentially acquired tracking lines [94]. The RF window size was equal to 5 wavelengths of the imaging probe

and the window overlap was 95%. A threshold ($R^2 > 0.7$) was applied to eliminate poor displacement estimation. The mean peak-to-peak HMI displacement amplitudes and standard deviation of the 10-cycle oscillations at 50 Hz were calculated based on the 200-RF lines or frames. The aforementioned processing was repeated at each raster scan point to obtain the 3D HMI displacement image for breast tumor detection. The range of the ROI was 5mm-diameter circle. On entire mastectomy images, a subset of the ROI was manually selected and ROI was located in a uniform region of tissue. Signal-to-noise ratio (SNR) is used to assess the quality of images and defined as:

$$SNR = \frac{\mu}{\sigma} \tag{6.1}$$

Where μ and σ are the mean and standard deviation of the displacement obtained in a homogenous region, respectively [137], [138].

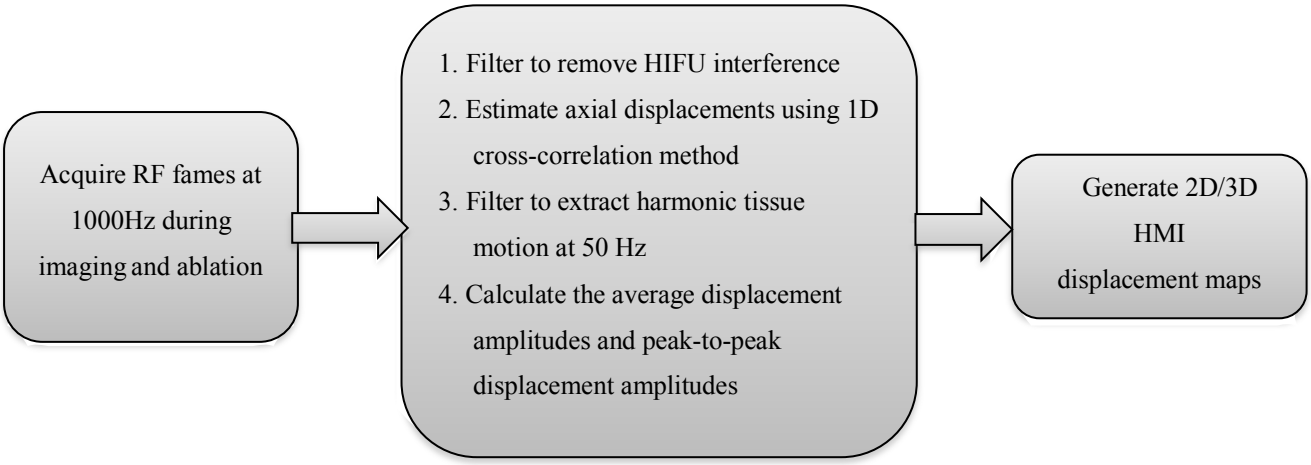

Figure 6.3 Schematic of HMIgFUS data acquisition and data processing.

For HMIgFUS ablation monitoring, the mean and standard deviation of the peak-to-peak amplitude of the estimated HMI displacements within the ROI were analyzed for the whole HMIFU ablation process. To compare among different targeted locations, normalization of the HMI displacements by the displacement obtained at t = 2 s was performed. Changes in the HMI

displacement amplitude were calculated by the percentage change in HMI displacement at the end of the thermal treatment over the displacement at t = 2 s.

A focal spot localization method [114] was used to define the ROI. A maximum peak-to-peak displacement value was estimated along the axial direction (1D) or the image (2D). Based on the maximum peak-to-peak displacement value, we calculated -3 dB displacement focal zone over the axial direction (1D) or the image (2D). In order to quantitatively analyze the relative tissue stiffness change during heating, the resulting displacement around the focal region was then averaged within the -3 dB region.

3D data rendering (Figure 6.5 B, D and F) was achieved using Amira (VSG, Burlington, MA). Matlab (Mathworks, Natick, MA, USA) was used for the statistical analysis. The results were presented in mean ± standard deviation format. A paired Student's t-test was used to determine a significant difference ($p < 0.05$) between before and after ablation.

6.2.3 Histology

The specimens were kept in 10% phosphate-buffered formalin at low temperature (4 ◦C) for at least 24 h. The specimens were then processed and embedded in paraffin, cut in 4-µm-thick slices, and stained with hematoxylin and eosin (H&E).

6.3 6.3 Results

6.3.1 Tumor characterization

6.3.1.1 Small piece breast specimen

Figure 6.4 shows the representative B-mode (A) image of a normal breast tissue. Plane wave 2D HMI (B, C) were shown within the ROI in (A) marked by dash line. Color in (B) and (C)

indicates the amplitude of HMI displacement. (B) shows the peak positive displacement, and (C) shows the peak negative displacement.

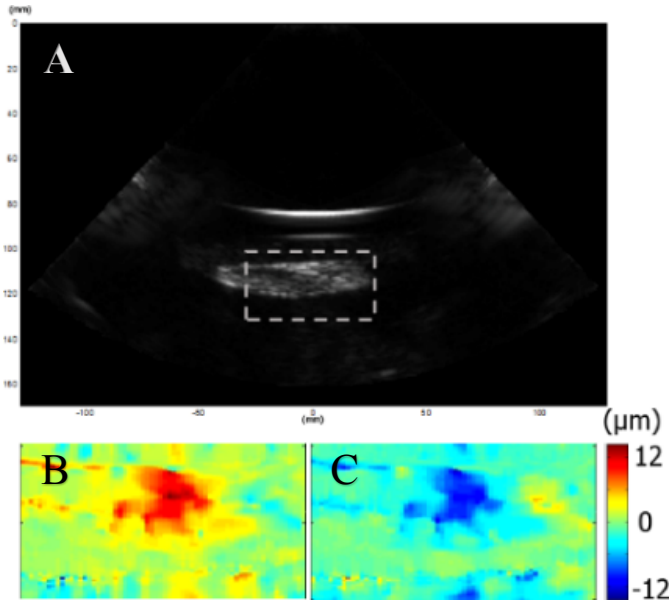

Figure 6.4 Representative B-mode (A) image of a normal breast tissue. Plane wave 2D HMI (B, C) were shown within the ROI in (A) marked by dash line. Color in (B) and (C) indicates the amplitude of HMI displacement. (B) shows the peak positive displacement, and (C) shows the peak negative displacement.

In Figure 6.5, the 3D HMI images of a normal breast specimen, a breast tumor specimen and a FA specimen before and after HMIFU ablation are shown in comparisons with the gross pathology images.

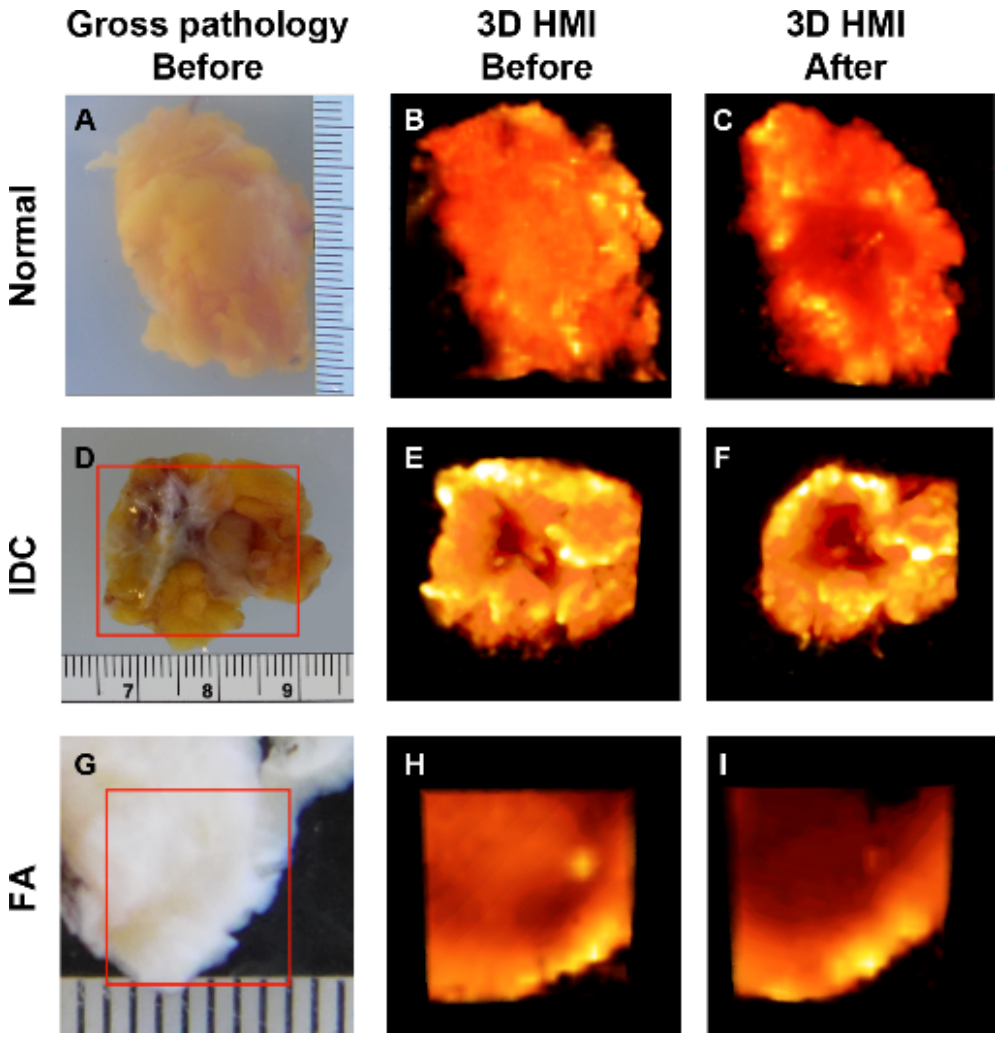

Figure 6.5 3D HMI displacement images of normal breast tissue, IDC and FA. (A) Gross pathology photograph of a normal breast specimen mounted on the gel matrix, the 3D reconstructed HMI of the selected tissue before (B) and after (C) HMIFU ablation. (D) Gross pathology photograph of a IDC specimen mounted on the gel matrix, and the 3D reconstructed HMI of the selected tissue before (E) and after (F) HMIFU ablation. (G) Gross pathology photograph of a FA specimen mounted on the gel matrix, the 3D reconstructed HMI of the selected tissue before (H) and after (I) HMIFU ablation. The brighter the color is indicating the higher HMI displacement and lower relative stiffness, and *vice versa*.

In the 1D system, the HMI displacement amplitudes of the normal breast, IDC and FA averaged within the -3dB regions were 40.10±15.50 μm (n = 9), 24.90±9.64 μm (n = 5) and 7.40 μm (n = 1), respectively (Fig. 3A); and 24.73±10.97 μm (n = 10), 12.77±10.30 μm (n = 10) and 2.56 μm (n = 1) with the 2D system (Fig. 3B). Histological analysis found no tissue damage in the normal breast tissue, IDC or FA from HMI imaging alone.

6.3.1.2 Entire mastectomy specimen

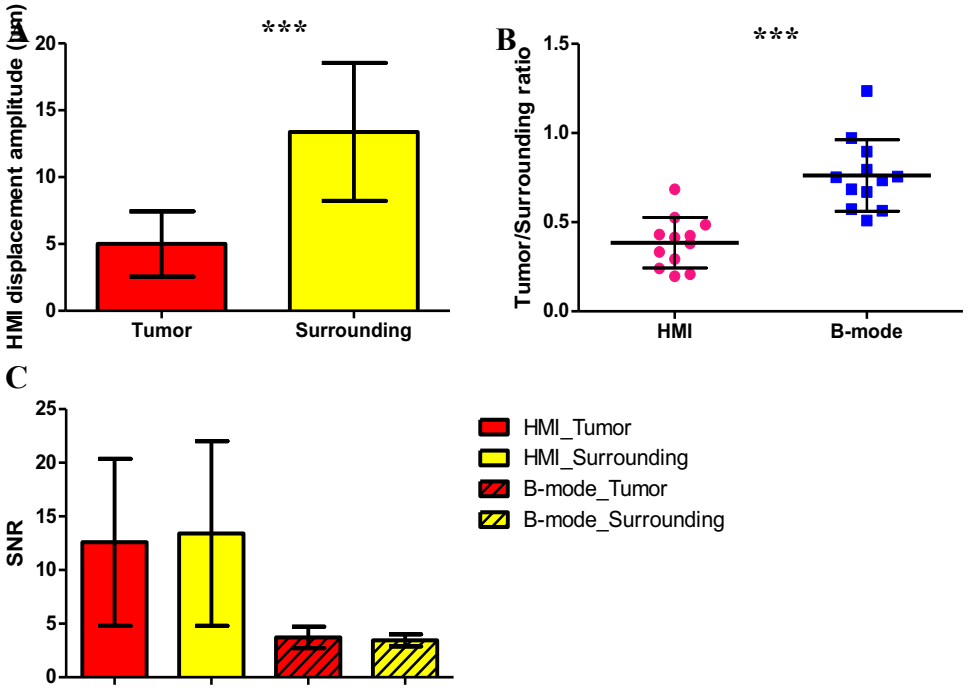

Figure 6.6 HMI displacement amplitude on entire mastectomy specimens. (A) HMI displacement amplitude on 12 tumors with corresponding surrounding tissue ($P < 0.0001$). (B) HMI displacement contrast ration between tumor and surrounding tissue in comparison with the contrast on corresponding B-mode images ($P < 0.0001$). (C) Image SNR comparison.

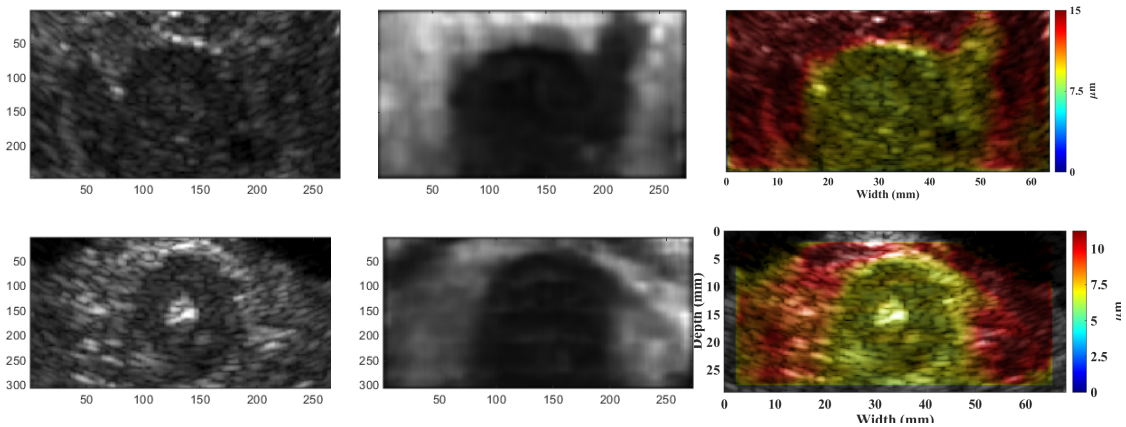

Figure 6.7 Representative B-mode images, HMI displacement maps and HMI displacement maps overlaid on corresponding B-mode images on entire mastectomy specimens.

The mean HMI displacement of the tumor and surrounding tissue were 5.00 ± 2.33 µm and 13.38 ± 4.94 µm respectively using the 2D system. The mean tumor/surround contrast ration of HMI maps and B-mode images were 0.38 ± 0.14 µm and 0.76 ± 0.19 µm respectively. The SNR of tumor and surrounding tissue on HMI maps were 12.59 ± 7.45 and 13.40 ± 8.24 µm respectively. And the SNR of tumor and surrounding tissue on B-mode images were 3.72 ± 0.96 and 3.44 ± 0.54 µm respectively (Figure 6.6).

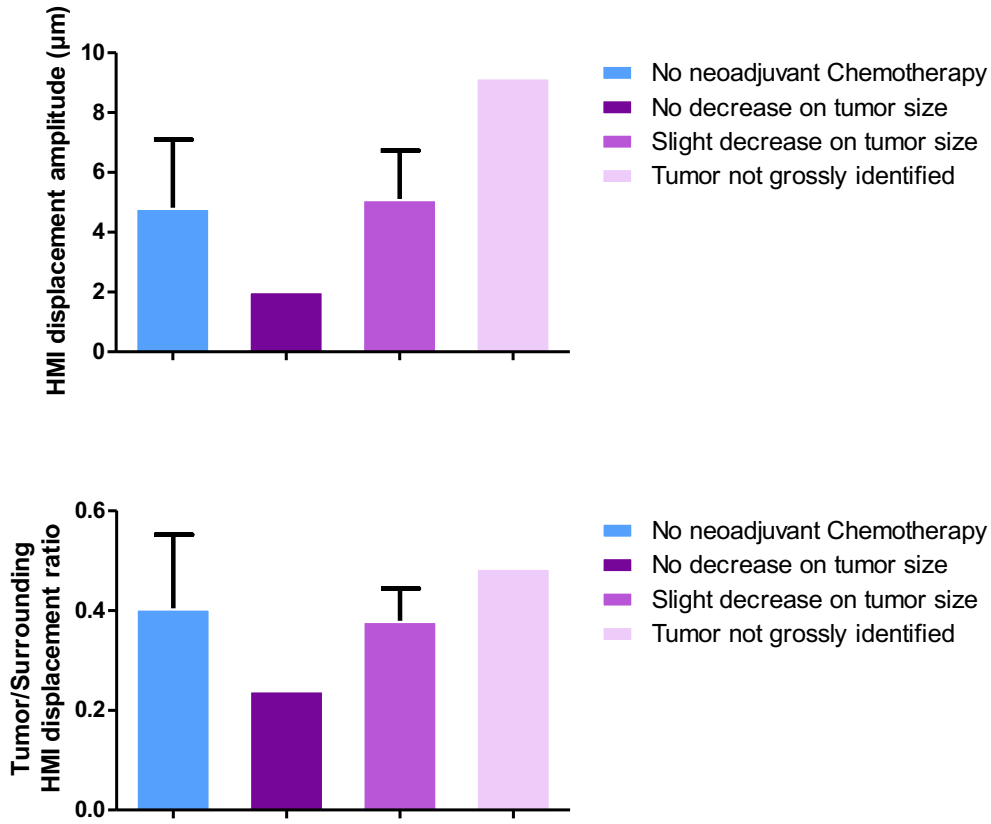

Figure 6.8 HMI displacement amplitude observation on neoadjuvant chemotherapy. No neoadjuvant Chemotherapy (n = 8), no decrease on tumor size after neoadjuvant chemotherapy (n = 1), slight decrease on tumor size after neoadjuvant chemotherapy (n = 2) and tumor not grossly identified after neoadjuvant chemotherapy (n = 1).

Figure 6.8 shows both HMI displacement amplitude of the tumor and HMI tumor/surrounding ration with corresponding neoadjuvant chemotherapy results. Among the 12 entire mastectomy specimens, 8 patients did not receive neoadjuvant chemotherapy prior to their surgery, and 4 patients received neoadjuvant chemotherapy prior to their surgery. The specimen from the patient whose tumor not grossly identified neoadjuvant chemotherapy has the highest

displacement. And the specimen from the patient whose tumor did not respond to neoadjuvant chemotherapy has the lowest displacement.

6.3.2 HMIgFUS ablation monitoring

Figure 6.9 shows HMI displacement change before and after HIFU ablation using the 1D (a) and 2D (b) systems. Tissue motion during heating is visible through the periodic variation in displacement amplitude, which is denoted by alternating red (positive) and blue (negative) displacement in Figure 6.9. Red denotes highest motion towards the transducer, and blue represents highest motion away from the transducer. Using the 1D HMI system, 9 out of 9 (100%) normal breast lesions, 5 out of 5 (100%) IDC lesions and 1 out of 1 (100%) FA lesions were found to have lower HMI displacement amplitude after HMIFU treatment indicating protein denaturation and necrosis. Using the 2D HMI system, 9 out of 10 (90%) normal breast lesions, 8 out of 10 (80%) IDC lesions and 1 out of 1 (100%) FA lesions were found to have lower HMI displacement after HMIFU treatment. HMI displacement before and after HMIFU ablation were compared by performing a paired Student's t-test. The mean HMI displacement before and after ablation is shown in Table 6.2.

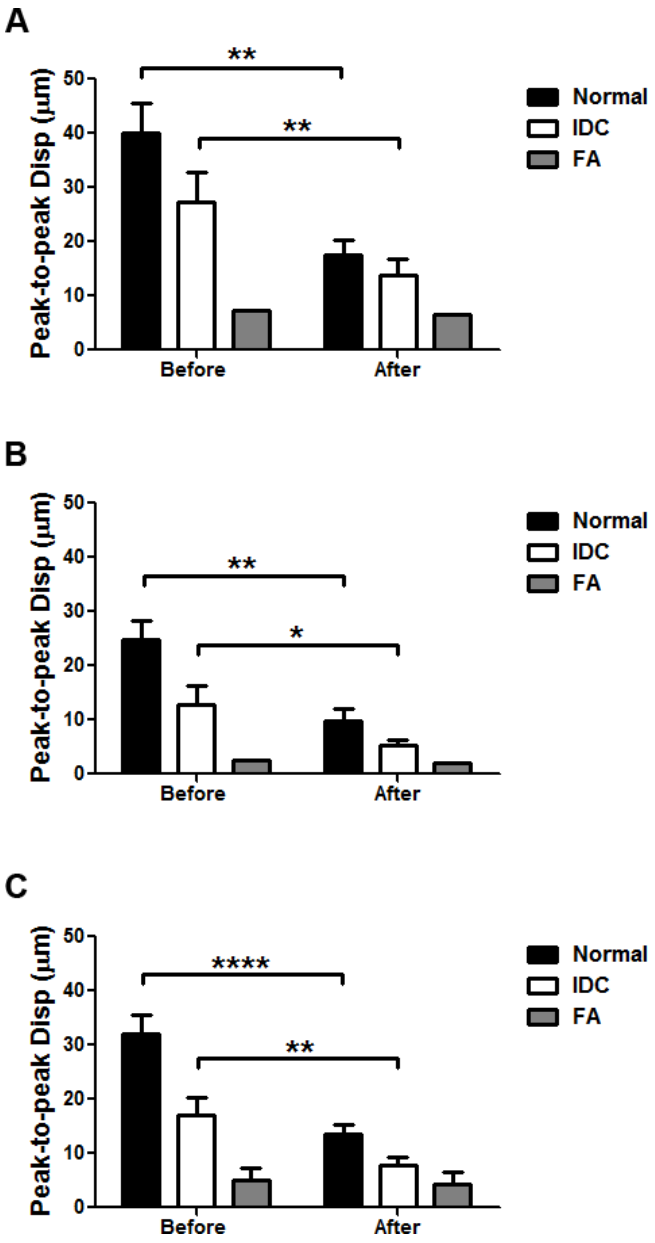

Figure 6.9 HMI displacement change before and after HMIFU ablation. (A) 9 normal, 5 IDC and 1 fibroadenoma specimens were imaged with 1D HMI system. (B) 10 normal, 10 IDC and 1 fibroadenoma specimens were imaged with 2D HMI system. (C) Combined results with both HMI systems. * indicates $p < 0.05$, ** indicates $p < 0.001$, and **** indicates $p < 0.00001$.

	1D SYSTEM				2D SYSTEM			
	Displacement (μm)				Displacement (μm)			
	Before	After	n	P value	Before	After	n	P value
NORMAL	40.10±15.50	17.49±7.85	9	0.0025	24.73±10.97	9.83±6.46	10	0.0048
IDC	24.90±9.64	12.28±5.44	5	0.0068	12.77±3.50	5.35±2.74	10	0.045
FA	7.34	6.58	1		2.56	2.06	1	

Table 6.2 HMI displacement before and after HMIFU ablation.

	Percentage of change	SD
Normal	-53.84%	25.60%
IDC	-44.69%	29.55%
FA	-15.33%	4.26%

Table 6.3 Normalized HMI displacement change over the entire HMIFU ablation process.

The mean HMI displacement of the normal breast tissue decreased from 40.10±15.50 μm to 17.49±7.85 μm (n = 9, p = 0.0025) using the 1D system, and from 24.73±10.97 μm to 9.83±6.46 μm (n = 10, p = 0.0048) using the 2D system. The mean HMI displacement of IDC decreased from 24.90±9.64 μm to 12.28±5.44 μm (n = 5, p = 0.0068) using the 1D system, and from 12.77±3.50 μm to 5.35±2.74 μm (n = 10, p = 0.045) using the 2D system. The mean HMI displacement of FA decreased from 7.34 μm to 6.58 μm (n = 1) using the 1D system, and from 2.56 μm to 2.06 μm (n = 1) using the 2D system. A similar decrease was also clearly imaged in 2-D, where the individual frameset consisted of peak negative displacement profiles as an example of a treated location.

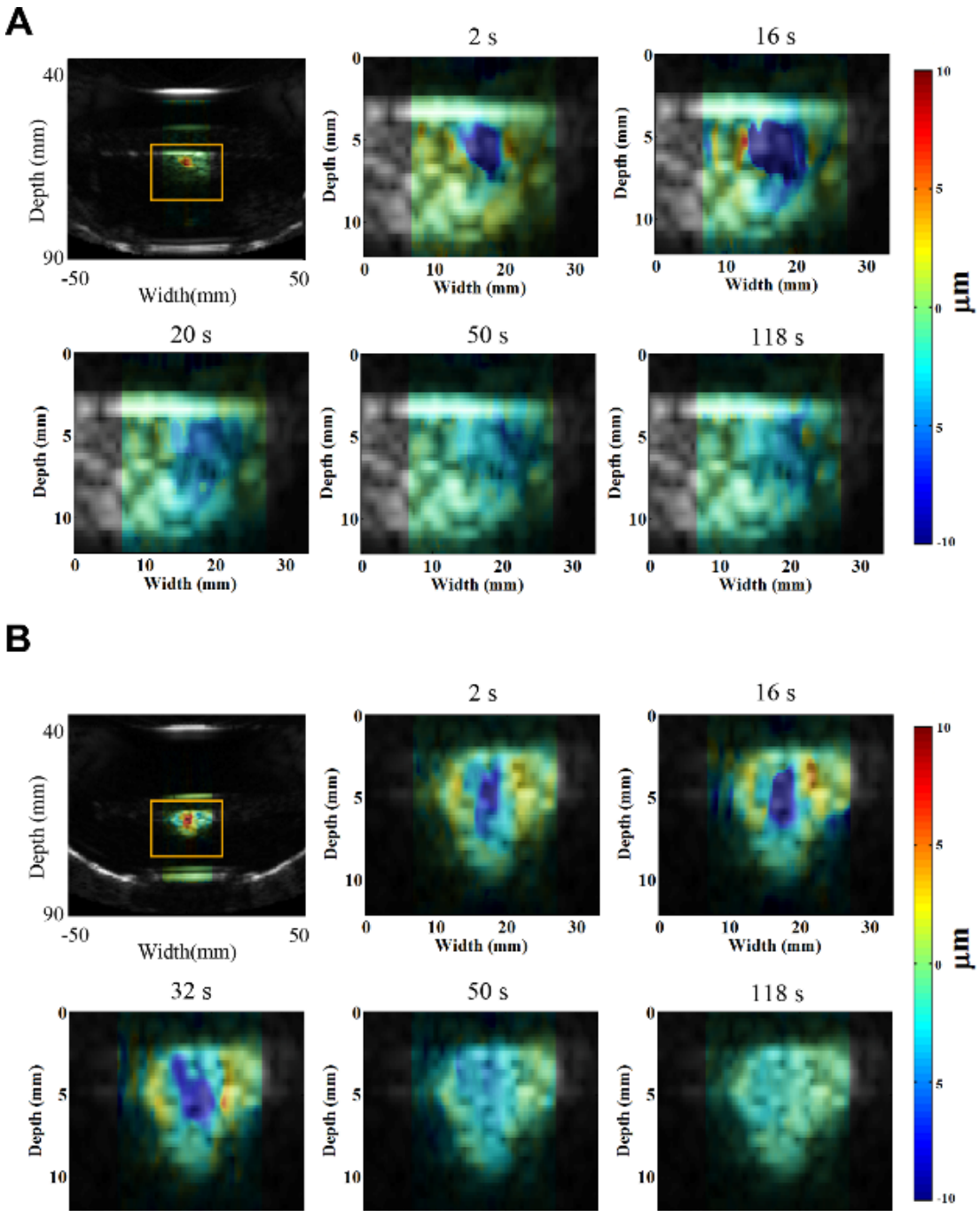

Figure 6.10 HMIgFUS ablation monitoring in 2D overlaying on B mode images in normal breast tissue (A) and IDC (B). Tissue motion during heating is denoted by alternating red and blue. In red, the motion moving toward the transducer, and in blue represents the motion moving away from the transducer. Peak negative HMI displacement frames during a 50-Hz cycle at 5

representative time points were selected from the HMIgFUS treatment monitoring sequence to show the decrease of focal displacement as the thermal lesion forms.

The normalized HMI displacement change over the entire HMIFU ablation process in all specimens is shown in Table 6.3. Compared to the initial displacement at the beginning (t = 2 s), the HMI displacement at the end (t = 118 s) of the HIFU ablation was observed. The HMI displacement amplitude in normal breast and IDC was 53.84% and 44.69% lower at the end of 2-min HMIFU ablation compared to those at the beginning of HMIFU exposure, showing consistent stiffening after HMIFU ablation. The representative H&E staining results after HMIFU are shown in Figure 6.11. Characteristic and similar histologic changes are seen in normal breast parenchyma, FA or IDC i.e. all tissues exposed to HIFU. The sections showed discrete hypereosinophilic areas reflecting changes occurring in the collagenous stroma as well as cautery like "streaming" phenomena in the HIFU ablated epithelial regions. The changes seen in the epithelium/nuclei are (non-neoplastic, benign or malignant) reminiscent to what is seen in tissue exposed to electrocautery change. Surrounding tissues are histologically unchanged.

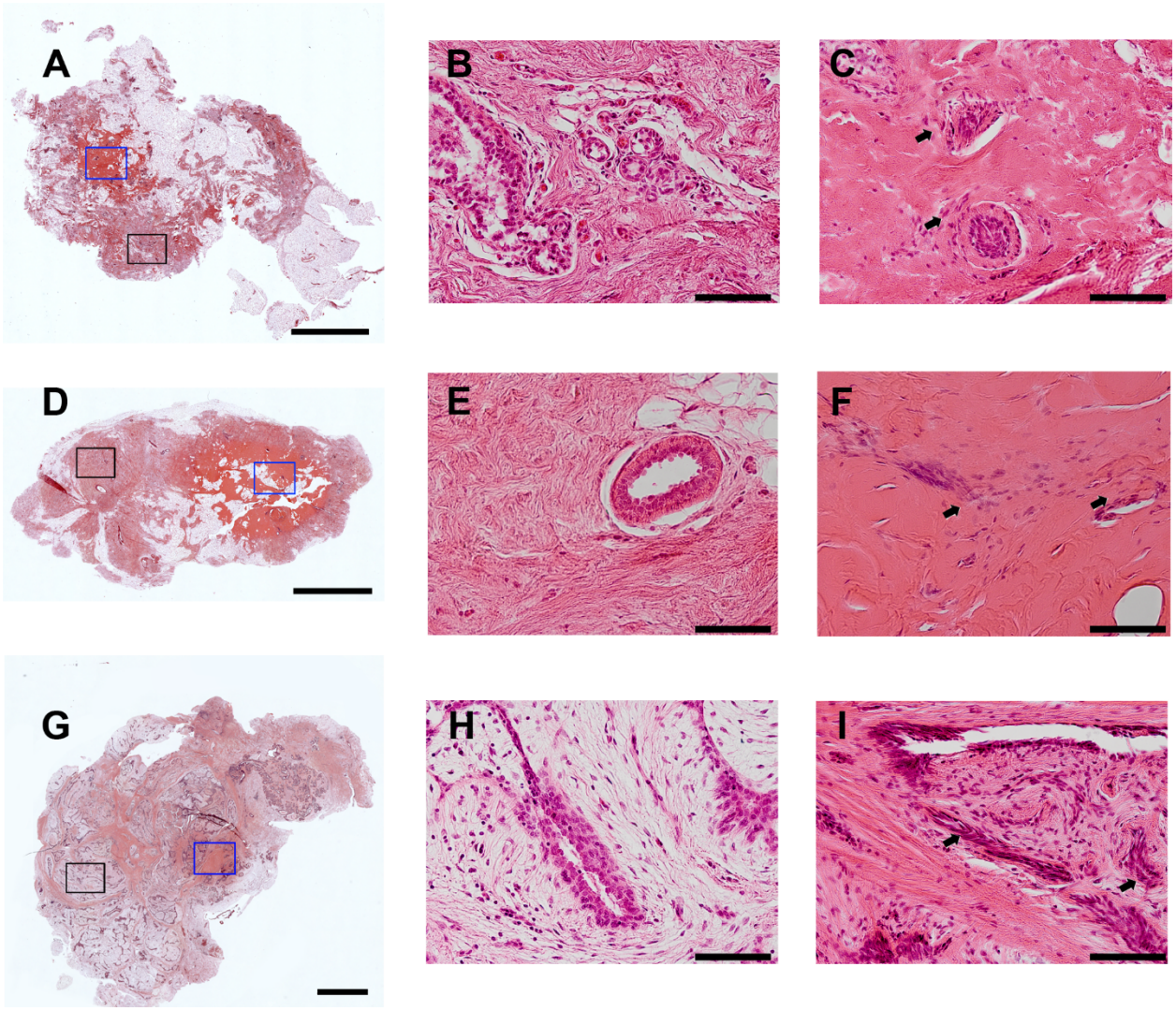

Figure 6.11 Example H&E staining of HMIFU ablated normal breast (A-C), IDC (D-F) and FA (G-I). In A, D and G, scale bar indicates 4 mm; in the rest of the images, scale bar indicates 0.1 mm. B, E and H are high magnification images of unablated region taken within the corresponding black frames, and C, F and I are high magnification images of ablated region taken within the corresponding blue frames. The ablated regions show discrete hypereosinophilic areas reflecting changes occurring in the collagenous stroma as well as cautery like "streaming" phenomena (arrow) in the HIFU ablated epithelial regions. The changes seen in the epithelium/nuclei are (non-

neoplastic, benign or malignant) reminiscent to what is seen in tissue exposed to electrocautery change. Surrounding tissues are histologically unchanged.

6.4 Discussion

The clinical application of HIFU in tumor treatment is currently hampered by the lack of a simple, cost-efficient device to reliably monitor HIFU treatment that can be utilized at the point-of-care. Experimental HMI images presented in this study demonstrate two important facts: 1) HMI is capable of detecting and imaging breast tumors in situ; 2) HMIFU provides the capability of monitoring tissue stiffness changes during simultaneously probing and forming lesions within the breast tissue.

It was found that HMI displacement amplitudes in the IDC and FA were on the average 43% and 85% lower than that in the normal breast, respectively. Although the tissue elasticity cannot be directly measured, this displacement contrast ratio can be indexed for relative stiffness of different types of tissues in the breast, considering a similar level of radiation force was applied. Histological analysis shows that in the setting of low FUS exposure during tumor detection, no tissue damage is found, which demonstrates that HMI can be performed without causing tissue damage.

In the entire mastectomy results, the malignant breast tumors have been observed to be stiffer than the surrounding tissue and sometimes larger in size in elasticity images than in B-mode images. This is consistent with observations in breast elastography [10], [139], [140] and can be attributed to the cancer infiltrating the surrounding tissue which serve to anchor the lesion and stiffen the surrounding tissue. One limitation of this study lies in the raster scanning method used

in the 2D HMI experiment. Depending on the size of the ROI, a raster scan covering the tumor and its surrounding area takes 2-3 minutes. Therefore, it may be subject to motion artifacts induced by respiratory motion in patients. Another ongoing study using electronic steering of the FUS beam to sweep the focal spot will help facilitate the imaging process.

Besides tumor detection, HMI offers unique solutions to HIFU tumor ablation monitoring. In this study, for the thermal treatment of tumors *ex vivo*, an acoustic power of 11 W or 8.7 W and a duration of exposure of 120 s for each location were used. Significant reduction (53.84% decrease in normal and 44.69% decrease in IDC) in the HMI displacement amplitude in the tumor after HIFU ablation was observed. This indicates that the HIFU induced lesions could be detected through the reduction in the harmonic motion amplitude. HMI monitors the lesion formation based on the underlying tissue stiffness changes. Therefore it can be more reliable than monitoring lesion formation by tracking the presence of cavitation or boiling bubbles, which are by definition stochastic phenomena used currently in the clinic for HIFU treatment monitoring [141]. We demonstrated that HMI is feasible for monitoring HIFU ablation in human breast tissue without interrupting HIFU treatment.

Application of HMI for breast imaging and HIFU monitoring is both promising and challenging. The overall displacement acquired with the 1D system was higher than that acquired with the 2D system due to the acoustic output difference between the 2 systems. It may be due to the higher efficiency of the 1D system which generated higher radiation force therefore higher displacement in the focal region. The output acoustic power used in the 2 systems were 11 W and 8.7 W, respectively. Both systems, however, showed similar displacement contrast between normal breast tissue, IDC and FA after normalization. Therefore, the power difference in this study does not influence the ability of HMI to differentiate abnormal from normal tissues. However, it

should be noted that the very low acoustic power output could potentially reduce the SNR with depth. Another limitation in this study lie in the raster scanning used in the experiment for 3D HMI. It involves a relatively lengthy process and thus will be subject to motion artifacts induced by respiratory and cardiac motions when applied in patients. Ongoing studies use electronic steering of the FUS beam to sweep the focal spot in order to facilitate the imaging process.

Furthermore, although off-line processing was used in this study, the 2D HMI system has the fundamental capability of on-line monitoring [99]. Ongoing work explores the potential of using on-line HMI to provide feedback control of the HMIFU ablation in order to control HMIFU therapy. Lastly, 2D HMI clearly located the HMIFU focal region and monitored the stiffness change of the focal region over time. However, because of the difficulty involved in sectioning through the excised breast to co-register with the imaging plane of the HMI, precise quantitative comparisons of actual lesion size and HMI displacement images cannot be performed with confidence. To assess the thermal lesion size based on the HMI images, additional studies are needed to correlate the HMI displacement map with histological measurements and define a quantitative threshold in HMIFU displacement change that corresponds to lesion formation, allowing physicians to easily identify the onset of lesion formation. Future studies will also consider the correlation between tissue structures and HMI characteristics to better understand tissue mechanical responses during HMIFU ablation.

HIFU has been available in the United States to treat uterine fibroids, prostate tumors and relieve pain from bone metastases. Moreover, there is a growing number of clinical applications at various stages of research and development around the world, including breast cancer [64], pancreatic cancer [35], and brain tumors [142]. MRgFUS has the advantage of high spatial resolution with thermometry capability. However, the intrinsic low frame rate of MRI prohibits

real-time monitoring of the treatment. On the other hand, USgFUS allows for real-time imaging at a relatively low cost. Different from conventional B-mode monitoring which relies on the appearance of hyperechoic spots resulting from boiling, HMIFU can provides relative tissue stiffness changes in real-time without interfering the HIFU treatment. Future clinical HMIFU could thus be used in an outpatient setting. In addition to relatively low costs associated, HMIFU will also be characterized by its non-invasive nature and reduced adverse effects.

The current study laid the foundations for future development of HMI as a clinical monitoring technique for breast HIFU with the added capability to detecting tumors for treatment planning, evaluate tissue stiffness change during HIFU ablation for treatment monitoring in real time, and assess the thermal lesion sizes after treatment evaluation.

6.5 Conclusions and Summary

In this chapter, we present a noninvasive imaging method for imaging *ex vivo* breast tumor specimens and monitoring of HIFU ablation. Results indicate that breast tumors confirmed with pathology can be detected by HMI. HMI has been experimentally shown to be capable of mapping and differentiating stiffness in normal and abnormal breast tissues. HMIgFUS can also successfully generate thermal lesions on normal and pathological breast tissues.

CHAPTER 7. *In vivo* human breast tumor characterization using Harmonic Motion Imaging (HMI)

7.1 Introduction

It has been established that cancer growth results in the alteration of the underlying mechanical properties of the breast tissue. In fact, the typical stiffening of tissues as a result of breast cancer is usually detected through palpation by the physician and/or self-examination. However, as a non-quantifiable diagnostic method, palpation is restricted to detection of tumors at locations close to the skin surface while standard techniques, such as mammography and sonography, cannot provide the difference in stiffness of the tumors in order to detect them at larger depths under the skin surface. Despite its proven high sensitivity, mammography has been shown to miss tumors that can be palpated, and is not as efficient in breast cancer screening in women below the age of 50. The National Cancer Institute states that the radiation-induced mutation can cause breast cancer, especially if exposed before the age of 30 years. Annual breast screening is recommended starting at (1) 40 years of age for the general population; (2) 25 to 30 years of age for carriers of the breast cancer 1 gene and untested relatives of carriers; (3) 25 to 30 years of age or 10 years earlier than the age of the affected relatives at diagnosis (whichever is later) for women with first degree relatives with premenopausal breast cancer or for women with lifetime risk for breast cancer 20% on the basis of family history [143]. There is a need to develop a highly reliable and low-cost imaging technique for characterization and differentiation tumor (begin and malignant) in breast, based on the distinct mechanical property of the tumor that can be 5-30 times harder than the normal tissues.

In this chapter, we propose to investigate the potential complementary role of a novel, non-ionizing and noninvasive imaging technique, Harmonic Motion Imaging (HMI), which can provide measurements of the locally generated mechanical responses and inherent mechanical properties of tissues. The result is a new image that contains unique localized information on the relative stiffness in and around the tumor. In addition, the vibratory nature of the excitation and localized response estimation allows for the direct measurement of tissue hardness. This allows for the tumor to be differentiated on the HMI image due to its distinct mechanical properties. The HMI technique does not share the requirements of previously developed mechanical methods, such as additional acoustical devices, use of external stimulus, or measurement of the response after stimulus application. The feasibility of the technique has already been demonstrated on theoretical models, tissue-mimicking materials, *in vivo* animal models and post-surgical human breast specimens. When it comes to the clinical translation of HMI, the limitation of the presented system in previous chapters lies in two aspects: immobility and relative slow raster scan schematic. The studies previously described rely on a 3D positioning system installed on an air table. Nevertheless, in a clinical setting where clinicians need to perform treatment localization, monitoring, and assessment, it is important to develop a mobile and compact HMI system with the same capability to hold and move the transducers precisely. The fast image reconstruction algorithm allows for real-time rendering with a temporal resolution of 4.5 Hz [99], [115]. This allows for the tumor to be differentiated on the HMI image due to its distinct mechanical properties. This chapter will test the initial feasibility on human subjects

A clinical HMI system will be built with a 4 degree of freedom robotic arm to be able to move the transducer precisely for raster scan. For the patients who are planned by their healthcare

providers to receive ultrasound-guided breast biopsy, the HMI scan will be performed in the biopsy room right before the biopsy procedure.

7.2 Methods

7.2.1 HMI clinical system

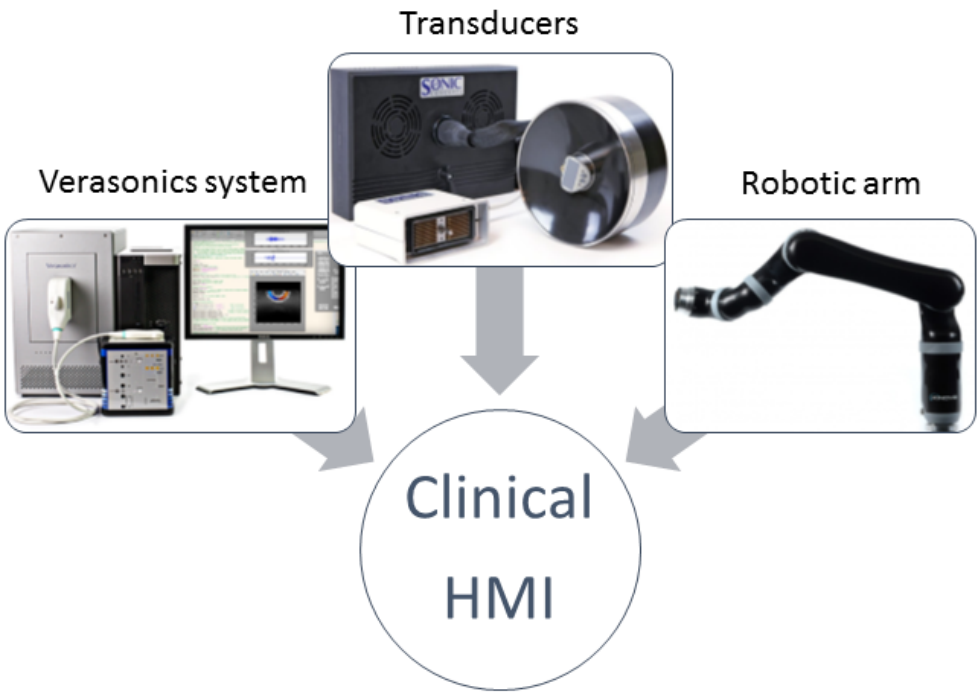

Figure 7.1 Schematic of 3 major components of HMI clinical system.

The HMI clinical system (Figure 7.1) consisted of 3 parts: 1) an ultrasound imaging research system (Vantage, Verasonics, Bothell, WA, USA) with a designated host PC (Precision T7500, Dell Inc., Austin, TX, USA) for system control, real-time display and data acquisition; 2) a FUS transducer (fc = 4 MHz, and D = 60 mm, Sonic Concepts Inc., Bothell WA, USA) and a phased array imaging probe (a 64-element phased array, fc = 2.5 MHz, P4-2, ATL/Philips, Bothell,

WA, USA) confocally-aligned through the central opening (diameter = 41 mm) of the FUS transducer for imaging and motion tracking; 3) a robotic arm (JACO2, Kinova inc., Boisbriand, Quebec, Canada) for automatic raster scan. The robotic arm was mounted on a mobile cart and controlled via either a joystick or the PC through a USB cable. The transducer pair was mechanically moved using the robotic arm for positioning and point-by-point raster scan as needed. In order to synchronize the acquisition of the monitoring signals (i.e., the pulse-echo imaging sequence) with the onset of HIFU treatment, the FUS transducer was simultaneously triggered with the Verasonics imaging system through a MATLAB-based (Mathworks, Natick, MA, USA) custom algorithm on a host PC.

The channel data signals were individually acquired through a 64-element phased array and the Verasonics system using a custom single-transmit based plane-wave wave front imaging sequence. The acquisition frame rate was set at 1000 frames/s, the analog-to-digital (A/D) sampling was chosen to be 10 MHz which is 4 samples per wavelength at a 2.5 MHz transmitting frequency. The acquisition sequence was repeated continuously while the acquired frames were transferred in a stacked set of 60 frames through an external function operated within the host PC. Additional reconstruction algorithms including beamforming and linear interpolation were computed offline to facilitate the data acquisition and data transferring processes.

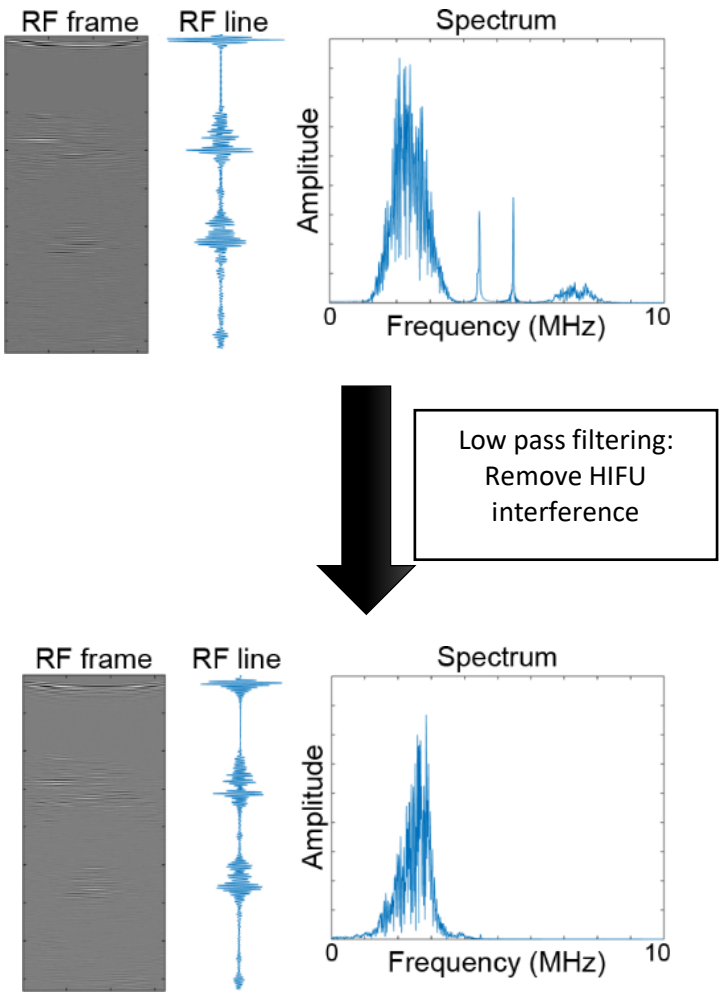

Figure 7.2 HMI data processing. Using lowpass filter to remove the interference from HIFU.

7.2.2 HMI clinical protocol

Patient recruitment process was approved by the institutional review board of Columbia University, and informed consent was obtained from all enrolled patients. In collaboration with the radiology department and the surgery department, patients who were planning to receive ultrasound-guided biopsy or breast surgery are eligible, were contacted by study coordinator after their office visit. After meeting with the patient and obtaining full consent for our ultrasound study,

we planned for HMI scan. The HMI scan was on the day of and prior to their scheduled biopsy or surgery. The HMI clinical study did not delay or hinder patient medical care, drug delivery, or time to biopsy or surgery. Patients received appropriate standard of care by their diagnostic and treating physicians regardless of whether they decide to participate in our study.

The inclusion and exclusion criteria are: 1) female patients (age > 18 years) with symptomatic breast mass which is visible on us; 2) female patients (age > 18 years) with breast mass which is invisible on us but palpable; 3) the ideal target lesion upper boundary should be within 10 mm from the skin; 4) the ideal target lesion lower boundary should be within 20 mm from the skin; 5) exclusion criteria are pregnant or lactating women, women with breast implants and women with a history of laser or radiation therapy to the targeted breast. All procedures relating to the research study was carried out in a private room. Our ultrasound exam took 15-20 minutes prior to their scheduled breast biopsy or surgery. Imaging data acquired during research procedures was anonymized and encrypted, and immediately removed from the ultrasound systems and transferred to the secure endpoint using an encrypted portable hard drive. After the transfer is complete, the imaging data was also being removed from the portable drive.

In the HMI imaging procedure, a B-mode ultrasound image was first obtained using the imaging probe only to locate the tumor. Then, a region of interest (ROI) area ranging from 20x20mm to 60x60mm was be chosen and specified on the PC. Then, a point-by-point HMI raster scan with a step size of 2-3 mm was performed within the ROI area to acquired 2D RF data. At each spot, the FUS exposure was 0.06 seconds long (3-cycle oscillations at 50 Hz), during which 60 RF frames at 1000 Hz pulse repetition frequency (PRF) were acquired. The 2D displacement data was be saved and reconstructed into 2D HMI image offline.

7.3 Results

7.3.1 Clinical system development

In order to test the acoustic output of our imaging probe, a standard experimental setup was used. The imaging ultrasound probes (P4-2, ATL/Philips, Bothell, WA, USA) was suspended in a degassed water bath with the transducers face oriented towards a hydrophone (Onda HGL-0400), a highly-sensitive device capable of measuring ultrasound pressures. The hydrophone was positioned in the spatial peak of the pressure field, and pressure measurements were digitized and saved onto a computer for post-processing. Pressure measurements were recorded for all possible output levels. The pressures recorded are related to both the $Ispta$ and MI, which were calculated from these measurements. This experiment was performed by two operators, who obtained similar results. Having obtained a calibration between output level (2-10V) and acoustic intensity, limits were incorporated into the Verasonics user interface. Calibration data is hard-coded in the ultrasound scanner, so the user will only be able to apply output levels from 0 to within 90% of the FDA limits ($Ispta$ of 84.6 mW per cm squared and MI of 1.71). Because two parameters are limiting the output, $Ispta$ and MI, the most restrictive limit will be used as our hardcoded output limit.

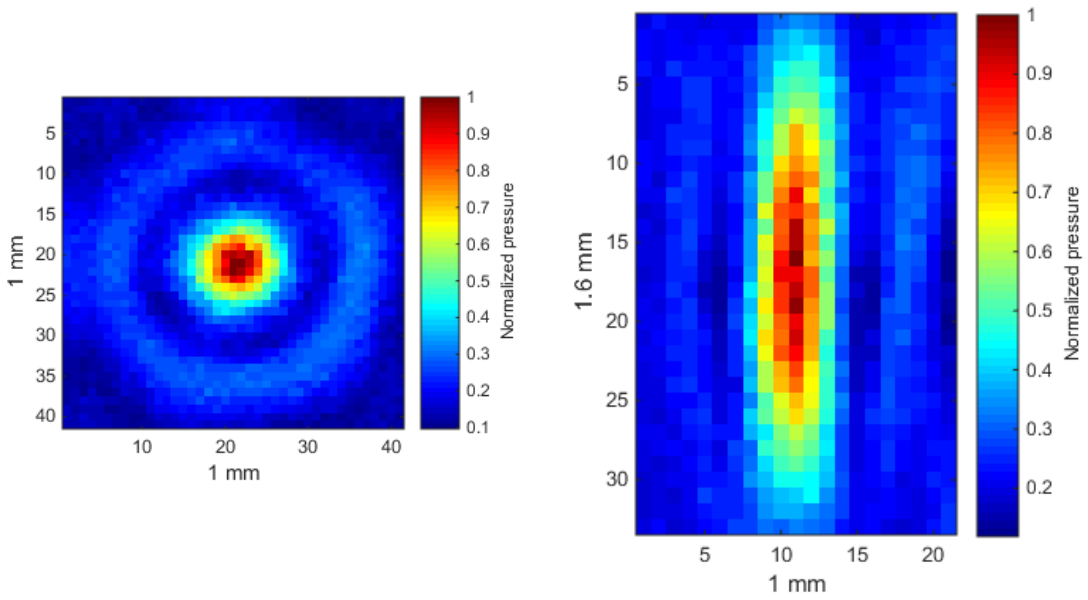

Figure 7.3 Normalized free field focal spot in transvers plane (left) and axial plane (right).

In order to test the acoustic radiation force output of our ultrasound system, a standard experimental setup similar to that described [144] was used. The *MI* of the pushing beams used for HMI imaging was less than the United States Food and Drug Administration limit of 1.9, and is consistent with those used in color Doppler imaging. Therefore, the potential for generating none-thermal bio effects (i.e., cavitation) with the HMI pushing beams is no greater than that for conventional color Doppler pulse sequences with a similar MI. A worst-case estimate of the potential temperature increase resulting from the pushing beams used in HMI imaging can be estimated by solving the Bioheat transfer equation [145] neglecting convection and conduction [146]. Under these assumptions, the equation becomes a first order linear differential equation, whose solution provides a linear relationship between temperature increase and application time:

$$dT = \frac{q_v t}{g_v} = \frac{2aIt}{g_v} \tag{7.1}$$

where T is the increase in temperature, q_v is the rate of heat production per unit volume, g_v is the volume specific heat for tissue, a is the absorption coefficient of tissue, I is the temporal average intensity of the acoustic beam in a given spatial location, and t is the application time. For the pushing beams used in HMI imaging, the peak anticipated temperature increase in each pushing location is 1°C ($a = 0.43\ Np/cm$ at 4.5 MHz), $I = 1000\ W/cm^2$ (in situ), $g_v = 4.2 \frac{J}{cm^3}/°C$, $t = 0.01\ s$). The spatial separation of the pushing locations results in minimal accumulation of heat between locations. Thermal increases by less than 1.0°C are considered acceptable during diagnostic US scanning [147];and, thus, the HMI push beam sequences used in these experiments do not pose an increased risk to the patient over that of conventional US imaging.

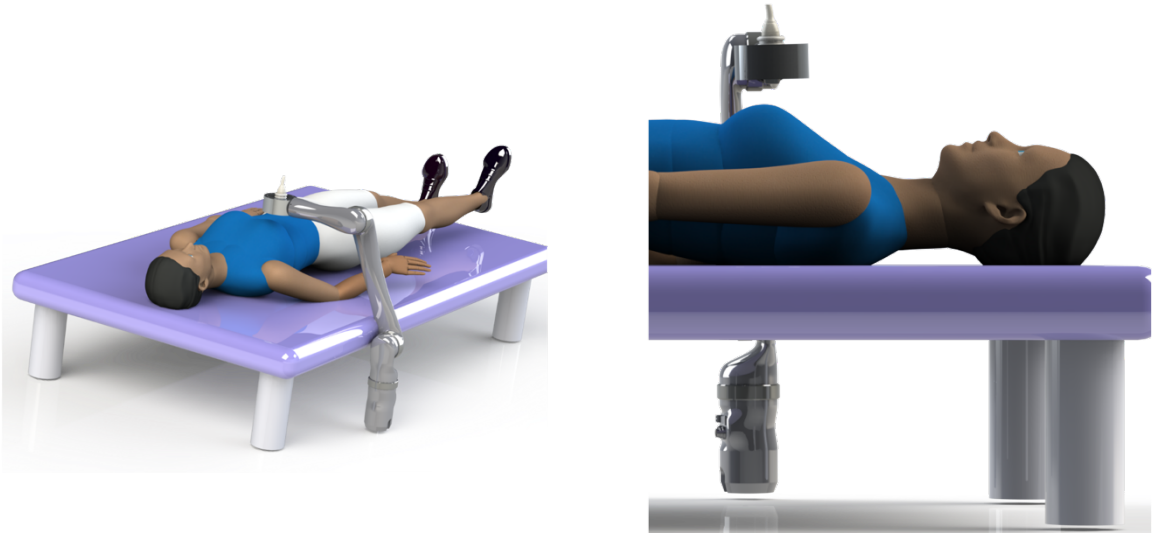

Figure 7.4 3D rendering of HMI clinical system robotic arm and transducers.

7.3.2 Patient results

From October 2017 to November 2017, 2 patients participated HMI clinical imaging study and 1 of the 2 patients had a biopsy after the HMI imaging procedure. The decision to biopsy was based on the clinical features, and HMI characteristics were not used to determine biopsy indications. HMI acquisition was performed the same day, just before the biopsy. Breast lesions from both patients were visible on ultrasound sonography (B-mode). The results from 1 patient was not considered due to the technical difficulty encountered during the data acquisition process.

A representative HMI map is shown in Figure 7.3 obtained from a patient with a known fibroadenoma (Figure 7.3 B-mode image shows a hypoechoic mass lesion within the yellow dashed rectangle area). The HMI images was taken from the 30x20 mm yellow dashed rectangle area denoted in the B-mode image. Normalized tissue displacement plotted in color map where blue shows low in displacement and re shows high in displacement. A 5mm-diameter circular region of interest (ROI) was chosen within the tumor area and the surrounding tissue with displacement amplitude of 1.90 ± 0.40 μm and 3.05 ± 0.60 μm in the fibroadenoma and the surrounding tissue respectively.

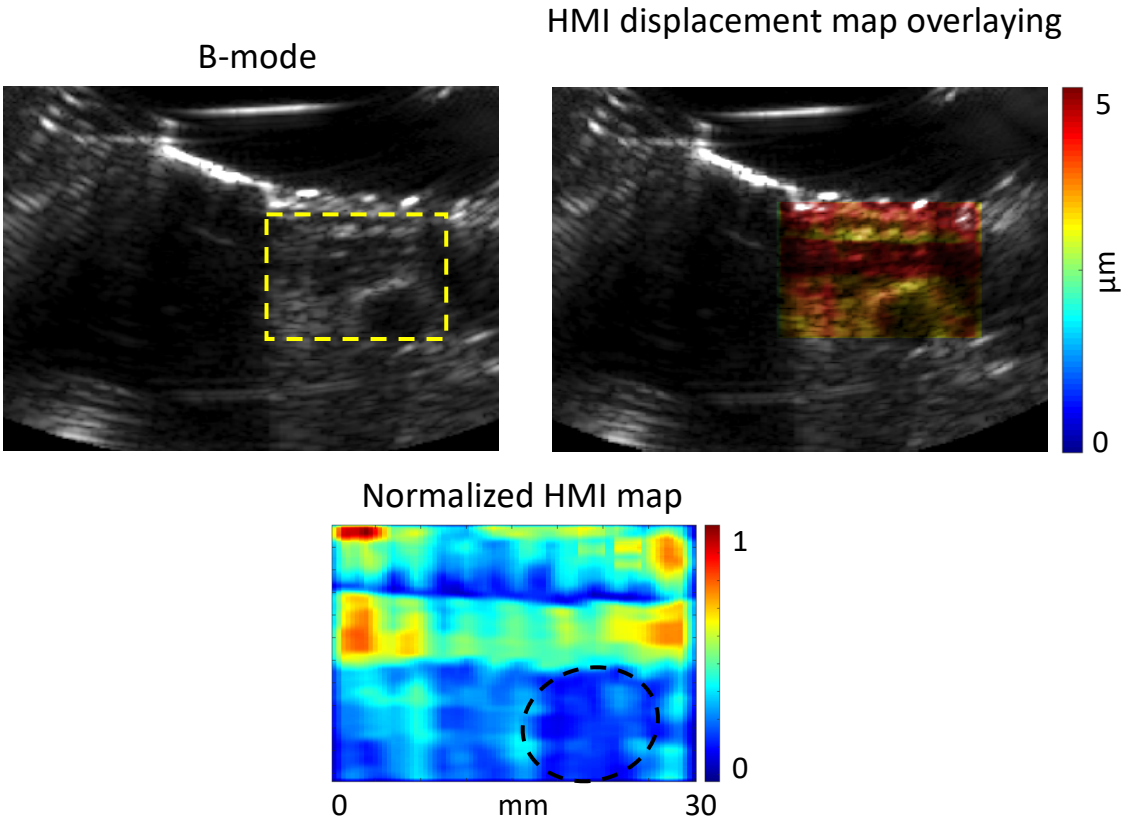

Figure 7.5 B-mode and HMI map of a patient with a fibroadenoma. The HMI images was taken from the yellow dashed square denoted area in the B-mode image. Normalized tissue displacement plotted in color map where blue shows low in displacement and red shows high in displacement.

7.4 Discussion

Harmonic Motion Imaging (HMI) is a novel imaging technique that applies an oscillatory force locally and at different depths in the tissue, in order to determine the characteristics of the resulting localized harmonic motion using high precision tracking methods. In this chapter, the first HMI system was developed and prototyped for the clinical application of breast tumor

characterization. The first HMI clinical trial was designed, proposed and been approved by the institutional review board of Columbia University. Chapter 6 has shown that, in *ex vivo* breast specimens, HMI displacement amplitudes in the invasive ductal carcinoma and fibroadenoma were, on average, 43 % and 85 % lower, respectively, than that in the surrounding breast tissue. In this chapter, we have further optimized HMI method for breast tumor characterization *in vivo* and evaluated of its potential clinical role in detection of breast cancer.

In comparison with other elasticity based technique, HMI has the advantage of using FUS transducer to generate a localized radiation force to probe deep tissue or tumor. Using HMI, highly localized harmonic motion can be noninvasively generated by ultrasonic beams deep inside the tissue and estimated at high precision, by using RF signals and cross-correlation methods. Due to the highly localized and harmonic nature of the response, the motion characteristics can be directly linked to the local tissue modulus.

Despite our successful implementation and feasibility study using the HMI clinical system for breast tumor characterization, there are several limitations of the first prototype HMI clinical platform. The current prototype requires a water bath for coupling in between the transducer and the skin in order to move laterally and axially. In the meanwhile, the raster scan procedure is relatively slow due to the mechanical movement. To overcome this limitation, using electronic beam steering for HMI as described in Chapter 5 can scan multiple points without mechanical movement of the transducer and the water bath is not needed anymore. Using electronic beam steering can also significantly increase the imaging speed and shorten the imaging duration from the order of minutes to the order of seconds. A FUS phased array is needed with higher number of elements and lower central frequency for increased steering range. Another limitation of the current HMI clinical system lies in the fact that all images of the 2D acquisition were constructed

offline after the imaging procedure. The beam forming and image reconstruction computational cost can vary between 5 and 20 minutes, depending on the matrix dimension of the specific raster scan, which depends on the tumor size and the ROI area. This hinders the clinical system from real-time visualization of the HMI displacement map over the ROI. Therefore, in order to successfully translate the first prototype HMI clinical system towards a more clinical friendly setting, it is necessary to implement a fast data storage and processing algorithm capable of processing displacement, combining raster scan points and streaming real-time HMI displacement map back to the user. Boundary conditions may also affect the measurements as they impact the oscillation of the tissues probed. The shear wave component resulting from reflection was ignored in this study. This assumption is based on the small size of foci (0.25×1.25 mm^2) compared to the size of tumor, and the fact that our measurement is confined to the focal region.

The preliminary results shown in this chapter indicate that HMI can may be an additional tool for breast tumor detection and localization, it may also be used as a technique to assess chemotherapeutic response during such therapy. This mechanical effect of chemotherapy was previously observed in breast cancer by Falou et al. [148]. In this study, 15 women received neoadjuvant chemotherapy and were monitored using elastography for 8 weeks. Responders demonstrated a significant decrease in mechanical properties 4 weeks after treatment initiation compared to non-responding patients. Moreover, elasticity imaging has shown interesting potential to predict response to neoadjuvant therapy in breast cancer [149]–[151] demonstrating the different uses of elasticity assessment for cancer therapy.

The study in this chapter has laid foundation for the development of a clinical Harmonic Motion Imaging guided Focused Ultrasound (HMIgFUS) system for breast tumor treatment and monitoring. HMIgFUS is an all-ultrasound-based non-invasive treatment technique with added

capability of real time treatment monitoring, which can be used to investigate the underlying local tissue mechanical property without stopping the HIFU treatment.

7.5 Conclusions and Summary

The first HMI clinical system has been built with a robotic arm for fast raster scan with added capability of GUP-based parallel beamforming. A clinical trial has been approved to image breast tumor on patient with breast mass. The HMI clinical system has shown to be able to map fibroadenoma mass on one patient with valid HMI displacement consistent with previous *ex vivo* studies. This imaging technique is a non-ionizing, noninvasive, and low-cost imaging technique compared to currently available methods. The study in this chapter may yield an assistive diagnostic technique for breast cancer providing further information on the relative stiffness of the tumor without any age discrimination. This chapter also lays foundation for future development of a clinical HMIgFUS system with the added capability of treatment planning, treatment monitoring and treatment assessment.

CHAPTER 8. Conclusion summary and future works

8.1 Conclusion & summary

The scope of this dissertation has been focused on the system optimization, prototyping and clinical feasibility testing of a biomechanical assessment and monitoring of thermal ablation using Harmonic Motion Imaging guided Focused Ultrasound (HMIgFUS) for the application of breast tumor.

In Chapter 3, a new HIFU treatment planning method was described that used oscillatory radiation force induced displacement amplitude variations to detect the HIFU focal spot before lesioning. This method was applied on tissue-mimicking phantoms and *in vitro* tissues with both the 1D and 2D tracking HMI systems. Using this method, we were able to visualize the HMIgFUS focal region at variable depths before applying HIFU treatment. By comparing the estimated displacement profiles with the actual lesion locations in pathology, we demonstrated the feasibility of using this HMI-based technique to localize the HIFU focal spot and predict lesion location during the treatment planning phase of a successful HIFU treatment. The same application feasibilities were also demonstrated in a 2D preclinical system. We concluded that HMI has the potential of providing the capacity for HIFU planning.

In Chapter 4, A HIFU lesion detection and ablation monitoring method was developed using oscillatory radiation force induced displacement amplitude variations in real time. Performances were assessed *in vitro* in canine liver, and *in vivo* initial feasibility was shown in a mouse pancreatic tumor model. Using this method, the HMIgFUS focal region and lesion formation were visualized in real time at a feedback rate of 2.4 Hz. By comparing the estimated lesion size against gross pathology, we demonstrated the feasibility of using HMIgFUS to monitor

treatment and lesion formation without interruption during the treatment monitoring phase of a successful HIFU treatment. We concluded that HMIgFUS has the potential of providing the capability for real-time HIFU monitoring.

In Chapter 5, it was shown that using the steered FUS beam using a 93-element phase-array FUS transducer, HMI can be used to image a 2.3 times larger ROI without physical movement of the transducer. Using steering for HMI can be used to shorten the total imaging duration without requiring physical movement of the transducer. The main limitation of this study lies in the design of the FUS transducer, which constrained the effective steering range of the FUS beam to +/-1.7 mm and +/-2 mm in the lateral and axial direction.

In Chapter 6, HMI and HMIgFUS were optimized and applied to *ex vivo* human breast tissue. A noninvasive imaging method for imaging postsurgical breast tumor specimens and monitoring of HIFU ablation was presented. The results showed that HMI is experimentally capable of mapping and differentiating stiffness in normal and abnormal *ex vivo* human breast tissues. HMIgFUS can also successfully generate thermal lesions on normal and pathological breast tissues. HMI has also been applied to post-surgical breast mastectomy specimens to mimic the *in vivo* environment.

In Chapter 7, the first HMI clinical system was reported with added capability of GUP-based parallel beamforming. A clinical trial has been proposed and approved at Columbia University to image breast tumor on human subjects. The HMI clinical system has shown to be able to map fibroadenoma mass on one subject with valid HMI displacement consistent with previous *ex vivo* studies. The study in this chapter may yield an early-detection technique for breast cancer without any age discrimination and thus, increase the survival rate. This imaging technique

is a non-ionizing, noninvasive, and low-cost imaging technique compared to currently available methods.

8.2 Future directions

In order to build an integrated, all-ultrasound-based clinical HIFU system for breast cancer with the added ability of tumor characterization, there are improvement need to work on the three stages: 1) Treatment planning, 2) Treatment monitoring, and 3) Treatment Assessment.

For the treatment planning stage, a user friendly interactive interface needs to be built for tumor localization. With the interface, the physician is able to outline the breast mass on consecutive sections of B-mode scans and HMI displacement maps in order to the position of the focal zone relative to the breast mass center. Thereafter, the number of treatment units and the time for treatment will be automatically calculated to cover the target volume with extra margin of normal tissue. A Systematic review [34] of HIFU ablation in the treatment of breast cancer including 9 studies has found the extra margin of normal tissue ablated around the target tumor in the included studies varied from 0.5 to 2 cm. The two studies [133], [152] with a margin of between 1.5 and 2 cm are the only two to report complete necrosis of the lesion in all patients, and both used ultrasound-guided HIFU therapy. In order to achieve complete necrosis of the lesion in all patient, a margin of 1.5 - 2 cm will be used in our study.

In treatment monitoring, ongoing efforts will focus on designing a FUS transducer with more elements and lower center frequency to enlarge the effective steering range for HMI. The feasibility of using electronic steering for HMIgFUS has been proven in Chapter 5 as it facilitates both HMI and HMIgFUS process by electronically steering the focal spot to several different predetermined locations. Using electronic steering can significantly increasing the

imaging/treatment area and shortening the imaging duration without physical movement of the transducer. However, the current steering range is limited by the design of the current FUS transducer. Therefore, designing a FUS transducer with more elements and lower center frequency can effectively enlarge both axial and lateral steering range for HMI. Other ongoing efforts include the on-line HMI focal spot localization to provide real-time feedback control to reduce treatment time and to enhance ablation accuracy during the HIFU treatment. Real-time feedback control algorithms for HIFU therapy based on pulse-echo ultrasound imaging have been tested in previous research [153]–[156]. Curiel et al. evaluated the feasibility of using localized HMI to monitor and control HIFU ablation in a rabbit tumor model. The treatments were automatically stopped if the detected localized harmonic motion amplitude at the focal spot dropped below a specified amplitude threshold in two consecutive measurements. This algorithm was able to successfully control ablation in 69% of the trials [154]. Using the real-time lesion detection and ablation monitoring method (Chapter 4), lesion size monitoring was achieved and lesion formation were visualized in real time at a feedback rate of 2.4 Hz. It also laid foundation for a real-time feedback control system based on the estimated lesion size growth curve. The treatments should automatically stop if the estimated lesion size is shown to not increase in size or the growth rate is under a set threshold.

From the system aspect, HMIgFUS can be integrated into commercial HIFU systems, such as the Theraclion Echopulse system (Figure 8.1). It has shown capability to effectively treat thyroid nodule with proven of macroscopic and microscopic histological examinations of thyroid tissue removed during surgery [32]. Echopulse is also in clinical trial overcome the prolonged treatment duration in benign breast tumor by applying HIFU pulses to the circumferential surface area rather than the whole volume with ultrasound B-mode guidance [157]. In another clinical trial, twenty

female patients diagnosed with palpable, non-calcified breast fibroadenomas 1cm or larger are enrolled in a single arm clinical trial and undergo HIFU treatment using the Echopulse system [158]. The Echopulse is equipped with a linear array imaging transducer (number of elements = 128, center frequency = 7.5 MHz) confocally-aligned with the focused ultrasound transducer to acquire B-mode images from the target area. This transducer is designed by Theraclion for the application in thyroid and breast, and has shown to be able to provide high quality B-mode images from 40 mm distance from the skin. This phased imaging array will also satisfy the imaging application in mice with sufficiently high in resolution due to the high center frequency. The HIFU and imaging frequencies are sufficiently distinct to effectively filter out the HIFU spectrum. Their clinical HIFU system will be programed to perform HMIgFUS in the Visualization and Treatment Unit (VTU) using their research platform that provides full control over the beamformer and overall programming in addition to the robotic arm. The imaging transducer can be operated by an open-architecture system (Vantage, Verasonics, Redmond, WA).

To test the feasibility of using Theraclion Echopulse for HMI, a Visualization and Treatment Unit (VTU) from the Echopulse system was modified to connect to an ultrasound imaging research system (Vantage, Verasonics, Bothell, WA, USA) to track the displacement in conjunction with a HIFU transducer as shown in Figure 8.3 shows the focal area and displacement over time detected by VTU on the *in vitro* liver specimen.

Figure 8.1 Echopulse, a high-intensity focused ultrasound (HIFU) treatment by Theraclion. Source: http://www.theraclion.com

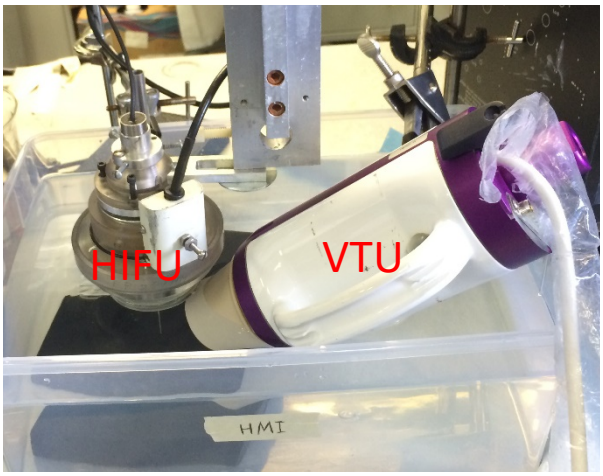

Figure 8.2 HMI feasibility test with Thercalion Echopulse VTU connected to a Verasonics system.

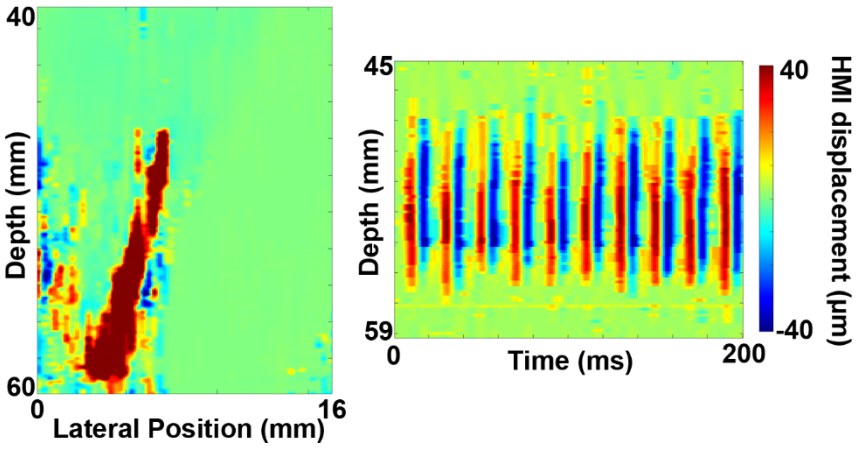

Figure 8.3 (Left) Theraclion VTU acquired HMI peak-to-peak displacement in liver specimen. (Right) Theraclion VTU acquired HMI displacement over time.

With the development of high-frequency ultrasound imaging array, the usefulness of high-frequency ultrasound as a tool for diagnosis has been evaluated in clinic. High-frequency ultrasound elastography (8 - 40 MHz) has been used to assess cutaneous melanoma in human subjects [159]. HMI, as an elasticity-based imaging technique, will also benefit from high-frequency imaging array for both diagnosis and treatment monitoring.

BIBLIOGRAPHY

[1] American Cancer Society, "Breast Cancer Facts & Figures 2017-2018," 2017.

[2] T. Faruk, M. K. Islam, S. Arefin, and M. Z. Haq, "The Journey of Elastography: Background, Current Status, and Future Possibilities in Breast Cancer Diagnosis," *Clin. Breast Cancer*, vol. 15, no. 5, pp. 313–324, 2015.

[3] A. Sarvazyan *et al.*, "Biophysical Bases of Elasticity Imaging," in *Acoutical Imaging*, vol. 21, 1995, p. 223.

[4] K. R. Nightingale, M. L. Palmeri, R. W. Nightingale, and G. E. Trahey, "On the feasibility of remote palpation using acoustic radiation force," *J. Acoust. Soc. Am.*, vol. 110, no. 1, pp. 625–634, 2001.

[5] L. Tabar, B. Vitak, H.-H. Chen, M.-F. Yen, S. W. Duffy, and R. A. Smith, "Beyond randomized controlled trials Organized Mammographic Screening Substantially Reduces Breast Carcinoma Mortality," *Cancer*, vol. 91, pp. 1724–31, 2001.

[6] S. W. Duffy, "Reduction in breast cancer mortality from organized service screening with mammography: 1. Further confirmation with extended data," *Cancer Epidemiol. Biomarkers Prev.*, vol. 15, no. 1, pp. 45–51, 2006.

[7] W. A. Berg, "Tailored supplemental screening for breast cancer: What now and what next?," *Am. J. Roentgenol.*, vol. 192, no. 2, pp. 390–399, 2009.

[8] C. D. Lehman *et al.*, "Cancer Yield of Mammography, MR, and US in High-Risk Women: Prospective Multi-Institution Breast Cancer Screening Study," *Radiology*, vol. 244, no. 2, pp. 381–388, 2007.

[9] A. I. Hagen *et al.*, "Sensitivity of MRI versus conventional screening in the diagnosis of BRCA-associated breast cancer in a national prospective series," *Breast*, vol. 16, no. 4, pp.

367–374, 2007.

[10] A. C. Sharma, M. S. Soo, G. E. Trahey, and K. R. Nightingale, “Acoustic Radiation Force Impulse imaging of in vivo breast masses,” vol. 0, no. c, pp. 728–731, 2004.

[11] M. Tozaki, S. Isobe, and M. Sakamoto, “Combination of elastography and tissue quantification using the acoustic radiation force impulse (ARFI) technology for differential diagnosis of breast masses,” *Jpn. J. Radiol.*, vol. 30, pp. 659–670, 2012.

[12] M. Fatemi, L. E. Wold, A. Alizad, and J. F. Greenleaf, “Vibro-acoustic tissue mammography.,” *IEEE Trans. Med. Imaging*, vol. 21, no. 1, pp. 1–8, Jan. 2002.

[13] A. Alizad *et al.*, “Breast vibro-acoustography: initial results show promise,” *Breast Cancer Res.*, vol. 14, no. 5, p. R128, 2012.

[14] M. Fink, “Supersonic Shear Imaging : A New Technique,” vol. 51, no. 4, pp. 396–409, 2004.

[15] A. Itoh *et al.*, “Breast Disease : Clinical Application Purpose : Methods : Results : Conclusion :,” vol. 239, no. 2, pp. 341–350, 2006.

[16] A. Athanasiou and A. Tardivon, “Breast Lesions : Quantitative Elastography with Supersonic Shear Imaging — Preliminary Results 1 Purpose : Methods : Results :,” vol. 256, no. 1, pp. 297–303, 2010.

[17] American Cancer Society, “Breast Cancer Facts & Figures 2015-2016,” 2016.

[18] M. Morrow *et al.*, “Society of Surgical Oncology–American Society for Radiation Oncology–American Society of Clinical Oncology Consensus Guideline on Margins for Breast-Conserving Surgery With Whole-Breast Irradiation in Ductal Carcinoma in Situ,” *Pract. Radiat. Oncol.*, vol. 6, no. 5, pp. 287–295, 2016.

[19] H. Furusawa *et al.*, “Magnetic Resonance-Guided Focused Ultrasound Surgery of Breast Cancer: Reliability and Effectiveness,” *J. Am. Coll. Surg.*, vol. 203, pp. 54–63, 2006.

[20] A. Hamza and S. Elrefaey, “Non-surgical treatment of early breast cancer: techniques on the way.,” *Gland Surg.*, vol. 3, no. 3, pp. 149–50, Aug. 2014.

[21] K. F. Chu and D. E. Dupuy, “Thermal ablation of tumours: biological mechanisms and advances in therapy.,” *Nat. Rev. Cancer*, vol. 14, no. 3, pp. 199–208, 2014.

[22] Z. Zhao and F. Wu, “Minimally-invasive thermal ablation of early-stage breast cancer: A systemic review,” *Eur. J. Surg. Oncol.*, vol. 36, pp. 1149–1155, 2010.

[23] S. S. Jeffery *et al.*, “Radiofrequency ablation of breast cancer: First Report of an Emerging Technology,” *Am. Surg.*, vol. 69, pp. 37–40, 1999.

[24] B. D. Fornage *et al.*, “Small Breast Cancer Treated with US-guided Radiofrequency Ablation: Feasibility Study,” *Radiology*, vol. 231, no. 11, pp. 215–224, 2004.

[25] T. Kinoshita, E. Iwamoto, H. Tsuda, and K. Seki, “Radiofrequency ablation as local therapy for early breast carcinomas,” *Breast Cancer*, vol. 18, pp. 10–17, 2011.

[26] T. Susini *et al.*, “Radiofrequency ablation for minimally invasive treatment of breast carcinoma. A pilot study in elderly inoperable patients,” *Gynecol. Oncol.*, vol. 104, pp. 304–310, 2007.

[27] B. D. Fornage and R. F. Hwang, “Current status of imaging-guided percutaneous ablation of breast cancer.,” *AJR. Am. J. Roentgenol.*, vol. 203, no. 2, pp. 442–8, Aug. 2014.

[28] E. Maloney and J. H. Hwang, “Emerging HIFU applications in cancer therapy,” *Int. J. Hyperth.*, vol. 31, no. 3, pp. 302–309, 2015.

[29] J. Lynn, R. Zwemer, and A. Chick, “The biological application of focused ultrasonic waves,” *Science (80-.).*, vol. 96, pp. 119–120, Aug. 1942.

[30] R. O. Illing *et al.*, “The safety and feasibility of extracorporeal high-intensity focused ultrasound (HIFU) for the treatment of liver and kidney tumours in a Western population,”

Br. J. Cancer, vol. 93, no. 8, pp. 890–5, Oct. 2005.

[31] J. E. Kennedy *et al.*, "High-intensity focused ultrasound for the treatment of liver tumours.," *Ultrasonics*, vol. 42, no. 1–9, pp. 931–5, Apr. 2004.

[32] O. Esnault *et al.*, "High-Intensity Focused Ultrasound Ablation of Thyroid Nodules: First Human Feasibility Study," *Thyroid*, vol. 21, no. 9, pp. 965–973, 2011.

[33] M. Warmuth, T. Johansson, and P. Mad, "Systematic review of the efficacy and safety of high-intensity focussed ultrasound for the primary and salvage treatment of prostate cancer," *Eur. Urol.*, vol. 58, no. 6, pp. 803–815, 2010.

[34] M. C. L. Peek *et al.*, "Systematic review of high-intensity focused ultrasound ablation in the treatment of breast cancer," *Br. J. Surg.*, vol. 102, no. 8, pp. 873–882, 2015.

[35] H. J. Jang, J.-Y. Lee, D.-H. Lee, W.-H. Kim, and J. H. Hwang, "Current and Future Clinical Applications of High-Intensity Focused Ultrasound (HIFU) for Pancreatic Cancer.," *Gut Liver*, vol. 4 Suppl 1, no. September, pp. S57-61, 2010.

[36] J. W. Wijlemans *et al.*, "Magnetic resonance-guided high-intensity focused ultrasound (MR-HIFU) ablation of liver tumours," *Cancer Imaging*, vol. 12, no. 2, pp. 387–394, 2012.

[37] G. ter Haar, "Ultrasound Focal Beam Surgery," *Ultrasound Med Biol*, vol. 21, no. 9, pp. 1089–1100, 1995.

[38] P. E. Huber *et al.*, "A New Noninvasive Approach in Breast Cancer Therapy Using Magnetic Resonance Imaging-guided Focused Ultrasound Surgery," pp. 8441–8447, 2001.

[39] F. Wu *et al.*, "A randomised clinical trial of high-intensity focused ultrasound ablation for the treatment of patients with localised breast cancer.," *Br. J. Cancer*, vol. 89, no. 12, pp. 2227–33, Dec. 2003.

[40] H. Furusawa *et al.*, "The evolving non-surgical ablation of breast cancer: MR guided

focused ultrasound (MRgFUS).," *Breast cancer*, vol. 14, no. 1, pp. 55–58, 2007.

[41] J. Z. Xia, F. L. Xie, L. F. Ran, X. P. Xie, Y. M. Fan, and F. Wu, "High-Intensity Focused Ultrasound Tumor Ablation Activates Autologous Tumor-Specific Cytotoxic T Lymphocytes," *Ultrasound Med. Biol.*, vol. 38, no. 8, pp. 1363–1371, 2012.

[42] Z. L. Xu, X. Q. Zhu, P. Lu, Q. Zhou, J. Zhang, and F. Wu, "Activation of Tumor-Infiltrating Antigen Presenting Cells by High Intensity Focused Ultrasound Ablation of Human Breast Cancer," *Ultrasound Med. Biol.*, vol. 35, no. 1, pp. 50–57, 2009.

[43] Q. Zhou, X. Q. Zhu, J. Zhang, Z. L. Xu, P. Lu, and F. Wu, "Changes in Circulating Immunosuppressive Cytokine Levels of Cancer Patients After High Intensity Focused Ultrasound Treatment," *Ultrasound Med. Biol.*, vol. 34, no. 1, pp. 81–87, 2008.

[44] J. Unga and M. Hashida, "Ultrasound induced cancer immunotherapy," *Adv. Drug Deliv. Rev.*, vol. 72, pp. 144–153, 2014.

[45] R. Cirincione *et al.*, "High-Intensity Focused Ultrasound– and Radiation Therapy–Induced Immuno-Modulation: Comparison and Potential Opportunities," *Ultrasound Med. Biol.*, vol. 43, no. 2, pp. 398–411, 2017.

[46] J. Ophir, I. Céspedes, H. Ponnekanti, Y. Yazdi, and X. Li, "Elastography: A Quantitative Method for Imaging the Elasticity of Biological Tissues," *Ultrason. Imaging*, vol. 13, no. 2, pp. 111–134, 1991.

[47] T. A. Krouskop, T. M. Wheeler, F. Kallel, B. S. Garra, and T. Hall, "Elastic Moduli of Breast and Prostate Tissues under Compression," *Ultrason. Imaging*, vol. 20, no. 4, pp. 260–274, 1998.

[48] M. Fatemi and J. F. Greenleaf, "Ultrasound-Stimulated Vibro-Acoustic Spectrography," *Science (80-.).*, vol. 280, no. 5360, pp. 82–85, Apr. 1998.

[49] E. E. Konofagou and K. Hynynen, “Localized harmonic motion imaging: theory, simulations and experiments,” *Ultrasound Med. Biol.*, vol. 29, no. 10, pp. 1405–1413, Oct. 2003.

[50] J. Bercoff, M. Tanter, and M. Fink, “Supersonic Shear Imaging : A New Technique for Soft Tissue Elasticity Mapping,” *IEEE Trans. Ultrason. Ferroelectr. Freq. Control*, vol. 51, no. 4, pp. 396–409, 2004.

[51] A. J. Bamber *et al.*, “EFSUMB Guidelines and Recommendations on the Clinical Use of Ultrasound Elastography. Part 1: Basic Principles and Technology,” *Ultraschall Med*, vol. 34, pp. 169–184, 2013.

[52] T. Shiina *et al.*, “WFUMB Guidelines and Recommendations for Clinical Use of Ultrasound Elastography: Part 1: Basic Principles and Terminology,” *Ultrasound Med. Biol.*, vol. 41, no. 5, pp. 1126–1147, 2015.

[53] R. M. S. Sigrist, J. Liau, A. El Kaffas, M. C. Chammas, and J. K. Willmann, “Ultrasound elastography: Review of techniques and clinical applications,” *Theranostics*, vol. 7, no. 5, pp. 1303–1329, 2017.

[54] C. Maleke, M. Pernot, and E. E. Konofagou, “Single-Element Focused Ultrasound Transducer Method for Harmonic Motion Imaging,” *Ultrason. Imaging*, vol. 28, pp. 144–158, 2006.

[55] C. Maleke, J. Luo, V. Gamarnik, X. L. Lu, and E. E. Konofagou, “Simulation Study of Amplitude-Modulated (AM) Harmonic Motion Imaging (HMI) for Stiffness Contrast Quantification with Experimental Validation,” *Ultrason. Imaging*, vol. 32, pp. 154–176, 2010.

[56] J. Chen, G. Y. Hou, F. Marquet, Y. Han, F. Camarena, and E. Konofagou, “Radiation-force-

based estimation of acoustic attenuation using harmonic motion imaging (HMI) in phantoms and *in vitro* livers before and after HIFU ablation," *Phys. Med. Biol.*, vol. 60, no. 19, pp. 7499–7512, 2015.

[57] J. Vappou, G. Y. Hou, F. Marquet, D. Shahmirzadi, J. Grondin, and E. E. Konofagou, "Non-contact, ultrasound-based indentation method for measuring elastic properties of biological tissues using harmonic motion imaging (HMI)," *Phys Med Biol*, vol. 60, no. 7, pp. 2853–2868, 2015.

[58] K. Hynynen, "Focused Ultrasound Surgery Guided by MRI," *Sci. Med. (Phila).*, vol. 3, no. 5, pp. 62–71, 1996.

[59] N. J. McDannold and F. a. Jolesz, "Magnetic Resonance Image-Guided Thermal Ablations," *Top. Magn. Reson. Imaging*, vol. 11, no. 3, pp. 191–202, Jun. 2000.

[60] K. Hynynen *et al.*, "MR Imaging-guided Focused Ultrasound Surgery of Fibroadenomas in the Breast : A Feasibility Study," *Radiology*, no. 219, 2001.

[61] G. K. Hesley, K. R. Gorny, and D. A. Woodrum, "MR-guided focused ultrasound for the treatment of uterine fibroids," *Cardiovasc. Intervent. Radiol.*, vol. 36, no. 1, pp. 5–13, 2013.

[62] S. M. Sprinkhuizen, M. K. Konings, M. J. Van Der Bom, M. A. Viergever, C. J. G. Bakker, and L. W. Bartels, "Temperature-induced tissue susceptibility changes lead to significant temperature errors in PRFS-based MR thermometry during thermal interventions," *Magn. Reson. Med.*, vol. 64, no. 5, pp. 1360–1372, 2010.

[63] N. H. G. M. Peters, L. W. Bartels, S. M. Sprinkhuizen, K. L. Vincken, and C. J. G. Bakker, "Do respiration and cardiac motion induce magnetic field fluctuations in the breast and Are there implications for MR thermometry?," *J. Magn. Reson. Imaging*, vol. 29, no. 3, pp. 731–735, 2009.

[64] L. G. Merckel *et al.*, "MR-guided high-intensity focused ultrasound ablation of breast cancer with a dedicated breast platform.," *Cardiovasc. Intervent. Radiol.*, vol. 36, no. 2, pp. 292–301, Apr. 2013.

[65] S. Sapareto and W. Dewey, "Thermal dose determination in cancer therapy," *Int. J. Radiat. Oncol. Biol. Phys*, vol. 10, pp. 787–800, 1984.

[66] P. S. Yarmolenko *et al.*, "Thresholds for thermal damage to normal tissues: An update," *Int. J. Hyperth.*, vol. 27, no. 4, pp. 320–343, 2011.

[67] T. Wu, J. P. Felmlee, J. F. Greenleaf, S. J. Riederer, and R. L. Ehman, "Assessment of thermal tissue ablation with MR elastography," *Magn. Reson. Med.*, vol. 45, no. September 2000, pp. 80–87, 2001.

[68] F. L. Lizzi *et al.*, "Radiation-force technique to monitor lesions during ultrasonic therapy," *Ultrasound Med. Biol.*, vol. 29, no. 11, pp. 1593–1605, Nov. 2003.

[69] R. Righetti *et al.*, "Elastographic Characterization of HIFU-induced Lesions in Canine Livers," *Ultrasound Med. Biol.*, vol. 25, no. 7, pp. 1099–1113, 1999.

[70] F. Kallel, R. J. Stafford, R. E. Price, R. Righetti, J. Ophir, and J. D. Hazle, "The feasibility of elastographic visualization of HIFU-induced thermal lesions in soft tissues," *Ultrasound Med. Biol.*, vol. 25, no. 4, pp. 641–647, 1999.

[71] R. Souchon *et al.*, "Visualisation of HIFU lesions using elastography of the human prostate in vivo: Preliminary results," *Ultrasound Med. Biol.*, vol. 29, no. 7, pp. 1007–1015, 2003.

[72] J. Bercoff, M. Pernot, M. Tanter, and M. Fink, "Monitoring Thermally-Induced Lesions with Supersonic Shear Imaging," *Ultrason. Imaging*, vol. 40, pp. 29–40, 2004.

[73] A. K. Thittai, B. Galaz, and J. Ophir, "Visualization of HIFU-Induced lesion boundaries by axial-shear strain elastography: A feasibility study," *Ultrasound Med. Biol.*, vol. 37, no. 3,

pp. 426–433, 2011.

[74] R. Xia and A. K. Thittai, “Real-Time Monitoring of High-Intensity Focused Ultrasound Treatment Using Axial Strain and Axial-Shear Strain Elastograms,” *Ultrasound Med. Biol.*, vol. 40, no. 3, pp. 485–495, 2014.

[75] a. Mariani *et al.*, “Real time shear waves elastography monitoring of thermal ablation: In vivo evaluation in pig livers,” *J. Surg. Res.*, vol. 188, no. 1, pp. 37–43, 2014.

[76] G. Y. Hou, J. Luo, F. Marquet, C. Maleke, J. Vappou, and E. E. Konofagou, “Performance assessment of HIFU lesion detection by harmonic motion imaging for focused ultrasound (HMIFU): a 3-D finite-element-based framework with experimental validation.,” *Ultrasound Med. Biol.*, vol. 37, no. 12, pp. 2013–27, Dec. 2011.

[77] G. Y. Hou, F. Marquet, S. Wang, I. Apostolakis, and E. E. Konofagou, “High-intensity focused ultrasound monitoring using harmonic motion imaging for focused ultrasound (HMIFU) under boiling or slow denaturation conditions.,” *IEEE Trans. Ultrason. Ferroelectr. Freq. Control*, vol. 62, no. 7, pp. 1308–19, 2015.

[78] G. Y. Hou, F. Marquet, S. Wang, and E. E. Konofagou, “Multi-parametric monitoring and assessment of high-intensity focused ultrasound (HIFU) boiling by harmonic motion imaging for focused ultrasound (HMIFU): an ex vivo feasibility study.,” *Phys. Med. Biol.*, vol. 59, no. 5, pp. 1121–45, Mar. 2014.

[79] C. Maleke and E. E. Konofagou, “In vivo feasibility of real-time monitoring of focused ultrasound surgery (FUS) using harmonic motion imaging (HMI).,” *IEEE Trans. Biomed. Eng.*, vol. 57, no. 1, pp. 7–11, Jan. 2010.

[80] H. Chen *et al.*, “Harmonic motion imaging in abdominal tumor detection and HIFU ablation monitoring: A feasibility study in a transgenic mouse model of pancreatic cancer,” *IEEE*

Trans. Ultrason. Ferroelectr. Freq. Control, vol. 62, no. 9, pp. 1662–1673, 2015.

[81] T. Payen *et al.*, "Elasticity mapping of murine abdominal organs in vivo using harmonic motion imaging (HMI)," *Phys. Med. Biol.*, vol. 61, no. 15, pp. 5741–5754, 2016.

[82] M. O. I. Donnell and S. W. Flax, "C 1998 Acndcmi : Press, mc .," vol. 11, pp. 1–11, 1988.

[83] a H. Chung, K. Hynynen, V. Colucci, K. Oshio, H. E. Cline, and F. a Jolesz, "Optimization of spoiled gradient-echo phase imaging for in vivo localization of a focused ultrasound beam.," *Magn. Reson. Med.*, vol. 36, no. 5, pp. 745–52, Nov. 1996.

[84] N. McDannold and S. E. Maier, "Magnetic resonance acoustic radiation force imaging," *Med. Phys.*, vol. 35, no. 8, pp. 3748–3758, 2008.

[85] E. A. Kaye, J. Chen, and K. B. Pauly, "Rapid MR-ARFI method for focal spot localization during focused ultrasound therapy," *Magn. Reson. Med.*, vol. 65, no. 3, pp. 738–743, 2011.

[86] V. Auboiroux *et al.*, "ARFI-prepared MRgHIFU in liver: Simultaneous mapping of ARFI-displacement and temperature elevation, using a fast GRE-EPI sequence," *Magn. Reson. Med.*, vol. 68, no. 3, pp. 932–946, 2012.

[87] V. Zderic, A. Keshavarzi, M. A. Andrew, S. Vaezy, and R. W. Martin, "Attenuation of porcine tissues in vivo after high-intensity ultrasound treatment," *Ultrasound Med. Biol.*, vol. 30, no. 1, pp. 61–66, 2004.

[88] J. C. Bamber and C. R. Hill, "Ultrasonic attenuation and propagation speed in mammalian tissues as a function of temperature.," *Ultrasound Med. Biol.*, vol. 5, no. 2, pp. 149–57, Jan. 1979.

[89] R. Seip and E. S. Ebbini, "Noninvasive estimation of tissue temperature response to heating fields using diagnostic ultrasound.," *IEEE Trans. Biomed. Eng.*, vol. 42, no. 8, pp. 828–39, Aug. 1995.

[90] C. Simon, P. Vanbaren, and E. S. Ebbini, “Two-dimensional temperature estimation using diagnostic ultrasound.,” *IEEE Trans. Ultrason. Ferroelectr. Freq. Control*, vol. 45, no. 4, pp. 1088–99, Jan. 1998.

[91] X. Zheng and S. Vaezy, “An acoustic backscatter-based method for localization of lesions induced by high-intensity focused ultrasound.,” *Ultrasound Med. Biol.*, vol. 36, no. 4, pp. 610–22, Apr. 2010.

[92] C. Maleke and E. E. Konofagou, “Harmonic motion imaging for focused ultrasound (HMIFU): a fully integrated technique for sonication and monitoring of thermal ablation in tissues.,” *Phys. Med. Biol.*, vol. 53, no. 6, pp. 1773–93, Mar. 2008.

[93] T. J. Hall, M. Bilgen, M. F. Insana, and T. A. Krouskop, “Phantom materials for elastography,” *IEEE Trans. Ultrason. Ferroelectr. Freq. Control*, vol. 44, no. 6, pp. 1355–1365, 1997.

[94] J. Luo and E. Konofagou, “A fast normalized cross-correlation calculation method for motion estimation.,” *IEEE Trans. Ultrason. Ferroelectr. Freq. Control*, vol. 57, no. 6, pp. 1347–57, Jun. 2010.

[95] W. Nyborg, “Acoustic streaming,” in *Physics aoustics*, 1965.

[96] M. L. Palmeri, S. Member, A. C. Sharma, R. R. Bouchard, R. W. Nightingale, and K. R. Nightingale, “A Finite-Element Method Model of Soft Tissue Force,” vol. 52, no. 10, pp. 1699–1712, 2005.

[97] L. Chang, K. Hsu, and P. Li, “Graphics Processing Unit-Based High-Frame- Rate Color Doppler Ultrasound Processing Li-Wen Chang, Ke-Hsin Hsu, and Pai-Chi Li,” *IEEE Trans. Ultrason. Ferroelectr. Freq. Control*, vol. 56, no. 9, pp. 1856–1860, 2009.

[98] Y.-F. Li and P.-C. Li, “Software beamforming: comparison between a phased array and

synthetic transmit aperture," *Ultrason. Imaging*, vol. 33, pp. 109–118, 2011.

[99] G. Hou *et al.*, "Sparse matrix beamforming and image reconstruction for real-time 2D HIFU monitoring using Harmonic Motion Imaging for Focused Ultrasound (HMIFU) with in vitro validation.," *IEEE Trans. Med. Imaging*, vol. 33, no. 11, pp. 2107–2117, Jun. 2014.

[100] J. F. Kruecker, G. L. LeCarpentier, J. B. Fowlkes, and P. L. Carson, "Rapid Elastic Image Registration for 3-D Ultrasound," *IEEE Trans. Med. Imaging*, vol. 21, no. 11, pp. 1384–1394, 2002.

[101] R. Mirzania, K. Shapoori, E. Malyarenko, and R. G. Maev, "Ultrasonic Imaging of Static Objects Through a Scattering Layer Using the Harmonic Phase Conjugation Approach," *Ultrasounics*, vol. 58, pp. 11–21, 2015.

[102] E. Sapin, J. L. Gennisson, M. Pernot, M. Fink, and M. Tanter, "Temperature dependence of the shear modulus of soft tissues assessed by ultrasound," *Proc. - IEEE Ultrason. Symp.*, vol. 1701, 2009.

[103] V. A. Khokhlova, M. R. Bailey, J. A. Reed, B. W. Cunitz, P. J. Kaczkowski, and L. A. Crum, "Effects of nonlinear propagation, cavitation, and boiling in lesion formation by high intensity focused ultrasound in a gel phantom," *J. Acoust. Soc. Am.*, vol. 119, no. 3, pp. 1834–1848, 2006.

[104] N. A. Watkin, G. R. Ter Haar, and I. Rivens, "The intensity dependence of the site of maximal energy deposition in focused ultrasound surgery," *Ultrasound Med. Biol.*, vol. 22, no. 4, pp. 483–491, 1996.

[105] M. R. Bailey *et al.*, "Use of overpressure to assess the role of bubbles in focused ultrasound lesion shape in vitro," *Ultrasound Med. Biol.*, vol. 27, no. 5, pp. 695–708, 2001.

[106] S. Dibaji, J. Wansapura, M. R. Myers, and R. K. Banerjee, "In Vivo Monitoring of HIFU

Induced Temperature Rise in Porcine Liver Using Magnetic Resonance Thermometry1," *J. Med. Device.*, vol. 8, no. 3, p. 30937, 2014.

[107] N. J. McDannold, R. L. King, F. a Jolesz, and K. H. Hynynen, "Usefulness of MR imaging-derived thermometry and dosimetry in determining the threshold for tissue damage induced by thermal surgery in rabbits.," *Radiology*, vol. 216, no. 11, pp. 517–523, 2000.

[108] T. Yu and C. Xu, "Hyperecho as the Indicator of Tissue Necrosis During Microbubble-Assisted High Intensity Focused Ultrasound: Sensitivity, Specificity and Predictive Value," *Ultrasound Med. Biol.*, vol. 34, no. 8, pp. 1343–1347, 2008.

[109] S. Ueno, M. Hashimoto, H. Fukukita, and T. Yano, "Ultrasound thermometry in hyperthermia," *Ultrason. Symp. 1990. Proceedings., IEEE 1990*, pp. 1645–1652 vol.3, 1990.

[110] C. R. Jensen, R. W. Ritchie, J. R. T. Collin, and T. Leslie, "Spatiotemporal Monitoring of High-Intensity Focused Ultrasound Therapy with Passive Acoustic Mapping," *Radiology*, vol. 262, no. 1, 2012.

[111] C. R. Jensen, R. O. Cleveland, and C. C. Coussios, "Real-time temperature estimation and monitoring of HIFU ablation through a combined modeling and passive acoustic mapping approach," *Phys. Med. Biol.*, vol. 58, no. 17, pp. 5833–5850, 2013.

[112] W. Kwiecinski *et al.*, "Cardiac shear-wave elastography using a transesophageal transducer: application to the mapping of thermal lesions in ultrasound transesophageal cardiac ablation," *Phys. Med. Biol.*, vol. 60, no. 20, pp. 7829–7846, 2015.

[113] Y. Han, S. Wang, H. Hibshoosh, B. Taback, and E. Konofagou, "Tumor characterization and treatment monitoring of postsurgical human breast specimens using harmonic motion imaging (HMI)," *Breast Cancer Res.*, vol. 18, no. 1, p. 46, 2016.

[114] Y. Han, G. Y. Hou, S. Wang, and E. Konofagou, "High intensity focused ultrasound (HIFU)

focal spot localization using harmonic motion imaging (HMI)," *Phys. Med. Biol.*, vol. 60, no. 15, pp. 5911–5924, 2015.

[115] J. Grondin, S. Wang, T. Payen de la Garanderie, and E. Konofagou, "Real-time monitoring of high intensity focused ultrasound (HIFU) ablation of in vitro canine livers using Harmonic Motion Imaging for Focused Ultrasound (HMIFU)," *J. Vis. Exp.*, 2015.

[116] K. Hynynen, "Acoustic power calibrations of cylindrical intracavitary ultrasound hyperthermia applicators.," *Med. Phys.*, vol. 20, no. 1993, pp. 129–134, 2011.

[117] K. P. Olive and D. A. Tuveson, "The use of targeted mouse models for preclinical testing of novel cancer therapeutics," *Clin. Cancer Res.*, vol. 12, no. 18, pp. 5277–5287, 2006.

[118] K. P. Olive *et al.*, "Inhibition of Hedgehog Signaling Enhances Delivery of Chemotherapy in a Mouse Model of Pancreatic Cancer," *Cancer Res.*, vol. 324, no. 5933, pp. 1457–1461, 2009.

[119] C. R. Hill, I. Rivens, M. G. Vaughan, and G. R. ter Haar, "Lesion development in focused ultrasound surgery: a general model," *Ultrasound Med. Biol.*, vol. 20, no. 3, pp. 259–269, 1994.

[120] R. Righetti *et al.*, "Elastographic characterization of HIFU-induced lesions in canine livers," *Ultrasound Med. Biol.*, vol. 25, no. 7, pp. 1099–1113, 1999.

[121] V. Suomi, Y. Han, E. Konofagou, and R. O. Cleveland, "The effect of temperature dependent tissue parameters on acoustic radiation force induced displacements," *Phys. Med. Biol.*, vol. 61, no. 20, pp. 7427–7447, 2016.

[122] J. R. Doherty, G. E. Trahey, K. R. Nightingale, and M. L. Palmeri, "Acoustic Radiation Force Elasticity Imaging in Diagnostic Ultrasound," *IEEE Trans. Ultrason. Ferroelectr. Freq. Control*, vol. 60, no. 4, pp. 685–701, 2013.

[123] M. Fatemi and J. F. Greenleaf, “Vibro-acoustography: an imaging modality based on ultrasound-stimulated acoustic emission.,” *Proc. Natl. Acad. Sci. U. S. A.*, vol. 96, no. 12, pp. 6603–8, Jun. 1999.

[124] A. P. Sarvazyan, O. V. Rudenko, S. D. Swanson, J. B. Fowlkes, and S. Y. Emelianov, “SHEAR WAVE ELASTICITY IMAGING : A NEW ULTRASONIC TECHNOLOGY OF MEDICAL DIAGNOSTICS,” *Ultrasound Med. Biol.*, vol. 24, no. 9, pp. 1419–1435, 1998.

[125] Y. Han, S. Wang, T. Payen, and E. Konofagou, “Fast lesion mapping during HIFU treatment using harmonic motion imaging guided focused ultrasound (HMIgFUS) in vitro and in vivo,” *Phys. Med. Biol.*, vol. 62, no. 8, p. 1361, 2017.

[126] D. R. Daum, N. B. Smith, R. King, and K. Hynynen, “In vivo demonstration of noninvasive thermal surgery of the liver and kidney using an ultrasonic phased array,” *Ultrasound Med. Biol.*, vol. 25, no. 7, pp. 1087–1098, 1999.

[127] L. R. Gavrilov and J. W. Hand, “A theorical assessment of the relative performance of spherical phase arrays for ultraosund surgery,” *IEEE Trans. Ultrason. Ferroelectr. Freq. Control. vol. 47, No. 1, January 2000*, vol. 47, no. 1, pp. 125–139, 2000.

[128] J. W. Hand, A. Shaw, N. Sadhoo, S. Rajagopal, R. J. Dickinson, and L. R. Gavrilov, “A random phased array device for delivery of high intensity focused ultrasound.,” *Phys. Med. Biol.*, vol. 54, no. 19, pp. 5675–93, 2009.

[129] American Cancer Society, “Breast Cancer Facts & Figures 2013-2014,” *Atlanta Am. Cancer Soc. Inc.*, 2014.

[130] M. Guray and A. Sahin, “Benign Breast Diseases: Classification, Diagnosis, and Management,” *Cancer*, pp. 435–449, 2006.

[131] R. Kovatcheva, J.-N. Guglielmina, M. Abehsera, L. Boulanger, N. Laurent, and E. Poncelet, "Ultrasound-guided high-intensity focused ultrasound treatment of breast fibroadenoma—a multicenter experience," *J. Ther. Ultrasound*, vol. 3, pp. 1–8, 2015.

[132] F. a Jolesz, "MRI-guided focused ultrasound surgery.," *Annu. Rev. Med.*, vol. 60, pp. 417–30, Jan. 2009.

[133] F. Wu *et al.*, "Extracorporeal high intensity focused ultrasound treatment for patients with breast cancer.," *Breast Cancer Res. Treat.*, vol. 92, no. 1, pp. 51–60, Jul. 2005.

[134] S. Madersbacher, M. Pedevilla, L. Vingers, M. Susani, and M. Marberger, "Effect of High-Intensity Focused Ultrasound on Human Prostate Cancer in Vivo," pp. 3346–3351, 1995.

[135] K. J. Parker, M. M. Doyley, and D. J. Rubens, "Imaging the elastic properties of tissue: the 20 year perspective.," *Phys. Med. Biol.*, vol. 56, no. 1, pp. R1–R29, Jan. 2011.

[136] A. P. Sarvazyan, M. W. Urban, and J. F. Greenleaf, "Acoustic Waves in Medical Imaging and Diagnostics," *Ultrasound Med Biol*, vol. 29, no. 7, pp. 997–1003, 2013.

[137] T. Varghese and J. Ophir, "A theoretical framework for performance characterization of elastography: The strain filter," *IEEE Trans. Ultrason. Ferroelectr. Freq. Control*, vol. 44, no. 1, pp. 164–172, 1997.

[138] S. Y. Lee, A. R. Cardones, J. Doherty, K. Nightingale, and M. Palmeri, "Preliminary results on the feasibility of using ARFI/SWEI to assess cutaneous sclerotic diseases," *Ultrasound Med. Biol.*, vol. 41, no. 11, pp. 2806–2819, 2015.

[139] T. Hall, "In vivo real-time freehand palpation imaging," *Ultrasound Med. Biol.*, vol. 29, no. 3, pp. 427–435, 2003.

[140] B. S. Garra, A. Zuurbier, M. Magnant, M. F. Pennanen, and R. Spratt, "Breast Elastography Initial Clinical of Breast Results ' Lesions :," pp. 79–86, 1997.

[141] Y. Zhou and W. G. X, “Variations of bubble cavitation and temperature elevation during lesion formation by high-intensity focused ultrasound.,” *J Acoust Soc Am*, vol. 134, no. 2, pp. 1683–1694, 2013.

[142] D. Coluccia *et al.*, “First noninvasive thermal ablation of a brain tumor with MR-guided focused ultrasound.,” *J. Ther. ultrasound*, vol. 2, p. 17, 2014.

[143] C. H. Lee *et al.*, “Breast Cancer Screening With Imaging: Recommendations From the Society of Breast Imaging and the ACR on the Use of Mammography, Breast MRI, Breast Ultrasound, and Other Technologies for the Detection of Clinically Occult Breast Cancer,” *J. Am. Coll. Radiol.*, vol. 7, no. 1, pp. 18–27, 2010.

[144] S. Maruvada, G. R. Harris, B. a Herman, and R. L. King, “Acoustic power calibration of high-intensity focused ultrasound transducers using a radiation force technique.,” *J. Acoust. Soc. Am.*, vol. 121, pp. 1434–1439, 2007.

[145] H. H. PENNES, “Analysis of Tissue and Arterial Blood Temperatures in the Resting Human Forearm,” *J. Appl. Physiol.*, 1948.

[146] W. L. Nyborg, “Solutions of the bio-heat transfer equation.,” *Phys. Med. Biol.*, vol. 33, pp. 785–792, 1988.

[147] CDRH, “Guidance for industry and FDA staff—information for manufacturers seeking marketing clearance of diagnostic ultrasound systems and transducers. 2008,” 2010.

[148] O. Falou *et al.*, “Evaluation of neoadjuvant chemotherapy response in women with locally advanced breast cancer using ultrasound elastography.,” *Transl. Oncol.*, vol. 6, no. 1, pp. 17–24, 2013.

[149] A. Evans *et al.*, “Can shear-wave elastography predict response to neoadjuvant chemotherapy in women with invasive breast cancer?,” *Br. J. Cancer*, vol. 109, no. 11, pp.

2798–802, 2013.

[150] Y. Ma, S. Zhang, J. Li, J. Li, Y. Kang, and W. Ren, "Comparison of strain and shear-wave ultrasounic elastography in predicting the pathological response to neoadjuvant chemotherapy in breast cancers," *Eur. Radiol.*, pp. 1–10, 2016.

[151] M. Hayashi *et al.*, "Evaluation of Tumor Stiffness by Elastography Is Predictive for Pathologic Complete Response to Neoadjuvant Chemotherapy in Patients with Breast Cancer," *Ann. Surg. Oncol.*, vol. 19, no. 9, pp. 3042–3049, 2012.

[152] F. Wu *et al.*, "Changes in biologic characteristics of breast cancer treated with high-intensity focused ultrasound," *Ultrasound Med. Biol.*, vol. 29, no. 10, pp. 1487–1492, 2003.

[153] R. Seip *et al.*, "High-intensity focused ultrasound (HIFU) multiple lesion imaging: comparison of detection algorithms for real-time treatment control," *2002 IEEE Ultrason. Symp. 2002. Proceedings.*, vol. 2, no. c, pp. 1427–1430, 2002.

[154] L. Curiel, Y. Huang, N. Vykhodtseva, and K. Hynynen, "Focused ultrasound treatment of VX2 tumors controlled by local harmonic motion," *Phys. Med. Biol.*, vol. 54, no. 11, pp. 3405–3419, 2009.

[155] R. Sugiyama *et al.*, "Real-time feedback control for high-intensity focused ultrasound system using localized motion imaging," *Jpn. J. Appl. Phys.*, vol. 54, no. 7, 2015.

[156] M. A. Abbass, J. K. Killin, N. Mahalingam, F. M. Hooi, P. G. Barthe, and T. D. Mast, "Real-Time Spatiotemporal Control of High-Intensity Focused Ultrasound Thermal Ablation Using Echo Decorrelation Imaging in ex Vivo Bovine Liver," *Ultrasound Med. Biol.*, vol. 44, no. 1, pp. 199–213, 2018.

[157] M. C. L. Peek, M. Ahmed, and M. Douek, "High-intensity focused ultrasound for the treatment of fibroadenomata (HIFU-F) study," *J. Ther. Ultrasound*, vol. 3, no. 1, p. 6, 2015.

[158] D. Brenin, “Treatment of breast fibroadenoma with high intensity focused ultrasound (HIFU): a feasibility study,” *J. Ther. Ultrasound*, vol. 3, no. Suppl 1, p. O78, 2015.

[159] C. M. Botar-Jid *et al.*, “Assessment of cutaneous melanoma by use of very-high-frequency ultrasound and real-time elastography,” *Am. J. Roentgenol.*, vol. 206, no. 4, pp. 699–704, 2016.